ANALYSIS OF PRINTED MONOPOLE ANTENNAS

SOMEN BHATTACHARJEE

DEPARTMENT OF ELECTRONICS AND ELECTRICAL ENGINEERING

INDIAN INSTITUTE OF TECHNOLOGY GUWAHATI

GUWAHATI - 781039, ASSAM, INDIA

ANALYSIS OF PRINTED MONOPOLE ANTENNAS

A

Thesis Submitted

in Partial Fulfilment of the Requirements

for the Degree of

DOCTOR OF PHILOSOPHY

By

SOMEN BHATTACHARJEE

Department of Electronics and Electrical Engineering

Indian Institute of Technology Guwahati

Guwahati - 781 039, INDIA.

May, 2016

Certificate

This is to certify that the thesis entitled "**ANALYSIS OF PRINTED MONOPOLE ANTENNAS**", submitted by **SOMEN BHATTACHARJEE** (11610238), a research scholar in the *Department of Electronics & Electrical Engineering, Indian Institute of Technology Guwahati*, for the award of the degree of **Doctor of Philosophy**, is a record of an original research work carried out by him under my supervision and guidance. The thesis has fulfilled all requirements as per the regulations of the institute and in my opinion has reached the standard needed for submission. The results embodied in this thesis have not been submitted to any other University or Institute for the award of any degree or diploma.

Dated:

Guwahati.

Dr. RAKHESH SINGH KSHETRIMAYUM
Dept. of Electronics & Electrical Engg.
Indian Institute of Technology Guwahati
Guwahati - 781039, Assam, India.

Prof. RATNAJIT BHATTACHARJEE
Dept. of Electronics & Electrical Engg.
Indian Institute of Technology Guwahati
Guwahati - 781039, Assam, India.

Acknowledgements

I would like to express my sincere gratitude to my supervisors, Dr. Rakhesh Singh Kshetrimayum and Prof. Ratnajit Bhattacharjee, for their excellent guidance and support throughout the course for this work. My heartfelt thanks to them for the unlimited support and patience shown to me. I would particularly like to thank for all his help in patiently and carefully correcting all my manuscripts.

I would like to thank my doctoral committee members Prof. A. K. Gogoi, Dr. S. K. Nayak and Dr. R. K. Sonkar for sparing their precious time to evaluate the progress of my work. Their suggestions have been valuable. I would also like to thank other faculty members for their kind help carried out during my academic studies. My special thanks to Mr. Sanjib, Mr. Utpal Kumar Sarma, and all the members of the High Frequency Laboratory for maintaining an excellent computing facility and providing various resources useful for the research work.

I had a great time with my many friends at IITG, including (but not limited to) Atul, Vinay, Brijesh, Murli, Shivanshu, Parveen, Himangshu, Ankit and Anand and the list goes on. I thank them for their support and encouragement. The company of my friends at IIT Guwahati proved to be a great asset which helped me stay relaxed throughout my research.

Among those deserving of a special mention is my wife Papiya, who had extended her wholehearted support to bring this work into existence. She has been able to take care of my daughter extremely well. I thank my daughter Soumyapriya for keeping me energetic and reducing my worries. Again, I am grateful to my parents (Sanjib Kumar Bhattacharjee and Rani Bhattacharjee), in-laws (Ashok Adhikary and Suniti Adhikary), whose love and encouragement made this research possible.

I also grateful acknowledge MHRD, Govt. of India for financing my studies at IIT Guwahati. Finally, I would like to thank the Almighty God for bestowing me this opportunity and showering his blessings on me to come out successful against all odds.

Somen Bhattacharjee

Abstract

Printed monopole antenna (PMA) is one of the most suitable antenna for achieving large bandwidth and omnidirectional radiation pattern. In the last one decade, several printed monopole antenna configurations have been proposed and such antennas have been designed using different simulation softwares (HFSS, IE3D, CST Microwave Studio etc) for various wireless communication applications such as wireless LAN, WiFi, UWB etc. However, very few theoretical works are reported for the analysis of printed monopole antennas. Our present work is devoted to development of analytical framework for investigation of printed monopole antennas. Full wave analysis using Mixed Potential Integral Equation is performed along with the derivation of spatial domain potential (scalar and vector) Green's function for horizontal electric dipole lying on an ungrounded dielectric layer. The input impedance and return loss of printed monopole antenna is calculated and validated by simulation (HFSS) and available experimental results.Approximate analysis of printed monopole antenna is also done to calculate input impedance using transmission line theory. In this, substrate is considered as a transmission line section terminated with free space characteristic impedance. The intrinsic impedance of the medium (substrate) depends on the thickness and the dielectric constant of the medium. Spectral domain Green's function for the field components is also derived in order to calculate the radiation pattern and gain of rectangular and circular printed monopole antenna and the theoretical results are validated by simulation (HFSS) and available experimental results. Next, the performance of printed monopole antenna with a magneto-dielectric cover and uniaxial substrate is investigated both in theory as well as in simulation (HFSS). Finally, appropriate circuit representation of printed monopole antenna is presented for different geometries of antenna and the ground plane, which are further verified by simulation (HFSS) and available experimental results.

CONTENTS

LIST OF FIGURES

LIST OF TABLES

ABBREVIATIONS

EFIE	Electric field integral equation
FDTD	Finite difference time domain
HED	Horizontal electric dipole
HFSS	High frequency structure simulator
MoM	Method of Moment
MPIE	Mixed potential integral equation
MSA	Microstrip antenna
PMA	Printed monopole antenna
TE	Transverse electric
TM	Transverse magnetic
UWB	Ultra wide band

MATHEMATICAL SYMBOLS

k_0	Free space wavenumber
$\vec{E}$	Electric field vector
$\vec{H}$	Magnetic field vector
$\tilde{E}$	Electric field representation in spectral domain
$\tilde{H}$	Magnetic field representation in spectral domain
$tan\delta$	Loss tangent
h	Substrate thickness
ε_r	Relative permittivity of a medium
ε_0	Free space permittivity
μ_r	Relative permeability of a medium
μ_0	Free space permeability
t	Time
Z_0	Characteristic impedance

CHAPTER 1

INTRODUCTION

1.1 Introduction to Printed Antennas

In the last two decades, due to rapid developments in the field of wireless communication, it has become necessary to develop antennas having features like compact size, light weight, low cost and easy to install on planar as well as nonplanar surfaces. Printed antennas are most suitable candidates for such applications. Among the different forms of printed antennas, microstrip antenna configuration is very popular for such applications. As shown in Fig. 1.1, a simple microstrip antenna (MSA) consists of radiating patch printed on one side of the dielectric substrate and the ground plane on the other side of the dielectric. The idea of MSA was first proposed by Deschamps [1] in 1953. In [2], different possible geometrical configurations of printed antennas have been discussed in detail including regular geometries like rectangular, circular, etc. One of the most prominent use of printed antenna is mobile satellite communication system [3]. In [4], printed antenna is used for global positioning system. Printed antennas are also used for radar and medical applications [5, 6].

Microstrip antenna have several advantages over conventional microwave antenna such as:

1. Light weight, low volume, low fabrication cost and conformable.

2. Linear and circular polarization both can be achieved using simple feed.

3. Can be easily integrated with microwave integrated circuits.

However, in spite of its popularity, microstrip antennas suffer from some drawbacks which are:

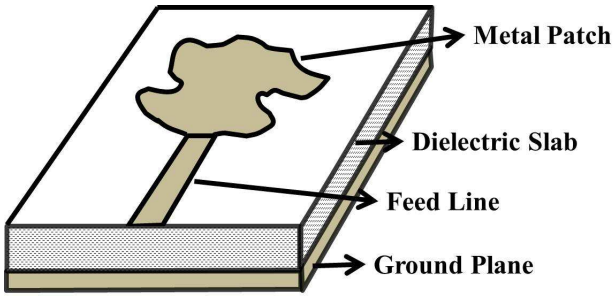

Figure 1.1: Layout of Microstrip Antenna

1. Narrow impedance bandwidth.
2. Low gain and efficiency.
3. Most microstrip antenna radiates in half space and polarization purity is less.

The above drawback of having narrow bandwidth of microstrip antenna can be avoided by using a printed monopole antenna (PMA). Structurally a PMA is slightly different from a microstrip antenna which is discussed in detail in the next section.

1.2 Printed Monopole Antenna

In high data rate wireless communication at GHz frequencies, antenna should be preferably small in size, have large bandwidth and possess omnidirectional radiation characteristics. These requirements can be easily met by printed monopole antennas. It has been observed in early 1930s that by thickening the arms of dipole or monopole antenna, bandwidth can be increased. The reason for increase of bandwidth with broadening the arms of dipole or monopole is the nature of current distribution, which no longer remains sinusoidal. The modified current distribution of such broadened antennas does not change the radiation pattern of the antenna appreciably, but it effects the input impedance considerably [7].

In broad sense, printed monopole antenna are categorized in three different configurations

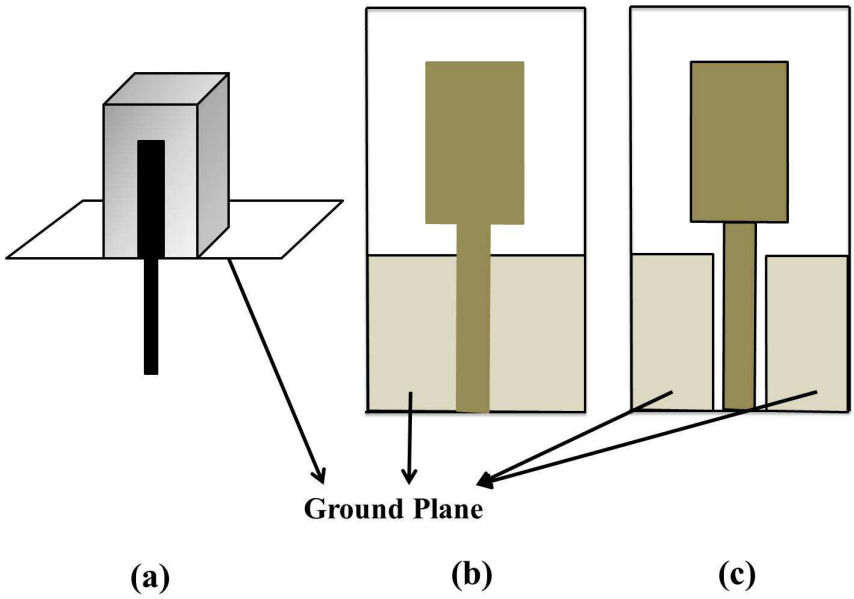

Figure 1.2: Different configuration of Printed Monopole Antenna

in terms of their excitation and location of the ground plane as shown in Fig. 1.2. The salient features of these different configurations are given below:

1. In the first configuration of PMA (Fig. 1.2(a)), ground plane is orthogonal to both patch as well as the dielectric, and the excitation is given by 50 Ω coaxial transmission line. This type of configuration with different shapes are discussed in [8] and analyzed using transmission line approach in [9].

2. The second configuration is microstrip line fed PMA (Fig. 1.2(b)), in which patch is excited via 50 Ω microstrip line [10]. Both the patch and the microstrip line, are lying on one side of the dielectric and the ground plane extends upto feed line only.

3. The third configuration is coplanar waveguide (CPW) fed PMA (Fig. 1.2(c)), in which ground and the patch are lying on same side of the dielectric whereas the other side of the dielectric is backed by free space [11].

The first configuration is not very popular as wireless handset antenna because of the com-

patibility with dimensions. Second and third configurations are more favorable printed antenna structures. These configurations are particularly useful for ultrawideband applications as well [12, 13]. The thesis is primarily devoted to the analysis and modeling of second configuration of PMAs.

Printed circuit version of the monopole antenna or printed monopole antenna are practically realized with finite sized ground plane. Fig. 1.3 depicts a strip monopole antenna on a dielectric substrate of thickness *h*, which is basically a 50 Ω microstrip transmission line extending beyond the rim of the ground plane. But as the strip monopole antenna is an extended part of the

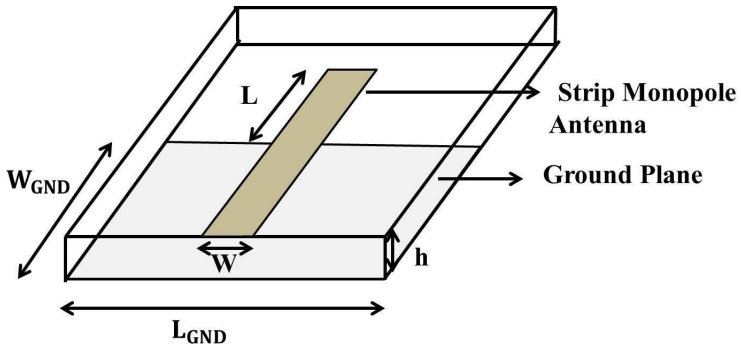

Figure 1.3: Layout of Strip Monopole Antenna

50 Ω transmission line, so similar to simple dipole or monopole antenna it doesn't provide large bandwidth. In order to achieve large bandwidth for the printed monopole antenna the arm of the strip is to be broadened only beyond the rim of the ground plane to form rectangular printed monopole antenna. For proper matching of the printed monopole with the microstrip feed line, the width of the feed, dielectric constant (ε_r) and thickness (h) of the substrate are to be chosen using the standard microstrip line design equations [14]

$$W/d = \begin{cases} \frac{8e^A}{e^{2A}-2}, & W/d < 2 \\ \frac{2}{\pi}\left[B-1-\ln(2B-1)+\frac{\varepsilon_r-1}{2\varepsilon_r}\left\{\ln(B-1)+0.39-\frac{0.61}{\varepsilon_r}\right\}\right], & W/d > 2 \end{cases}$$

where

$$A = \frac{Z_0}{60}\sqrt{\frac{\varepsilon_r+1}{2}} + \frac{\varepsilon_r-1}{\varepsilon_r+1}\left(0.23+\frac{0.11}{\varepsilon_r}\right)$$

$$B = \frac{377\pi}{2Z_0\sqrt{\varepsilon_r}}$$

Thus a microstrip fed printed monopole antenna shown in Fig. 1.3 can be considered as an asymmetrically driven dipole antenna, in which the strip form one arm of the dipole and the ground plane form the other arm. It can be further realized as combination of two grounded monopole antenna, one monopole is the strip and the other is the ground plane. For printed monopole antennas, the radiation field is found by considering the contribution of both the patch and the ground plane.

1.3 Analytical Modeling of PMAs: Related Issues

To understand the physical phenomena and its corresponding characteristics of printed antennas, especially microstrip antenna, various analytical and numerical method have been developed. The available methods for the analysis of microstrip antenna are as follows:

- **Cavity Model Analysis**

  In cavity model analysis, the microstrip patch antenna is modeled as a lossy cavity. The cavity is formed enclosing a dielectric region by electric conductors at the top and bottom while by magnetic walls along the perimeter of the patch. The fields within the cavity are expressed as the summation of the fields of various resonant modes while far fields are computed from the equivalent magnetic currents around the periphery [7]. The cavity model can take into account the higher order resonant modes and the feed inductance. It offers a simple yet clear physical understanding of the resonant behavior of microstrip patch antennas. However, this model is applicable only to regular patch shapes.

- **Transmission Line Analysis**

  Microstrip antenna was first analyzed by Munson in 1974 using transmission line model [15]. In transmission line model of rectangular microstrip antenna, two radiating slots (which accounts for the fringing fields) separated by a distance equal to the length of the patch accounts for the radiation from patch. Since these slots are in the vicinity of

the ground plane, image theory is made use of to compute the radiated fields.Further, each of the radiating slot is equivalent to parallel admittance comprise of conductance and susceptance. Mutual coupling effect between the radiating edges using transmission line method is discussed in [16]. The transmission line model, usually applies to only rectangular patch. But this limitation can be avoided to great extent by modeling through generalized transmission line theory. In this method, circular, annular sector, ring shaped structures can be modeled [17–19].

In another method, using transmission line approach proposed by Jackson and Alexopoulous in which substrate is considered as transmission line and combining with reciprocity theorem, far field components of printed antennas are derived analytically [20].

- **Full Wave Analysis**

  Cavity model and transmission line model analysis works well with thin substrates only. It is difficult to model different feed configuration, patches with anisotropic substrate and cross polarization can't be predicted because of single mode analysis. Most of the drawbacks are overcome by using fullwave analysis. In this method the substrate and ground plane are assume to be infinite. The effect of dielectric and its corresponding thickness are accounted by Green's function evaluated by imposing boundary condition at the interfaces. The evaluated Green's function are further employed in integral equation method such as Electric Field Integral Equation (EFIE) or Mixed Potential Integral Equation (MPIE) [2, 21, 22], in which the current distribution over the metallic patch is calculated using Method of Moment (MoM). This method provides accurate results for impedance and radiation characteristics of printed antennas. It is possible to analyze arbitrary shaped structures, it can account surface wave, dielectric and radiation losses. Apart from these, this technique is also able to analyze patch antenna on anisotropic substrates. Apart from MoM, Finite Difference Time Domain Method (FDTD) method [23, 24] is also a full wave technique with the difference that it computes in time domain and the derivation of Green's function is not required. Due to volumetric discretization employed in FDTD, MoM is a better choice which uses surface discretization. Besides, in FDTD, in

order to truncate the infinite simulation domain, a proper absorbing boundary conditions is necessitated.

In the above mentioned methods for the analysis of printed antennas, each methods have their individual advantages and disadvantages. But to predict the performance of the antennas it is necessary to know the physics of the problem. Though above methods give accurate results, approximate analysis on the performance of these antennas are also useful. PMA analysis using any of the above mentioned technique is not done earlier even for the basic antenna geometry. So the thesis attempts the analysis of PMAs using the above mentioned methods.

In order to understand the operation of printed monopole antennas, a proper and accurate model is necessary. The existing models developed for the microstrip antennas are not directly applicable to PMA due to its partial ground plane on the back side of the substrate. Here, we point out few such differences between traditional microstrip antennas and PMAs which suggest that further modifications are required in existing models to make them more suitable for the printed monopole antennas.

❖ In microstrip antennas substrate is fully backed by the metallic ground plane whereas for the microstrip transmission line fed PMA, substrate is backed by partial ground plane. In printed monopole antenna case, the ground plane extends up to the microstrip line.

❖ As the boundary conditions for a PMA are different than those of a microstrip antenna, the Green's function for a PMA needs to be evaluated appropriately considering the boundary conditions of a PMA.

❖ In transmission line model for the microstrip antennas using the approach given in [20], the length of the transmission line is considered to be the height of the substrate which is terminated on short circuit due to presence of ground plane below the patch, whereas for PMAs due to absence of ground plane transmission line doesn't terminate on a short circuit.

❖ As mentioned earlier, ground plane takes part in the radiation phenomena for PMAs. It forms asymmetric dipole antenna which can be further realized as a combination of two grounded monopole antenna. Hence the dimension of the ground plane plays a key role in overall characteristics of PMAs.

❖ In microstrip antennas magneto dielectric based substrate are important for miniaturization purposes but the same may not helpful for the miniaturization purposes for PMAs.

The above discussion indicates the possible differences in the design aspects of printed antennas and PMAs. Therefore, a new model need to be developed for printed monopole antennas by modifying the existing models for microstrip antennas. Another issue which we needs to be taken care of while developing a model for printed monopole antennas is the location of poles in the Sommerfeld integral.

In [25], the transmission line analysis combined with the reciprocity theorem is proposed for microstrip antenna to calculate radiation characteristics of the antenna. But to apply the same approach for printed monopole antennas, some modifications are required. In Green's function evaluation for microstrip antennas, the boundary conditions are applied at patch dielectric interface and at the ground plane on the backside of the dielectric. But to evaluate Green's function, different boundary conditions is required in PMA at the backside of the dielectric air interface due to absence of metallic ground plane. In our work, Mixed Potential Integral Equation based approach is used along with MoM to calculate current distribution over the metallic patch. In order to calculate MPIE, spatial domain Green's function (vector and scalar) are required which are basically a definite integral of Sommerfeld type [2, 21]. Since the Green's function derived here is different from the Green's function of microstrip antennas, the issues of identification of poles in Sommerfeld integral must be taken into care for this case as well.

1.4 Motivation of the Present Work: Thesis Objective

As mentioned in the previous sections, primarily simulation and measurement based studies about PMA have been reported in literature. Not many works are available dealing with analytical modeling of PMA. Analytical modeling of PMA is important to understand the interdependence of various parameters of PMA and its performance as well as arriving at the initial design of PMAs to be fine tuned through commercial simulators. Keeping in this view, analytical modeling of PMAs have been considered in detail in this thesis. The objective of the thesis is to develop simplified approximate analytical models and rigorous full wave analysis for different PMA configurations. The validity of such modeling is established in comparison with simulation and available experimental results. In order to analyze PMA, some modifications on the existing models are required. Such modifications are listed below:

- For the transmission line analysis of microstrip antenna following [20], the substrate is modeled as a transmission line which terminates on short circuited line because of the presence of ground plane whereas for PMAs the same terminates on free space characteristic impedance due to absence of ground plane.

- In PMAs the spectral domain Green's functions are derived to account for the effect of substrate and its corresponding thickness by imposing boundary conditions at the patch-dielectric and dielectric-air interfaces (due to absence of the ground plane). Further, to implement Green's function in MPIE, spatial domain Green's function is required which can be obtained using inverse Fourier Transform of spectral domain Green's function. This gives rise to integral of Sommerfeld type. This type of integrals requires careful handling because of the poles. The number of poles and its location for PMAs may be different from microstrip antennas.

- As mentioned before, ground plane plays a key role for the radiation of PMAs. The ground plane effect is also accounted for the theoretical radiation characteristic of PMAs by considering it as another arm of the asymmetric dipole antenna.

In the next section we will discuss about the contribution of the thesis.

1.5 Thesis Contributions

The main contributions of this thesis in the theoretical modeling and analysis of PMAs are:

1. Approximate equivalent transmission line modelling of PMAs. The modelling is carried out through derivation of Green's function for an HED on an ungrounde substrate and equivalent transmission line representation of the dielectric substrate. Theoretical models have been developed for rectangular and circular PMA for evaluating various antenna parameters.

2. Analysis of PMA through derivation of scalar and vector Green's function and combining the same with MPIE-MoM. Evaluation of input impedance of rectangular and F shaped PMA are presented as case study for the proposed approach.

3. Derivation of analytical expressions for far field and gain of rectangular and circular PMA considering PMAs as asymmetric dipole by taking into account of the contribution of the ground plane.

4. Investigation of bandwidth enhancement of rectangular PMA using magneto-dielectric substrate.

5. Performance analysis of PMA on uniaxial substrate employing spectral domain immittance approach.

6. Accurate circuit representation of different printed monopole antennas (strip, rectangular, bend strip, bend strip with protruding stub in the ground, circular).

1.6 Thesis Organization

The thesis is organized as follows:

- **Chapter 1** discusses about the issues with the existing theoretical models of microstrip antennas which needs to be considered for analysis of PMA and the motivation behind the present work. This chapter highlights the basics of printed antennas as well as printed monopole antennas. A brief introduction of the issues related to existing model and corresponding modifications required to analyze PMAs are presented here. This chapter also

provides the thesis contribution along with a brief outline of the thesis organization.

- **Chapter 2** presents a literature survey of related works in the area of modeling and analysis of printed antennas using transmission line approach, full wave technique (MPIE), spectral domain method, spectral domain immittance approach and related works on magneto-dielectric and uniaxial substrate for printed antennas. It also presents a survey on the works related to PMAs in terms of simulation and experiments as well related few theoretical works.

- **Chapter 3** presents the derivation of a closed form expression for input admittance of horizontal electric dipole over an ungrounded substrate using transmission line analogy. The derived expression is then used to calculate reflection coefficient of rectangular and circular printed monopole antenna (PMA) fed by a microstrip line. Analytical result for the reflection coefficient of both rectangular and circular PMA is verified using High Frequency Structure Simulator (HFSS). For circular PMA, analytical, and simulated results are also compared with the measured results available in literature. Effect of the dimension and dielectric material on the antenna bandwidth is also studied and verified by HFSS.

- **Chapter 4** presents spatial domain potential Green's functions of a horizontal electric dipole (HED) lying on an ungrounded dielectric slab. The full wave technique (MoM) based Mixed Potential Integral Equation (MPIE), involving the derived potential Green's functions, is used to calculate the input impedance as well as the reflection coefficient of printed monopole antennas (PMAs). The performance of rectangular and F shaped PMAs are evaluated using MPIE-MoM. The computed results for the input impedance and reflection coefficient of rectangular PMA are verified with HFSS results. Further, refection coefficient of F-shaped PMA is computed using MPIE-MoM which is verified by HFSS simulation and available experimental result.

- **Chapter 5** presents the theoretical analysis of radiation characteristics of PMAs. Theoret-

ical analysis of radiation characteristics of PMAs is not adequately dealt in the literature. By applying appropriate boundary conditions, spectral domain Greens functions for a horizontal electric dipole lying on an ungrounded dielectric substrate is derived and making use of the same, the expressions for the radiated fields and gain for PMAs are then obtained. The derived far field expressions for rectangular and circular PMAs are verified with available experimental results as well as by comparing with the results computed using HFSS. The theoretical gain for rectangular and circular monopole antennas are also computed and compared with HFSS simulation results.

- **Chapter 6** presents the enhancement of bandwidth in traditional printed monopole antenna (PMA) using a cover of magneto-dielectric material in the 8-18 GHz range. Analytical expression for the far field radiation pattern of PMA with magneto-dielectric cover using transmission line analogy is derived. The advantage of using magneto-dielectric cover on PMA is shown by comparing the antenna performance of PMA having dielectric cover and no cover, using HFSS software package.

- **Chapter 7** presents the performance of printed monopole antennas (PMA) on uniaxial substrate and the same is theoretically analyzed using spectral domain immittance approach. Using immittance approach, field components of unit current source is evaluated first and then directivity is also calculated. The theoretical values of the far field radiation pattern and directivity of uniaxial substrate based rectangular printed monopole antenna are validated by HFSS whereas return loss is calculated using HFSS.

- **Chapter 8** presents circuit representation of printed monopole antennas for different cases. In general, a simple parallel RLC circuit is enough to represent a particular operating frequency band of an antenna. Similarly, for multiple resonating antenna, each resonance can be modeled by their equivalent parallel RLC circuit. Thus overall circuit of a lossy one port device such as antenna can be modeled by series inductance and capacitance in connection with parallel RLC circuit(s). But the effect of capacitance in series is not relevant for printed monopole antennas since ground plane below the patch is absent

for such cases. Thus circuit representation is presented for different printed monopole antennas cases with their individual lumped element values for each design of the antenna which are further verified by HFSS and available experimental results.

- **Chapter 9** concludes this thesis with a summary of the work done and the related work which may be investigated in future.

CHAPTER 2

LITERATURE SURVEY: REVIEW OF RELATED WORKS

The present chapter provides detailed literature review on the existing models on printed antennas and available literatures related to PMAs. A list of existing models which are considered in this thesis for analysis of PMA as well as their principles of operation are shown in Table 2.1. In the following sections, we will discuss each model in brief with reference to available literatures.

2.1 Transmission Line Model

In transmission line model, radiating slot acts as parallel admittance which consists of conductance and susceptance. Munson et al. [15] first proposed transmission line analysis of rectangular microstrip antenna. But the model proposed by Munson has some disadvantages such as the expressions derived for admittance are not valid for narrow patches, the mutual coupling effect between the radiating slots are neglected. The solution to some of the stated problems are provided in [16, 27]. In [28], the loss due to radiation and lossy dielectric material for printed antennas are accounted by transmission line theory. Transmission line analysis for aperture coupled microstrip antenna is given in [29]. The earlier methods discussed are limited to rectangular patches only. The analysis for other patch shape, viz. circular, annular and ring shaped geometries are performed using generalized transmission line model in [17–19]. Such

Table. 2.1: Various models for printed antenna analysis

Analytical Model	***Principle on which model is developed***	***Remark***
Transmission Line Model [20]	Green's function is derived for an HED on grounded substrate. Substrate is modeled as a transmission line and the length of the line is equal to the thickness of the substrate. Reciprocity is used for calculation of pattern	Multilayered geometry can be modeled. Calculation of radiation pattern and input impedance is possible.
Full Wave Analysis using Method of Moments [2]	Green's function is derived by imposing boundary conditions at the interfaces which is required for solving integral equation. Integral equation may be solved using MoM.	Radiation parameters estimation for any arbitrary shaped antennas is possible.
Spectral Domain Immittance Approach [26]	Green's function for multilayered geometry can be evaluated from decoupled TM and TE field components.	Radiation parameters estimation for any arbitrary shaped antennas is possible.

analysis is based on microstrip patch configuration having separable geometries. Quasi TEM transmission line model is used to analyze circular printed antennas and arbitrary shaped antennas [30], [31]. Lebbar et al. [9], proposed transmission line analysis of printed monopole antenna. The PMA discussed in [9], is printed line on a lossy dielectric substrate which is mounted over ground plane and coaxial fed excitation is provided to the antenna via ground plane.

In another method proposed by Jackson et. al [20], antenna is represented in terms of unit horizontal electric dipole placed on substrate superstrate geometry. Each of the substrate and superstrate is represented by transmission line, where the substrate thickness represents the length of the transmission line and its corresponding characteristic impedance is dependent on the material properties (dielectric constant and relative permeability). Further, the far field radiation pattern of the antenna of given geometry is calculated. In [25], the same methodology is used to analyze simple microstrip antenna. It may be noted that the above mentioned modeling techniques were developed in the context of microstrip antennas. In this thesis, we explore

whether such models with appropriate modification can model the PMA configuration under consideration.

Table. 2.2: Summary of the available work for printed antennas using transmission line approach

Reference	***Summary of the work***	***Remark***
Munson *et al*. [15]	Patch and the ground plane together consist the transmission line	Limited to rectangular patch
Bhattacharyya *et al*. [17]	Patch is modelled as transmission line	Circular shaped patch
Dubost *et al*. [31]	Patch is modelled as transmission line along with quasi TEM mode analysis	Arbitrary shaped patch
Jackson *et al*. [25]	Substrate acts as transmission line	Rectangular patch is analyzed
Lebbar *et al*. [9]	Patch acts as transmission line	Stripline is analyzed

2.2 Full Wave Analysis

Although transmission line based analysis is relatively simpler, it has some limitations.The inherent limitations of transmission line approach are overcome by using full wave technique. The full wave technique is the most suitable form of analysis in terms of accuracy, completeness and versatility. However, such techniques involve tedious numerical computation. The popular techniques for carrying out full wave analysis of printed antennas are:

1. Spectral Domain MoM
2. MPIE-MoM Approach
3. Finite Difference Time Domain Technique (FDTD).
4. Finite Element Method (FEM)

In the following section, we present the literature review of the related work based on the full wave techniques. Since FDTD and FEM techniques have not been used in thesis for the analysis

of PMAs, so review of related literatures are not presented here. However, it is worth mentioning that the results obtained using the analytical models proposed in this thesis are compared with the results obtained using an FEM based simulator, HFSS. It is well known fact that MoM is more efficient for analysis of open structures like antenna problems. Besides, unlike FEM and FDTD, MoM involves surface discretization which makes it faster for implementation. Summary of the available work for printed antennas using full wave technique in tabular format is shown in Table 2.3

2.2.1 Spectral Domain MoM Approach

Spectral domain approach [32, 33], utilizes spectral domain Green's function to analyze printed antennas. Green's functions are generally employed for solving electric field integral equation (EFIE) over the patch metallization by applying appropriate boundary conditions over the patch. Green's function for printed antennas [34], are special cases of horizontal electric dipole (HED) in presence of multilayered region [35–37]. Fields of an HED in presence of three and four layered region are available in [38] and [39, 40]. Printed antenna is the case of an HED in a three layered region, first region is free space where field is to be determined, second is the dielectric in which HED is located on the top surface and the third is the metallic ground plane [41, 42]. In the following literatures, spectral domain technique for the analysis of rectangular patch [43], circular [44], elliptical [45], ring [46], printed dipole [41], patch of arbitrary shape [47] are available. Analysis of anisotropic substrate based printed antenna is available in [33]. Handling of different feed mechanism in case of printed antennas is possible in spectral domain approach, [48] focus on proximity coupled microstrip fed antenna and [49–52] on aperture coupled antenna. Mutual coupling between antennas is considered in [43]. [53] accounts the far field radiation pattern of printed antennas using stationary phase method. The theoretical formulation of radiation pattern of rectangular microstrip antenna is given in [54].

2.2.1.1 Spectral Domain Immittance Approach

Spectral domain immittance approach is the most effective technique particularly for the analysis of multilayered microstrip structures. Itoh et. al. [26], first proposed the immittance ap-

proach based analysis for dispersion characteristics of printed transmission lines. In [55], the analysis of open microstrip structure is presented. Green's function for multilayered geometry can be evaluated from decoupled TM and TE field components. Green's function related to TM and TE fields, are identified as inverse of wave admittances observed from HED located at the interface of free space and grounded dielectric for printed open microstrip structures.

2.2.2 Mixed Potential Integral Equation (MPIE) - MoM Approach

In general, spectral domain Green's function is used for electric field integral equation. But in MPIE, as the name suggests, instead of field, spatial domain potential (scalar and vector) Green's function are utilized in integral equation evaluation. In the following literatures, MPIE based analysis of rectangular patch [56], circular patch [57], arbitrary shape patch [58, 59] are available. MPIE analysis of anisotropic substrate based printed antenna is available in [58]. [60] reports aperture coupled antenna analysis utilizing MPIE. Mutual coupling between antennas is considered in [61].

2.2.2.1 Singularity Issues with MPIE Approach

In order to solve MPIE, spatial domain Green's function is required. To get spatial domain Green's function from its spectral domain counterpart, inverse Fourier transform or Fourier-Bessel transform is performed, and is given by,

$$f(\rho) = \int_0^\infty J_0(k_\rho \rho)\, \tilde{f}(k_\rho)\, k_\rho dk_\rho \tag{2.1}$$

where ρ is the radial distance between source and the observer and $J_0(\cdot)$ is the Bessel function of first kind.

The equation in (2.1) is an integration of Sommerfeld type. This type of integration are generally associated with the poles in the integrand. To avoid such pole(s) from the integrand is one of the most challenging issue in the present approach. One such method to avoid the pole(s) is pencil function method, which was first proposed by Hua and Sarkar [62], some of the related literatures are also available in [63, 64]. In another method proposed in [34, 42, 65], poles

are eliminated from the integrand to make the integration smooth. In [21], the integration is performed using weighted average algorithm to overcome the issue associated with the poles.

2.2.3 Method of Moment

The spectral domain electric field integral equation or MPIE are solved for unknown surface current density J_s using method of moment [66]. In this method, unknown current density J_s is expanded in terms of known basis function with unknown coefficients. The resulting integral equation is tested through another set of function known as testing function, which provides a set of simultaneous equations in matrix format. Solving the matrix equation, unknown coefficients of the current density are found out. Using the surface current over the patch one can calculate different antenna parameters like input impedance, return loss and radiation pattern. Basis function can be further subdivided into entire domain basis function and subdomain basis function. Entire domain basis function are generally used for regular shaped patches [67], whereas for irregular shaped structure, subdomain basis function [49, 68] are used.

Table. 2.3: Summary of the available work for printed antennas using full wave technique

Reference	***Summary of the work***	***Remark***
Shively *et al*. [47]	Spectral domain electric field integral equation approach	Arbitrary shaped patch
Perlmutter *et al*. [54]	Spectral domain method for radiation pattern calculation	Rectangular patch is analyzed
Itoh *et al*. [55]	Spectral domain immittance approach	Open microstrip structures
Uckun *et al*. [59]	Mixed potential integral equation approach	Arbitrary shaped patch

2.3 Effect of Substrate Material on the Performance of Printed Antennas

In this section, the performance of printed antennas on different substrates such as uniaxial, magneto-dielectric are discussed along with available literatures.

2.3.1 Magneto-dielectric Substrate

In [69], magnetodielectric is used as substrate in printed antennas. The advantages and limitations of such materials are also presented. Mosallaei et al. [70], proposed periodic configurations of magneto-dielectric material for applications in VHF-UHF applications. Magneto dielectric based nanocomposite is used in planar inverted F antenna for reduction in specific absorption rate (SAR) [71]. Some of the practical magnetodielectric based substrate material are discussed in [72]. One of the most important feature of magnetodielectric based materials is that it provides antenna miniaturization [73, 74].

2.3.2 Uniaxial Substrate

Spectral domain approach based analysis for printed antennas on uniaxial substrate is given in [33], whereas MPIE based analysis for the same is available in [75]. Some of the work related to printed structures on uniaxial substrate are available in [76, 77].

2.4 Summary

This chapter provides an review of some of works related to printed antenna models that have been reported in the literature. Different aspects of printed antenna modeling using transmission line and full wave techniques have been discussed in detail. Some issues related to extending such modeling techniques to include PMAs have been highlighted. This chapter also provides a brief discussion of the magneto-dielectric and uniaxial substrates.

Table. 2.4: Summary of the available theoretical work for printed antennas on magnetodielectric and uniaxial substrate.

Reference	***Summary of the work***	***Remark***
Hansen *et al*. [69]	Transmission line modelling for magnetodielectric substrate based printed antenna	Limited to square patch
Pozar *et al*. [33]	Full wave analysis using spectral domain approach for printed antenna on uniaxial substrate	Rectangular patch
Plet *et al*. [75]	Full wave analysis using MPIE approach for printed antenna on multilayered scenario	Rectangular patch

CHAPTER 3

APPROXIMATE ANALYSIS USING TRANSMISSION LINE APPROACH

3.1 Introduction

Printed monopole antenna (PMA) is one of the most suitable choices for wideband and ultra wideband applications due to its large impedance bandwidth and nearly omnidirectional radiation pattern. Most of the experimental and simulation work on different PMA structure has already been done and some of them are available in the literature [78–80]. FDTD and characteristic mode theory based analysis of PMA fed by CPW are available in [81] and [82] respectively. Electric Field Integral Equation and Method of Moment (EFIE MoM) analysis of printed strip monopole antenna is also presented in [83]. The present chapter discusses about the analytical evaluation of input impedance as well as reflection coefficient of rectangular PMA. Analytical model of antennas provide physical insight into the antenna operation and the same helps in preliminary design of antennas which can be refined further using different CAD tools available. An analytical model of PMA using transmission line analogy provides useful information on the dependence of antenna parameters on its dimensions and substrate material. PMA is structurally similar to simple microstrip antenna (MSA) with only difference that the ground plane is removed below the patch. Thus PMA can be modeled in terms of unit horizontal electric dipole (HED) lying on a substrate which is not backed by a ground plane. Thus transmission line analogy is an effective way to derive the closed form expressions for the input impedance and reflection coefficient of PMA. The substrate layer can be modelled as a

transmission line with characteristic impedance and propagation constant depends on angle of incidence θ [20]. Since the characteristic impedance also depends on the substrate material, thus the expression for theoretical input impedance gives some physical insight on the behavior of PMA with respect to variation in ε_r and substrate thickness h . Results for the reflection coefficient evaluated from the theoretical input impedance expression of a rectangular PMA fed by 50 Ω microstrip line is compared with Ansoft High Frequency Structure Simulator (HFSS) results. Reflection coefficient of a circular PMA is also evaluated using the theoretical method proposed in this work and the same is compared with simulation (HFSS) results as well as results already available in literature [79]. Dependence of impedance bandwidth on substrate material and dimensions of the antenna is also discussed in the result section.

3.2 Theory

Assume a horizontal electric dipole (HED) lying on a lossy and ungrounded dielectric substrate as shown in Fig. 3.1. The input admittance Y_{in} is evaluated in the dielectric when source is in

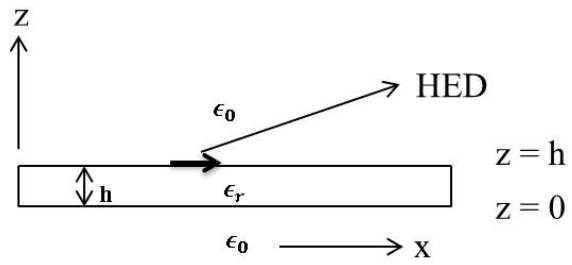

Figure 3.1: Geometry of HED along x-axis on the interface of dielectric and free space

the air at an specified angles θ, ϕ in spherical coordinates. Using reciprocity theorem Y_{in}^{TE} or Y_{in}^{TM} is the admittance due to the source lying on the interface (between air and dielectric) seen from air for transverse electric (TE) or transverse magnetic (TM) cases. The admittance Y_{in}^{TE} or Y_{in}^{TM} depends on the angle of incidence θ. The source accounted for reciprocity on the interface

can be represented by the plane wave incident on transmission line of length equal to height of the dielectric layer. Fig. 3.2 represent the wave incident from Region 2 (air) on the dielectric at an angle θ, enters into Region 1 (dielectric) at an angle θ_1 and wave emerges out to Region 0 (air) at an angle θ_2.

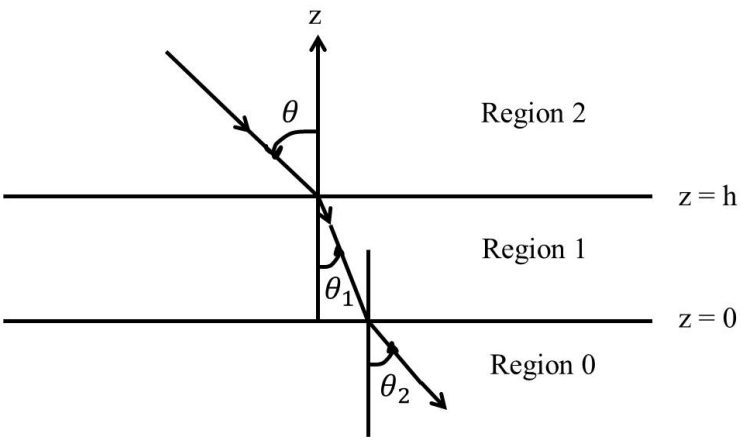

Figure 3.2: Wave propagation in a three layered region

3.2.1 Transmission Line Equivalent of PMA

Here, the substrate layer is modeled as transmission line with the length equal to the substrate thickness h and propagation constant depends on angle θ [20], which terminates at the characteristic impedance of air Z_{c2} .

Now using the equivalent transmission line model for PMA as shown in Fig. 3.3, the input admittance for the TE polarization case can be expressed as

$$Y_{in}^{TE} = \frac{n_1(\theta)}{\eta_0} \frac{\frac{\eta_0}{n_1(\theta)} + j\eta_0 \sec(\theta)\tan(\beta_1 h)}{\eta_0 \sec(\theta) + j\frac{\eta_0}{n_1(\theta)}\tan(\beta_1 h)} \tag{3.1}$$

The above expression for input admittance of a HED on an ungrounded substrate for TE polarization case can be derived using [20] in which characteristic impedance of air (Z_{c0} and Z_{c2}) is $\eta_0 sec(\theta)$, whereas characteristic impedance of substrate (Z_{c1}) is $\eta_0/n_1(\theta)$, $n_1(\theta)$ is the effective refractive index of the dielectric which is dependent on angle θ, equal to $\sqrt{\varepsilon_r - \sin^2(\theta)}$

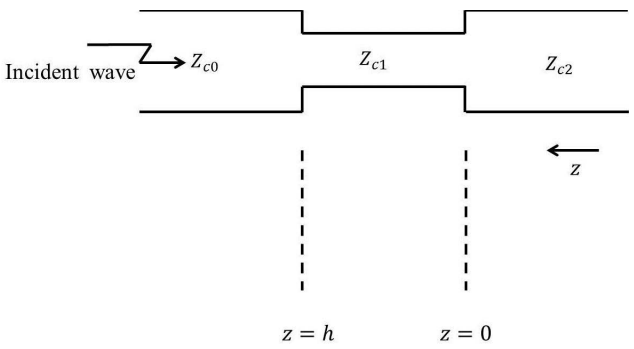

Figure 3.3: Transmission line model of printed monopole antenna

and propagation constant $\beta_1 = k_0 n_1(\theta)$. Similarly, input admittance for TM polarization case can be written as

$$Y_{in}^{TM} = \frac{\varepsilon_r}{\eta_0 n_1(\theta)} \frac{\frac{\eta_0 n_1(\theta)}{\varepsilon_r} + j\eta_0 \cos(\theta) \tan(\beta_1 h)}{\eta_0 \cos(\theta) + j\frac{\eta_0 n_1(\theta)}{\varepsilon_r} \tan(\beta_1 h)} \tag{3.2}$$

In this case characteristic impedance for air is $\eta_0 cos(\theta)$, whereas characteristic impedance for substrate is $\frac{\eta_0 n_1(\theta)}{\varepsilon_r}$, and rest of the parameter are same as in TE polarization case. For most of the practical cases, printed monopole antennas have very thin substrate thickness, so for thin substrate cases i.e. when h is small and $\theta = 0$ (for perpendicular incidence) both equations (3.1) and (3.2) becomes

$$Y_{in} = \frac{1}{\eta_0} + j\frac{k_0 h}{\eta_0}(\varepsilon_r - 1) \tag{3.3}$$

Now replacing ε_r by $\varepsilon_r(1 - jtan(\delta))$ in 3.3, where $tan(\delta)$ is very small amount of dielectric loss in the substrate, then after some calculations equation (3.3) gives overall resistance $R = \eta_0 / (1 + k_0 h \varepsilon_r \tan(\delta))$, capacitance $C = k_0 h(\varepsilon_r - 1)/\omega_0 \eta_0$ and inductance $L = \eta_0 / \omega_0 k_0 h(\varepsilon_r - 1)$ respectively.

Here ω_0 is resonant frequency of the structure and η_0 is the free space characteristic impedance nearly equal to 377 Ω. Using the value of R, L, C one can evaluate the Q value for shunt RLC circuit, thus the bandwidth of the structure is shown in Fig. 3.1. Hence bandwidth (BW) can be

expressed as

$$BW = \frac{1}{k_0 h(\varepsilon_r - 1)} + \frac{\varepsilon_r \tan(\delta)}{(\varepsilon_r - 1)} \tag{3.4}$$

The value of first and second term for BW expression in equation (3.4) for different substrate material of thickness $h = 1.59$ mm with operating frequency of 3 GHz are listed below in Table. 3.1.

Table. 3.1: Bandwidth calculation

Substrate	*1st term in* (3.4)	*2nd term in* (3.4)
FR4 epoxy	3	0.03
RT Duriod 5870	7.5	0.002
RT Duriod 5880	8.3	0.001

From Table. 3.1, it can be observed that the value of second term in (3.4) is very small compared to the first term, so the second term can be neglected. Hence equation (3.4) can be written as

$$BW \approx \frac{1}{k_0 h(\varepsilon_r - 1)} \tag{3.5}$$

3.3 Results

The above results are limited to the HED, input impedance calculation for printed monopole antenna is carried out using the following equation [84]

$$Z_{in} = -\frac{hI_s}{I_0}\left(\frac{1}{Y_{in(TEorTM)}}\right) \tag{3.6}$$

where I_s is the current set up by the microstrip line feed on the antenna which is given by $I_0 \sin\left(\pi(x - 0.5L)/L\right)/W$. Thus reflection coefficient can be effectively evaluated from input impedance of printed rectangular monopole antenna. The proposed technique is validated by HFSS simulation using rectangular PMA on FR4 substrate ($\varepsilon_r = 4.4$) having thickness 1.59 mm with loss tangent of 0.02 fed by a 50 Ω microstrip line. The geometry of the antenna is shown in Fig. 4. The detailed dimensions of the rectangular printed monopole antenna shown in Fig. 3.4 are listed below in Table. 3.2. The performance of this transmission line based approach has also been verified in case of a circular PMA [79].

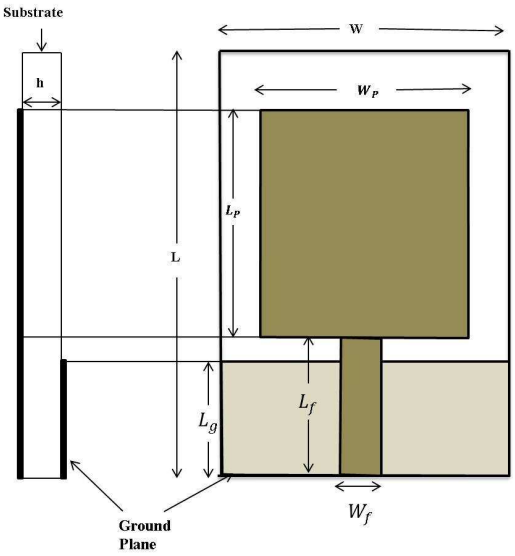

Figure 3.4: Geometry of a rectangular printed monopole antenna

Table. 3.2: Detail dimensions of rectangular PMA

	Dimension of Rectangular PMA							
Parameters	L_p	W_p	L_f	W_f	L_g	L	W	h
Units (in mm)	46	42	17.8	2.96	15	76	81	1.59

3.3.1 Discussions

Fig. 3.5 shows both theoretical as well simulation results of reflection coefficient (in dB) of simple rectangular printed monopole antenna which is in good agreement. Equivalent surface area model of square and circular patch discussed in [85] is used to calculate reflection coefficient of printed circular printed monopole antenna and the theoretical results are validated by HFSS. In Fig. 3.6, the theoretical and HFSS results are compared with the results of circular PMA available in [79]. It may be noted that [79] provides simulation results of circular PMA computed using CST Microwave Studio as well as measured data. It is interesting to note that bandwidth gets affected by broadening the width of the rectangular printed monopole antenna as shown in Fig. 3.7. Fig. 3.8 shows that the impedance bandwidth degrades with the increase in dielectric constant and follows equation (3.5) developed in theory section. Increase in dielectric constant

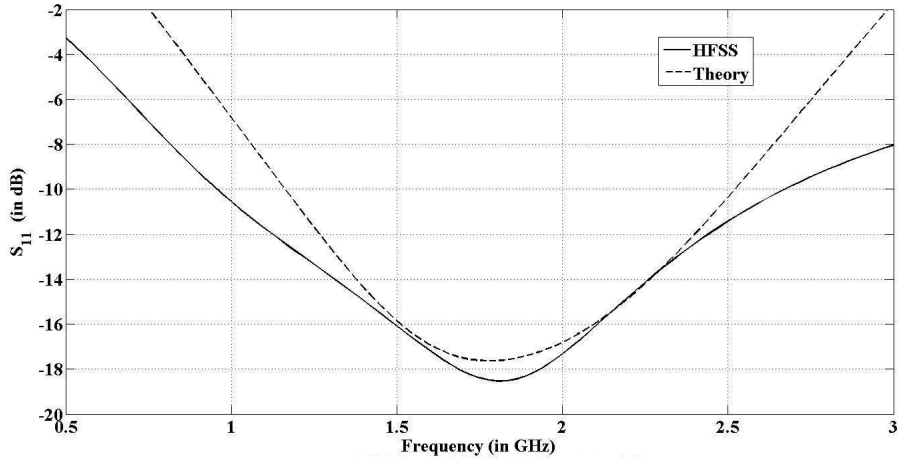

Figure 3.5: Plot of reflection coefficient of a rectangular printed monopole antenna in dB

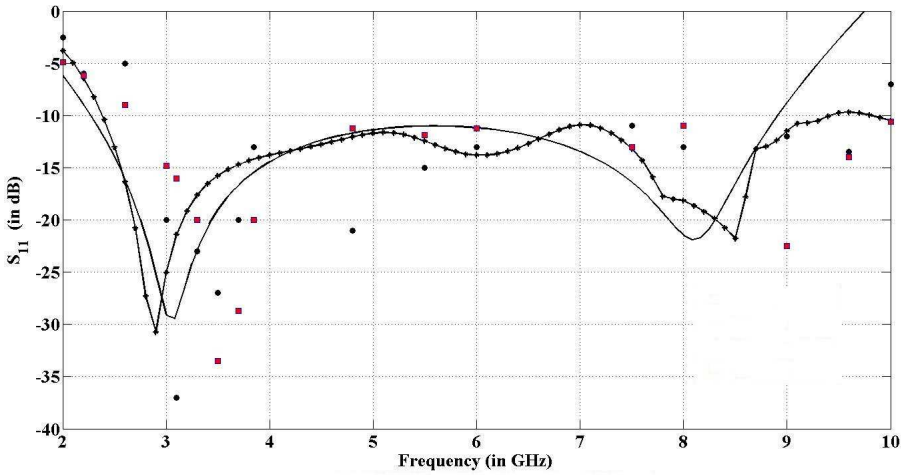

Figure 3.6: Plot of reflection coefficient (theory (—), HFSS (—⋆—), CST (.) and measured (●)) of a circular printed monopole antenna in dB

raises surface wave which in turn reduces the radiated power.

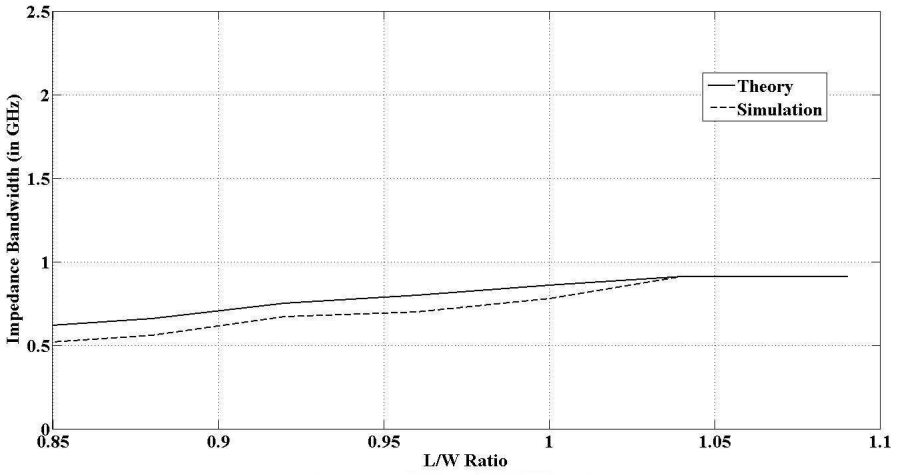

Figure 3.7: Plot of L/W (Length to width) ratio to Bandwidth in case of rectangular PMA

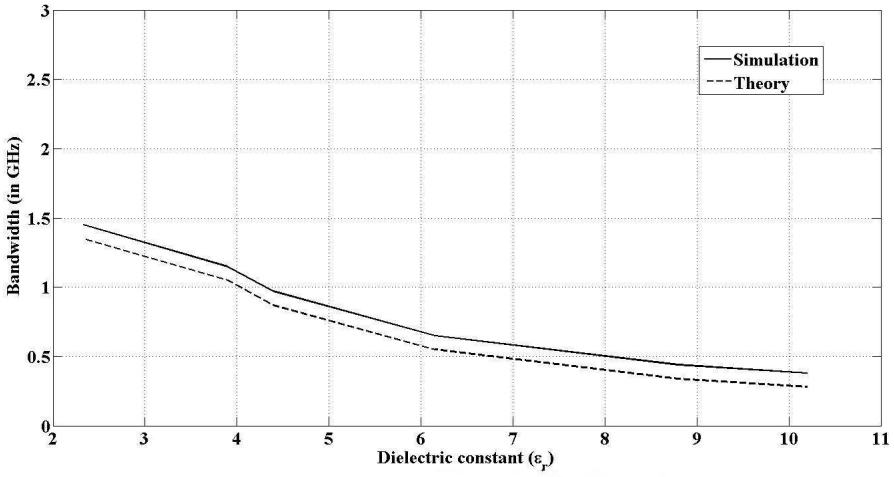

Figure 3.8: Plot of Dielectric constant (ε_r) to Bandwidth in case of rectangular PMA

3.4 Summary

Input impedance of a HED on an ungrounded substrate is first derived using transmission line analogy. We extract the circuit parameters with closed form expressions for resistive and reactive parts for both TE and TM polarization case. Circuit representation for PMA is used to

calculate reflection coefficient. The theoretical results for reflection coefficient of rectangular and circular are compared with simulation results obtained using HFSS software. The proposed method is also found to be reasonably accurate for modelling circular PMA. Besides these the effect of broadening the width of the patch on the impedance bandwidth for rectangular PMA is also shown in the result section. Impact of dielectric constant of the substrate material on impedance bandwidth is also presented here. Though the formulation provides us some physical insight, method is an approximate one and applicable to to rectangular and circular PMAs only. In addition to this, the effect of ground plane is not considered here but for a PMA it plays a major role. So keeping this drawback in mind, the next chapter is dedicated to use of rigorous full wave technique for the analysis of PMA.

CHAPTER 4

POTENTIAL GREEN'S FUNCTIONS OF UNGROUNDED DIELECTRIC SLAB AND ITS APPLICATION IN FULL WAVE ANALYSIS

4.1 Introduction

The electromagnetic field of a horizontal electric dipole in multilayered dielectric media has applications in theoretical analysis of antenna, geophysical analysis, and radar. The present chapter is based on the derivation of potential (scalar and vector) Green's function for a horizontal electric dipole (HED) on an ungrounded dielectric slab for the analysis of printed monopole antennas (PMAs), using mixed potential integral equation and method of moments (MPIE-MoM). MPIE-MoM is preferred over traditional Electric Field Integral Equation (EFIE) because of the fact that both scalar and vector potentials vary as $1/R$, where R represents the distance of the observation point from the antenna and therefore less singular compared to traditional EFIE [86]. The exact Green's function formulation in different dielectric media required for full wave analysis of microstrip antenna (MSA) are available in [33], [37], [87], [88]. In MPIE, Green's function needs to satisfy the boundary condition on the patch metallization. A simple PMA is structurally similar to a microstrip line fed patch antenna with the difference that the ground plane below the patch is removed. Thus the metallic patch of PMA can be modeled analytically in terms of unit horizontal electric dipole (HED) lying on a dielectric slab which is not backed by a ground plane. By applying boundary conditions on the tangential electric and

magnetic field components at the two interfaces: first between air and the face of the dielectric slab on which the HED is kept and the second between the opposite face of the same dielectric slab and air, the field components are then determined in the spectral domain. The exact magnetic vector potential is obtained from magnetic field components and then using Lorentz Gauge condition, one can evaluate the scalar potential. It may be mentioned here that the scalar and vector potential Green's function expressions which are derived here are major contributions of this chapter. After getting both scalar and vector potential in spectral domain, spatial domain counterpart can be obtained using inverse Fourier Transform. Integral which represents Inverse Fourier Transform here is an integral of Sommerfeld type. Solutions of such type of integral are discussed in literatures [21, 89, 90]. After the integral being evaluated, the Mixed Potential Integral Equation (MPIE) involving spatial domain vector and scalar potential Green function can be solved for unknown current distribution over the metallic patch using Galerkin's Method. Resulting current distribution is used to calculate input impedance and reflection coefficient of the rectangular PMA and the results are compared using Ansoft High Frequency Structure Simulator (HFSS). HFSS results are in good agreement with the one computed using the proposed MPIE-MoM approach. An F shaped printed monopole antenna is also analyzed using the proposed MPIE-MoM approach and the theoretical results are in good agreement with HFSS and experimental results reported in [80].

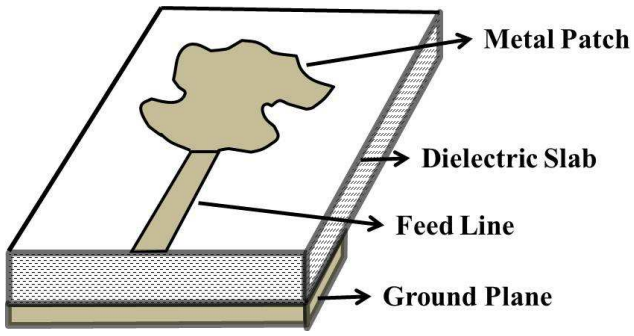

Figure 4.1: Layout of a printed monopole antenna

4.2 Potential Green's functions of a HED over Ungrounded Dielectric Slab

Fig. 4.1 depicts a PMA of arbitrary shape printed on a lossless dielectric slab of relative permittivity ε_r and thickness h. It may be noted that PMA has a ground plane extending up to the feed line only i.e. the ground plane under the patch has been removed. Hence, this structure of PMA is different from the conventional microstrip antenna.

Therefore, the potential Green's function for PMA will be inherently different from that of MSA [34]. In the next section derivation of the spectral domain potential Green's functions is presented.

4.2.1 Potential Green's Functions in Spectral Domain

Green's function is used in full wave analysis to satisfy the boundary condition over the patch metallization, which is modeled in terms of a horizontal electric dipole (HED). So, in order to derive spectral domain Green's function, an HED lying on a lossless and ungrounded dielectric slab is considered first (since the ground plane under the patch has been removed for PMAs) as shown in Fig. 4.2. It may be noted that the case of an HED on a grounded dielectric substrate has been well investigated in the literature [34].

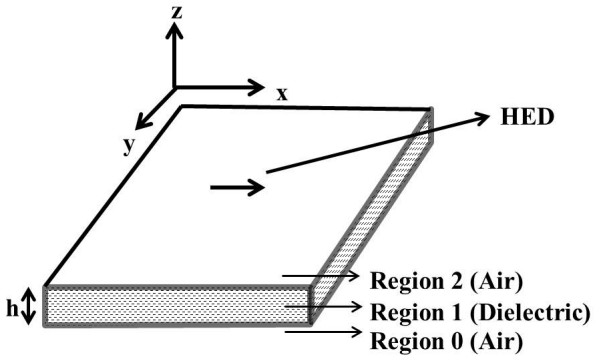

Figure 4.2: Geometry of HED along x- axis on the interface of dielectric and free space

To derive potential Green's function, let us consider an HED on a lossless dielectric slab located at (x_0, y_0) shown in Fig. 4.2, the x-directed current is defined as $J_x = \hat{x}\delta(x-x_0)(y-y_0)$ at $z = d$ and the effect of J_x is considered through boundary condition. The source free Maxwell's equations in frequency domain can be written as,

$$\nabla \times \vec{E} = -j\omega\mu_0\vec{H} \tag{4.1a}$$

$$\nabla \times \vec{H} = j\omega\varepsilon_0\varepsilon_r\vec{E} \tag{4.1b}$$

The above equations can be explicitly written after Fourier transform is applied to equation (4.1a) ($\frac{\partial}{\partial x} \rightarrow jk_x, \frac{\partial}{\partial y} \rightarrow jk_y$) as,

$$jk_y\tilde{E}_z - \frac{\partial \tilde{E}_y}{\partial z} = -j\omega\mu_0\tilde{H}_x \tag{4.2a}$$

$$\frac{\partial \tilde{E}_x}{\partial z} - jk_x\tilde{E}_z = -j\omega\mu_0\tilde{H}_y \tag{4.2b}$$

$$jk_x\tilde{E}_y - jk_y\tilde{E}_x = -j\omega\mu_0\tilde{H}_z \tag{4.2c}$$

Similarly for equation (4.1b) can be given as

$$jk_y\tilde{H}_z - \frac{\partial \tilde{H}_y}{\partial z} = j\omega\varepsilon_0\varepsilon_r\tilde{E}_x \tag{4.3a}$$

$$\frac{\partial \tilde{H}_x}{\partial z} - jk_x\tilde{H}_z = j\omega\varepsilon_0\varepsilon_r\tilde{E}_y \tag{4.3b}$$

$$jk_x\tilde{H}_y - jk_y\tilde{H}_x = j\omega\varepsilon_0\varepsilon_r\tilde{E}_z \tag{4.3c}$$

Now, after differentiating equation (4.2b) w.r.t z, the equation can be rewritten as

$$j\frac{\partial \tilde{H}_y}{\partial z} = \frac{jk_x}{\omega\mu_0}\frac{\partial \tilde{E}_z}{\partial z} - \frac{1}{\omega\mu_0}\frac{\partial^2 \tilde{E}_x}{\partial z^2} \tag{4.4}$$

The term $\frac{\partial \tilde{H}_y}{\partial z}$ in equation (4.4) can be replaced by equation (4.3a) and then after some simple algebraic calculation we get [33],

$$k_\rho^2\tilde{E}_x = jk_x\dot{\tilde{E}}_z - \omega\mu_0 k_y\tilde{H}_z \tag{4.5}$$

Similarly, the following expressions can also be obtained:

$$k_\rho^2\tilde{E}_y = jk_y\dot{\tilde{E}}_z + \omega\mu_0 k_x\tilde{H}_z \tag{4.6a}$$

$$k_\rho^2\tilde{H}_x = jk_x\dot{\tilde{H}}_z + \omega\varepsilon_0\varepsilon_r k_y\tilde{E}_z \tag{4.6b}$$

$$k_\rho^2 \tilde{H}_y = jk_y \dot{\tilde{H}}_z - \omega\varepsilon_0\varepsilon_r k_x \tilde{E}_z \tag{4.6c}$$

Here $\tilde{E}$ and $\tilde{H}$ are Fourier Transform representation of the fields, $\dot{\tilde{E}}$ and $\dot{\tilde{H}}$ are spatial derivatives of Fourier Transform representation of the fields. For the present case, since there is no ground plane, we need to divide the equivalent antenna structure into three regions. Region 2 and Region 0 signifies region above the top and below the bottom region of the dielectric slab respectively, whereas Region 1 denotes the dielectric slab itself as shown in Fig. 4.2. The general solutions assumed for the Regions 0, 1 and 2 are as follows: For Region 2,

$$\widetilde{E}_{z2} = Ae^{-u_2 z} \qquad for \qquad z > h \tag{4.7}$$

$$\widetilde{H}_{z2} = Be^{-u_2 z} \qquad for \qquad z > h \tag{4.8}$$

where $u_2^2 = -k_z^2 = k_\rho^2 - k_0^2$ and $Im(u_2) > 0$.

For Region 1,

$$\widetilde{E}_{z1} = Ccosh(u_1 z) + Dsinh(u_1 z) \qquad for \qquad 0 \le z \le h \tag{4.9}$$

$$\widetilde{H}_{z1} = Esinh(u_1 z) + Fcosh(u_1 z) \qquad for \qquad 0 \le z \le h \tag{4.10}$$

where $u_1^2 = -k_z^2 = k_\rho^2 - \varepsilon_r k_0^2$ and $Im(u_1) > 0$.

For Region 0,

$$\widetilde{E}_{z0} = Me^{u_0 z} \qquad for \qquad z < 0 \tag{4.11}$$

$$\widetilde{H}_{z0} = Ne^{u_0 z} \qquad for \qquad z < 0 \tag{4.12}$$

where $u_0^2 = -k_z^2 = k_\rho^2 - k_0^2$, $k_\rho^2 = k_x^2 + k_y^2$ and $Im(u_0) > 0$. Now, in order to find the arbitrary constants A, B, C, D, E, F, M and N respectively, the boundary conditions are applied as follows: (i) $\tilde{E}_x$, $\tilde{E}_y$ and $\tilde{H}_x$, $\tilde{H}_y$ are continuous at the interface between Region 0 and 1 $(z = 0)$, (ii) $\tilde{E}_x$, $\tilde{E}_y$ and $\tilde{H}_x$ are continous, whereas $\tilde{H}_y$ is discontinuous by an amount of $\tilde{J}_x$ at the interface between Region 1 and 2 $(z = h)$. After applying the above boundary conditions in equations (4.5) to (4.6c) through (4.7) to (4.12), we get,

$$\tilde{E}_{z2} = \frac{\tilde{J}_x k_x e^{-u_2(z-h)}}{\omega\varepsilon_0 D_{TM}} \tag{4.13}$$

$$\tilde{H}_{z2} = \frac{-j\tilde{J}_x k_y e^{-u_2(z-h)}}{D_{TE}} \tag{4.14}$$

where $D_{TM} = 1 + \frac{u_2\varepsilon_r(u_1+u_0\varepsilon_r tanh(u_1h))}{u_1(u_0\varepsilon_r+u_1 tanh(u_1h))}$ and $D_{TE} = u_2 + \frac{(u_0+u_1 tanh(u_1h))}{\left(1+\frac{u_0}{u_1}tanh(u_1h)\right)}$. It may be noted that the above expressions for D_{TE} and D_{TM} are different from that of the grounded dielectric slab in [34].

The relation required to derive vector potential Green's functions using magnetic field components can be expressed as

$$\mu_0\vec{H} = \nabla \times \vec{A} \tag{4.15}$$

The equation in (4.15) can be explicitly written after Fourier Transform ($\frac{\partial}{\partial x} \rightarrow jk_x, \frac{\partial}{\partial y} \rightarrow jk_y$) as,

$$\mu_0\tilde{H}_x = -jk_y\tilde{A}_z \tag{4.16a}$$

$$\mu_0\tilde{H}_y = \frac{\partial\tilde{A}_x}{\partial z} - jk_x\tilde{A}_z \tag{4.16b}$$

$$\mu_0\tilde{H}_z = -jk_y\tilde{A}_x \tag{4.16c}$$

Now, equation (4.13) and (4.14) together with equations (4.16a) to (4.16c), spectral domain vector potential Green's function at the interface ($z = h$) can be written as:

$$\tilde{G}_A^{xx} = \frac{\mu_0}{2\pi D_{TE}} \tag{4.17}$$

$$\tilde{G}_A^{zx} = \frac{j\mu_0(1-\varepsilon_r)k_x tanh(u_1h)\left[\frac{1}{u_1} + \frac{u_0\left(1-tanh^2(u_1h)\right)}{(u_0\varepsilon_r+u_1 tanh(u_1h))(u_1+u_0 tanh(u_1h))}\right]}{2\pi D_{TE}D_{TM}} \tag{4.18}$$

Spectral domain scalar potential Green's function can be derived from vector potential components using Lorentz Gauge condition $\nabla\cdot\vec{A} + j\omega\mu_0\varepsilon_0\varepsilon_r V = 0$, and the same can be obtained as

$$\tilde{G}_V = \frac{1}{2\pi\varepsilon_0}\left[\frac{D_{TM} - (\varepsilon_r-1)u_2 tanh(u_1h)\left\{\frac{1}{u_1} + \frac{u_0\left(1-tanh^2(u_1h)\right)}{(u_0\varepsilon_r+u_1 tanh(u_1h))(u_1+u_0 tanh(u_1h))}\right\}}{D_{TE}D_{TM}}\right] \tag{4.19}$$

It may be pointed out here that the above expressions for vector potential ($\tilde{G}_A^{xx}$ and $\tilde{G}_A^{zx}$) and

scalar potential Green's functions ($\tilde{G}_V$) are not readily available in existing literature and they are different from potential Green's function of HED on a grounded dielectric substrate.

The above expressions in equation (4.17) and (4.19) are the spectral domain Green's function for ungrounded dielectric slab. But in order to solve MPIE spatial domain Green's function is required. To get spatial domain Green's function from its spectral domain counterpart, inverse Fourier transform or Fourier-Bessel transform is performed, and the same is given by

$$f(\rho) = \int_0^\infty J_0\left(k_\rho \rho\right) \tilde{f}\left(k_\rho\right) k_\rho dk_\rho \tag{4.20}$$

where ρ is the radial distance between source and the observer and $J_0(\cdot)$ is the Bessel function of first kind. Now using equation (4.20) spatial domain vector and scalar potential Green's function can be expressed as

$$G_A^{xx} = \frac{\mu_0}{2\pi} \int_0^\infty \tilde{G}_A^{xx} J_0(k_\rho \rho) k_\rho dk_\rho \tag{4.21}$$

$$G_V = \frac{1}{2\pi\varepsilon_0} \int_0^\infty \tilde{G}_V J_0(k_\rho \rho) k_\rho dk_\rho \tag{4.22}$$

4.3 Numerical Evaluation of Spatial Domain Vector and Scalar Potential Green Functions

Both equations (4.21) and (4.22) are spatial domain vector and scalar potential Green's function, for HED on a lossless ungrounded dielectric slab as shown in Fig. 4.2 and have the nature of Sommerfeld integral. Generally such integrals are numerically computed as they can't be solved analytically. Many authors have already discussed about the solution of such type of integral using different methods. One such method is Matrix Pencil Method discussed in detail in [62, 64]. Another method used Complex Residue approach for singularity extraction [21, 42], in which poles appear due to zeros in denominator of the integrand. This poles make the integrand highly oscillatory, thus poles are eliminated from the integrand using residue theorem to make the integration smooth. Next, spatial domain integrals of Sommerfeld type which arises in equations (4.21) and (4.22) are discussed in detail.

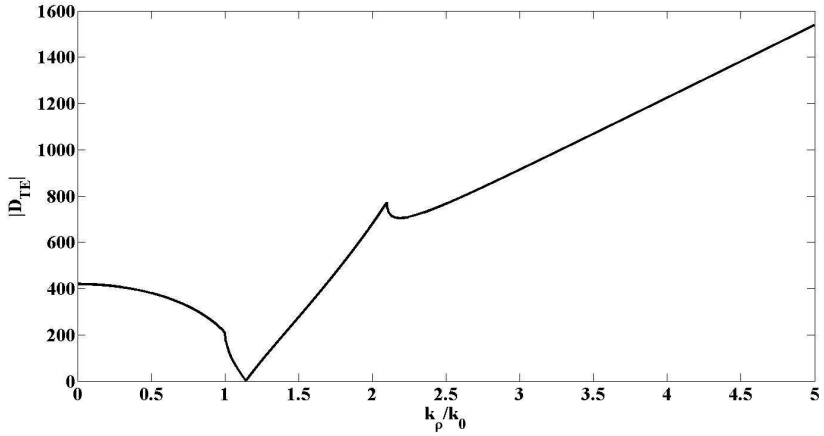

(a)

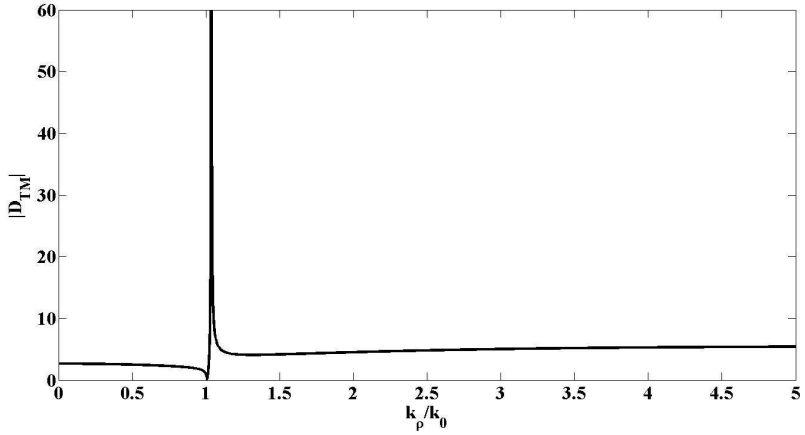

(b)

Figure 4.3: Plot of denominator terms of the integrand (a) Magnitude plot of D_{TE} vs. k_ρ/k_0 (b) Magnitude plot of D_{TM} vs. k_ρ/k_0.

4.3.1 Approximation of Vector and Scalar Potential Green's Function for a HED on an Ungrounded Dielectric Slab

Since spatial domain potential (vector and scalar) Green's function in integral form have no analytical solution, such integrals are evaluated numerically. To evaluate the integrals, the integrand needs to be examined carefully in order to locate and avoid the pole(s). Roots of the functions D_{TE} and D_{TM} appear as poles in the integrand. In Fig. 4.3 magnitude of D_{TE} and D_{TM} for HED

on an ungrounded dielectric slab is plotted as a function of normalized wave number. From Fig. 4.3, it can be observed that the term D_{TE} has one root between k_0 and $1.5k_0$, i.e., there is one pole in the integrand of spatial domain magnetic vector potential Green's function G_A^{xx}. The expression for spectral domain vector potential Green's function for very thin substrate with moderate dielectric constant can be obtained by setting $u_0 = u_1$ for the term D_{TE} in equation (4.17). In addition to this it can be noted that u_0 and u_2 are equal since both the expressions indicate free space region. Then using the integral in equation (4.21), the expression for spatial domain vector potential Green's function can be given as

$$G_A^{xx} = \frac{\mu_0}{4\pi}\frac{e^{-jk_0R_0}}{R_0} \tag{4.23}$$

where $R_0^2 = \rho^2$ and $\rho = \sqrt{(x-x_0)^2+(y-y_0)^2}$ is the radial distance between source and the observer. It can be noted that for thin substrate case, the magnetic vector potential G_A^{xx} is free space Green's function, and thus the expression become independent of the thickness and dielectric constant of the substrate. In addition to these equation (4.23) is low frequency approximation for vector potential Green's function of a HED on an ungrounded dielectric slab.

Similarly, low frequency approximation for spatial domain scalar potential Green's function by setting $u_0 = u_1$ in equation (4.22) can be obtained, which can be expressed as [42],

$$G_V = \left(K + \frac{1}{1+\varepsilon_r}\right)\left[\frac{e^{-jk_0R_0}}{R_0} - (1-K)\sum_{i=1}^{\infty} K^{2i-1}\frac{e^{-jk_0R_i}}{R_i}\right] \tag{4.24}$$

where $K = \frac{1-\varepsilon_r}{1+\varepsilon_r}$, $R_0^2 = \rho^2$ and $R_i^2 = \rho^2 + (2ih)^2$.

4.3.2 Evaluation of Numerical Integration for Spatial Domain Potential Green's Function

In the previous section, it has been observed that the term D_{TE} gives rise to a pole in the integrand of spatial domain vector potential Green's function. Since for most of the practical cases PMA has a thin substrate, hence the expression in equation (4.23) can be directly used in MPIE for carrying out the analysis. Similar expression is also derived for thin and moderate dielectric constant material in case of scalar potential Green's function in equation (4.24). Even though

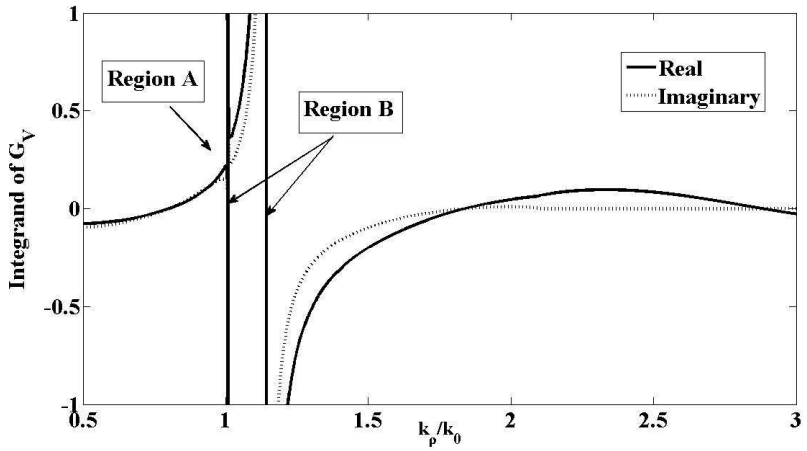

(a)

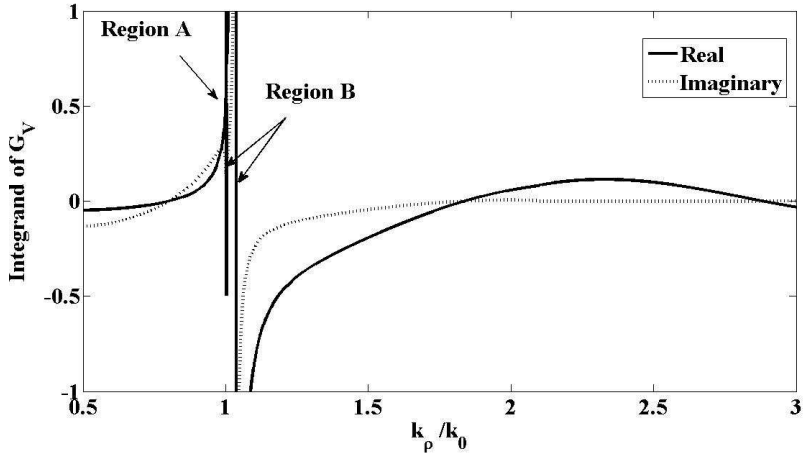

(b)

Figure 4.4: Plot of spatial domain scalar potential G_V at different frequencies (a) Variation of integrand of G_V (real and imaginary) with normalized distance k_ρ/k_0 for the parameter $\varepsilon_r = 4.4$, $h = 1.52$ mm and $k_0\rho$ = 3 at 10GHz (b) Variation of integrand of G_V (real and imaginary) with normalized distance k_ρ/k_0 for the parameter $\varepsilon_r = 4.4$, $h = 1.52$ mm and $k_0\rho$ = 3 at 5 GHz.

the substrate thickness is small, the expression in equation (4.24) depends both on thickness as well as dielectric constant. So, in order to analyze the effect of both thickness and dielectric constant of the substrate on PMA, the integrand of spatial domain scalar potential Green's function G_V has been investigated in detail followed by numerical integration. Thus, instead of

using equation (4.24) directly in MPIE, numerical integration of G_V is performed next. Fig. 4.4, shows the plot of the integrand of spatial domain scalar potential Green function G_V of a HED on an ungrounded dielectric slab at two different frequencies. For a given dielectric constant and substrate thickness, the branch cut and pole(s) are separate and distinct, which are denoted as Region A and Region B, respectively. Region A indicates the branch cut at k_0 whereas Region B comprises both of TE and TM poles. The poles which arises due to zeros of D_{TE} and D_{TM} in the denominator of the integrand G_V are denoted as TM and TE surface wave pole. The number of pole increases with the increase of surface waves. For an HED over thin ungrounded lossless dielectric slab, the pole is real and it location can be theoretically estimated by

$$\frac{k_\rho}{k_0} \approx 1 + \frac{(\varepsilon_r - 1)^{\frac{3}{2}} k_0 h}{4\varepsilon_r} \qquad for \qquad D_{TM} \tag{4.25a}$$

$$\frac{k_\rho}{k_0} \approx 1 + \frac{(\varepsilon_r - 1)^{\frac{3}{2}} k_0 h}{4} \qquad for \qquad D_{TE} \tag{4.25b}$$

Using equation (4.25), theoretically the location of TE and TM pole can be found out and they are located at $1.1k_0$ and $1.49k_0$ respectively, where as the graphical location of TE and TM pole are at $1.01k_0$ and $1.2k_0$ as shown in Fig. 4.4(a). The difference between theoretical and graphical location of both the poles depend on the choice of operating frequency. In Fig. 4.4(a) the operating frequency is 10 GHz, where the difference is quite pronounced whereas Fig. 4.4(b) shows the location of TE and TM pole obtained analytically and graphically at lower frequency of 5 GHz. It can be seen that in Fig. 4.4(b) the theoretical location of TE and TM pole are at $1.02k_0$ and $1.05k_0$ whereas graphically same is obtained at $1k_0$ and $1.04k_0$. Thus we find that at lower operating frequencies the TE and TM pole can be found more accurately by using equation (4.25). Now, the branch cut for the present case occur at $k_\rho = \pm k_0$ due to zeros of the function $u_0 = 0$. For the case of u_1, the terms in the integrand of G_V are even functions of u_1. Hence, branch cut is only considered for u_0. In addition to this it has also been observed that lowering the substrate thickness the surface wave pole and branch cut coincides in the complex plane, which makes nearly omnidirectional radiation pattern [91]. Now, to evaluate the spatial domain scalar potential Green's function G_V, branch cut at k_0 and poles singularity at $1.01k_0$ and $1.2k_0$ must be avoided which are located on k_ρ axis in order to integrate the function in a

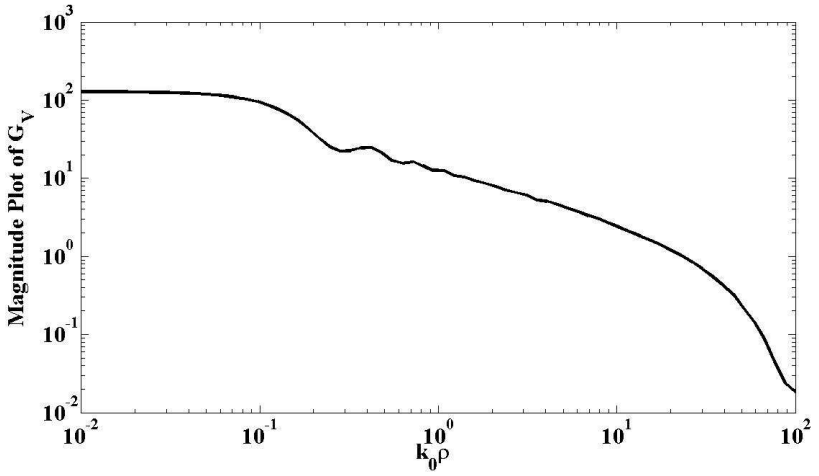

(a)

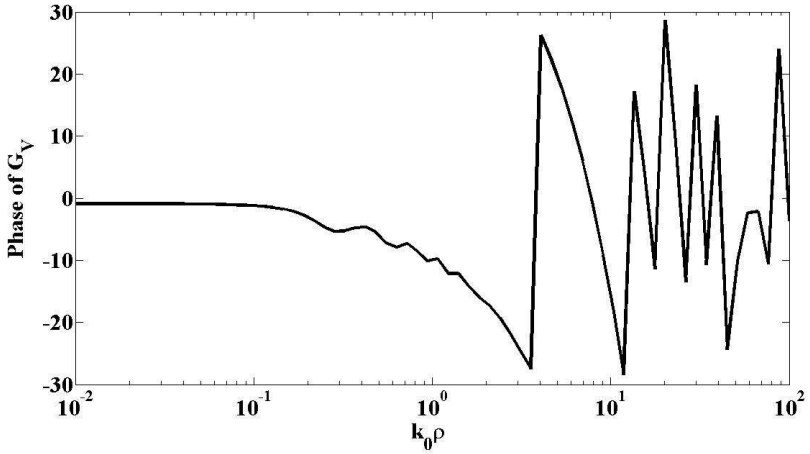

(b)

Figure 4.5: Plot of magnitude and phase of spatial domain scalar potential G_V (a) Variation of magnitude of scalar potential Green's function G_V with radial distance $k_0\rho$ of HED on ungrounded dielectric slab of dielectric constant $\varepsilon_r = 4.4$ and thickness $h = 1.52mm$ (b) Variation of phase of scalar potential Green's function G_V with radial distance $k_0\rho$ of HED on ungrounded dielectric slab of dielectric constant $\varepsilon_r = 4.4$ and thickness $h = 1.52mm$.

smooth manner. To overcome the branch cut, the integration is performed by substituting k_ρ with $k_0 cos(ht)$ in the limit $[0, k_0]$, and to avoid the poles which are located in the limit $[k_0, \infty]$ the integration is performed using [21]. The magnitude and phase variation of spatial domain scalar potential Green's function G_V with distance is shown in Fig. 4.5. The magnitude plot

of G_V in Fig. 4.5 shows the formation of near field for the initial values of the distance is of the nature $1/\rho$ whereas for the farthest value of distance, far field become more dominant of behavior $1/\sqrt{\rho}$. The transition of near field region to far field is shown by rapid variation of phase in phase plot of Fig. 4.5.

4.3.3 Effect of Substrate Thickness and Dielectric Constant on Scalar Potential Green's Function

In this section the effect of substrate material and its thickness on scalar potential Green's function G_V is considered. It can be noted from Fig. 4.6(a) that the normalized scalar potential Green's function for a HED with ungrounded dielectric slab attains far field conditions more quickly in low thickness cases compared to high thickness cases. As surface waves are trapped more in thick substrate, the radiating power is reduced. Similarly from Fig. 4.6(b), it can be concluded that though both lower and higher dielectric constant material attains far field condition in similar fashion but for larger values of dielectric constant, far field condition degrades rapidly with increased distance, because for large dielectric constant material, fields becomes highly confined within high dielectric region. Hence, it can be seen that for practical printed monopole antennas low thickness and low dielectric constant material are preferred to get maximum radiation characteristics. The issues discussed regarding the variation of scalar potential Green's function are important, since for practical PMAs, selection of the thickness and dielectric constant of the substrate are important in getting proper radiation characteristics required for specific design.

4.4 Full Wave Analysis of Printed Monopole Antenna Using MPIE MoM

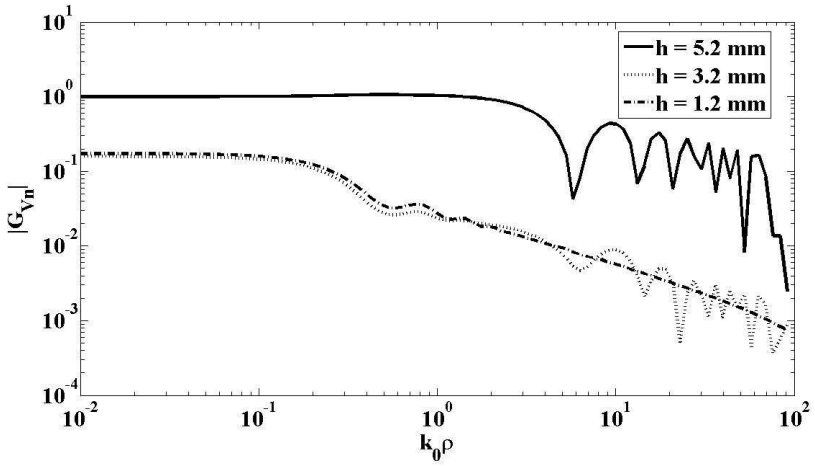

(a)

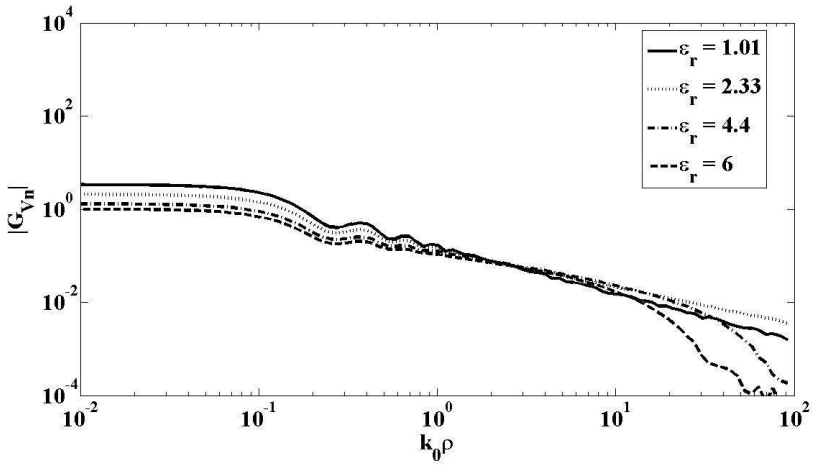

(b)

Figure 4.6: Plot of scalar potential Green's function variation with varying thickness (h) and dielectric constant (ε_r) of the substrate (a) Plot of normalized scalar potential Green function $|G_{Vn}|$ vs. radial distance of a HED on a lossless ungrounded dielectric slab with varying thickness of slab having dielectric constant $\varepsilon_r = 4.4$ (b) Plot of normalized scalar potential Green function $|G_{Vn}|$ vs. radial distance of a HED on a lossless ungrounded dielectric slab with varying dielectric constant having fixed slab thickness of $h = 1.52mm$.

In this section, the Mixed Potential Integral Equation (MPIE) which is discussed in [92–94] is solved for PMA, using the vector and scalar potential Green's function derived in equations (4.21) and (4.22). The solution is based on solving the integral equation for unknown current

and charge density using Method of Moment (MoM). Now, the MPIE can be expressed as

$$\vec{E} = j\omega \int\int G_A \cdot \vec{J}_s dS + \nabla \int\int G_V \cdot \frac{\nabla \cdot \vec{J}_s}{j\omega} dS \tag{4.26}$$

The unknown current density $\vec{J}_s$ and charge density q_s can be written as

$$\vec{J}_s = \sum_{i=1}^{N} \alpha_i \vec{T}_i(\rho) \tag{4.27}$$

$$q_s = \sum_{i=1}^{N} \alpha_i \pi_i(\rho) \tag{4.28}$$

where $\vec{T}_i(\rho)$, $\pi_i(\rho)$ are the basis function for current and charge density, and α_i are the unknown coefficients in equations (4.27) and (4.28).

The charge density basis functions can be related to current density basis function through the continuity equation which can be written as

$$\pi_i(\rho) = -\frac{\nabla \cdot \vec{T}_i(\rho)}{j\omega} \tag{4.29}$$

Here, piecewise sinusoidal subdomain function is used as current density basis function for $\vec{T}_i(\rho)$.

By applying Method of Moment to the integral equation in equation (4.26), we get a matrix equation of the form

$$[Z][\alpha] = [b] \tag{4.30}$$

where $[Z]$ is the 2×2 impedance matrix and $[\alpha]$, $[b]$ are the column matrix of unknown coefficients and known excitation voltage. Thus, the elements of the impedance matrix can be expressed as $Z_{ij} = a_{ij} + v_{ij}$, where a_{ij} represent the contribution due to vector potential $\vec{A}$ is given by $a_{ij} = j\omega \int \vec{T}_i(\rho) \cdot \int G_A \cdot \vec{T}_j(\rho) dS' dS$ whereas for scalar potential V can be written as $v_{ij} = \frac{1}{j\omega} \int \nabla \cdot \vec{T}_i(\rho) \cdot \int G_V \nabla \cdot \vec{T}_j(\rho) dS' dS$. The elements of the 2×2 impedance matrix can be explicitly written as

$$Z_{xx} = j\omega \int \vec{T}_i(x) \cdot \int G_A^{xx} \cdot \vec{T}_j(x') \, dx' dx + \frac{1}{j\omega} \int \frac{\partial}{\partial x} \cdot \vec{T}_i(x) \cdot \int G_V \frac{\partial}{\partial x'} \cdot \vec{T}_j(x') \, dx' dx \tag{4.31}$$

$$Z_{yy} = j\omega \int \vec{T}_i(y) \cdot \int G_A^{yy} \cdot \vec{T}_j(y') \, dy' dy + \frac{1}{j\omega} \int \frac{\partial}{\partial y} \cdot \vec{T}_i(y) \cdot \int G_V \frac{\partial}{\partial y'} \cdot \vec{T}_j(y') \, dy' dy \tag{4.32}$$

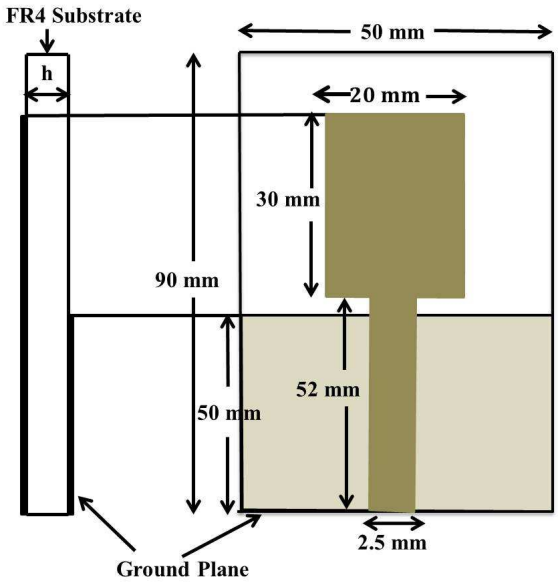

Figure 4.7: Geometry of a simple rectangular printed monopole antenna on a substrate having thickness $h = 1.52mm$ and dielectric constant $\varepsilon_r = 4.3$.

$$Z_{xy} = \frac{1}{\omega^2} \int \frac{\partial}{\partial x} \cdot \vec{T}_i(x) \cdot \int G_V \frac{\partial}{\partial y'} \cdot \vec{T}_j(y')\, dy' dx \tag{4.33}$$

$$Z_{yx} = \frac{1}{\omega^2} \int \frac{\partial}{\partial y} \cdot \vec{T}_i(y) \cdot \int G_V \frac{\partial}{\partial x'} \cdot \vec{T}_j(x')\, dx' dy \tag{4.34}$$

where $G_A^{xx} = G_A^{yy}$

Hence, using the four elements of 2×2 impedance matrix $[Z]$, equation (4.30) can be solved for unknown coefficients of α. Now as the current density becomes known, the parameter like input impedance and reflection coefficient for printed monopole antenna of given dimension can be found out easily.

4.4.1 Results and Discussion

The layout of a simple rectangular printed monopole antenna is shown in Fig. 4.7. The computed MPIE-MoM results for input impedance and reflection coefficient of printed rectangular monopole antenna are compared with HFSS results, which shows agreement as shown in Fig. 4.8 (a), (b) and Fig. 4.9. However, results shows some deviation in Fig. 4.8(a),(b) and

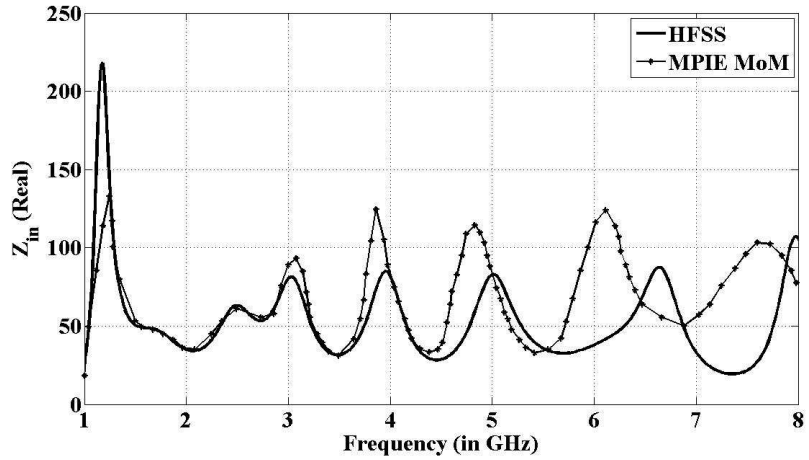

(a)

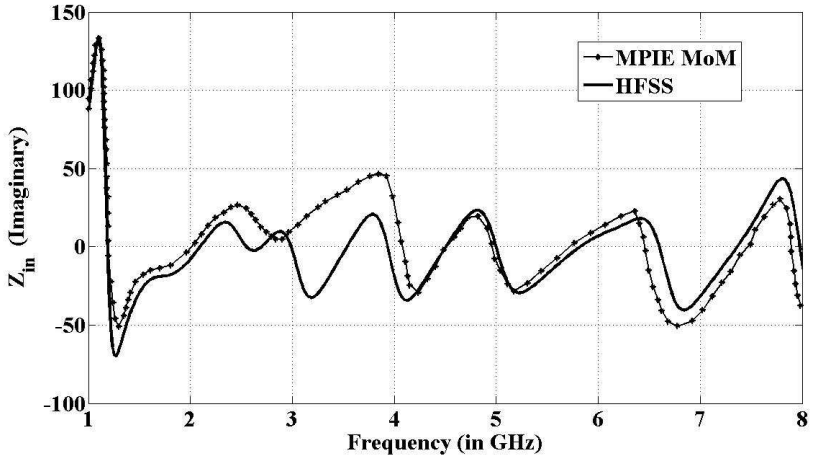

(b)

Figure 4.8: Plot of input impedance of a simple rectangular printed monopole antenna shown in Fig. 4.7 (a) Plot of input impedance (Real) in Ω of a simple rectangular PMA (b) Plot of input impedance (Imaginary) in Ω of a simple rectangular PMA.

Fig. 4.9 which may be attributed to fact that in theory, the feed gap between the patch and the ground is not being considered since in general Green's function is evaluated for patch metallization only.

The detailed geometry of F shaped PMA of [80] is depicted in Fig. 4.10, and Fig. 4.11 shows the verification of reflection coefficient of F shaped PMA using MPIE MoM and compared with

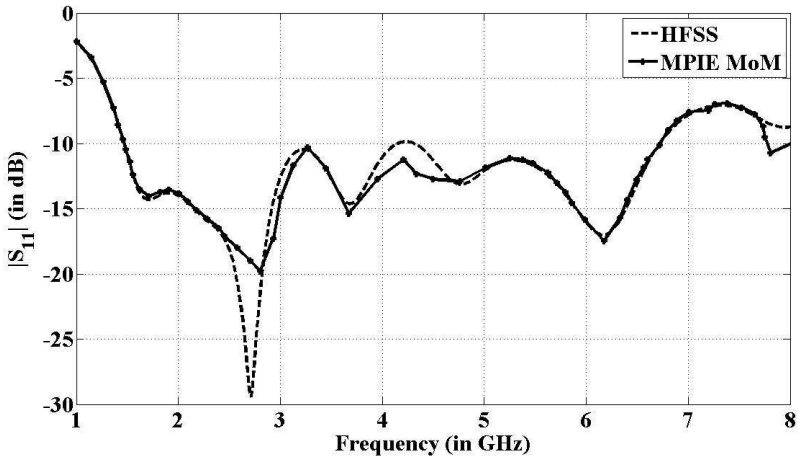

Figure 4.9: Plot of reflection coefficent of a simple rectangular printed monopole antenna shown in Fig. 4.7.

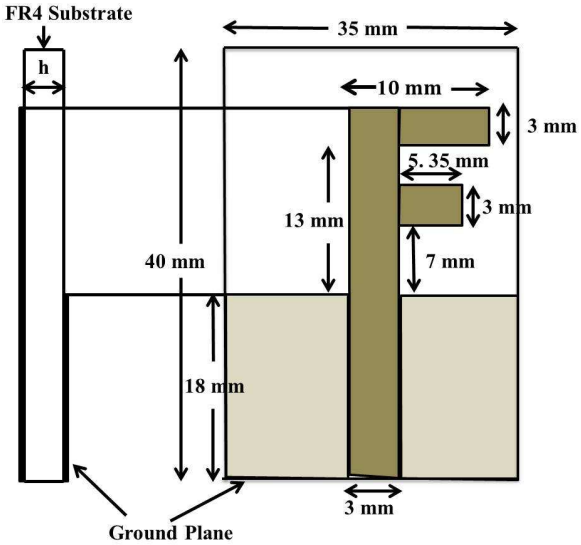

Figure 4.10: Geometry of F shaped printed monopole antenna.

HFSS and experimental results addressed in [80].

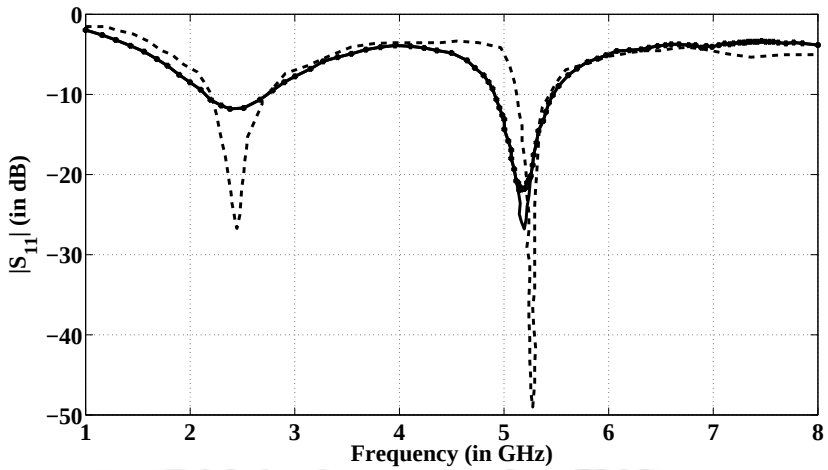

Figure 4.11: Plot of reflection coefficent theory (—•—), HFSS (—), and measured [] (– –) of a F shaped printed monopole antenna shown in Fig. 4.10.

4.5 Summary

Green's potential functions (both scalar and vector) in spectral domain are derived for horizontal electric dipole on a lossless dielectric slab which is not backed by conducting ground plane. Expressions for Green potential functions in spatial domain are derived here and are not available in existing literature. In addition to this the variation of potential Green's functions with dielectric constant and substrate thickness have also been reported here. Applying the potential Green's function to integral equation and solved using MoM based on Galerkin's method to calculate input impedance and reflection coefficient of a printed rectangular monopole antenna. The computed results using MPIE MoM are validated with simulated one using HFSS. Further, the reflection coefficient of a F shaped PMA has also been evaluated using MPIE MoM and the results are verified using both HFSS and available experimental results.

CHAPTER 5

ANALYSIS OF RADIATION CHARACTERISTICS OF PRINTED MONOPOLE ANTENNAS

5.1 Introduction

Printed monopole antenna (PMA) is considered as one of the most suitable antenna for broadband and ultra wideband applications due to its very large impedance bandwidth and omnidirectional radiation patterns. Some of the simulation and experimental works on PMAs are available in the literature [78–80, 95, 96]. However, theoretical analysis of radiation characteristics of PMAs is not adequately dealt in the literature. Microstrip excited printed monopole antenna can be considered as an asymmetrically driven dipole antenna, in which the patch and the ground plane form two arms of the dipole [97]. Since both the antenna as well as the ground plane lie on a dielectric substrate, it is necessary to derive Green's function taking the effect of the dielectric into account. To derive Green's function, the field components of an infinitesimal current source on an ungrounded dielectric layer are found using proper boundary conditions at the interfaces. Then, this analysis is further extended for calculation of the overall radiation characteristics of PMA taking into account the current distribution on the patch as well the effect of the ground plane below the feed line. Theoretical treatment of PMA along with closed form expressions for the far field radiation patterns of rectangular, circular PMA has been pre-

sented in this chapter. In our proposed method of analysis of PMA which is described in detail in the next section, the field components are determined in the spectral domain. The spectral domain field components are then used to calculate far field radiation patterns and gain for PMAs. The theoretical results of radiation patterns for rectangular and circular PMAs fed by 50 Ω microstrip line are compared with experimental data given in [95] and [79], and simulation results obtained using HFSS. In addition to this, the calculated theoretical gain is also verified by HFSS simulation results.

5.2 Theory

The radiated fields of a PMA can be formulated using Green's function of an HED lying on an ungrounded substrate and from the knowledge of current distribution on the patch as well as the ground plane below the feed line. The procedure for derivation of spectral domain electric and magnetic field Green's function has already been discussed in section 4.2.

Using the equations (4.5) and (4.6a), $\tilde{E}_x$ and $\tilde{E}_y$ at $x = h$ are given by

$$\tilde{E}_x = \frac{j}{\omega\varepsilon_0 k_\rho^2}\left[\frac{k_x^2 u_2}{D_{TM}} + \frac{k_0^2 k_y^2}{D_{TE}}\right]\tilde{J}_x \tag{5.1}$$

$$\tilde{E}_y = \frac{j}{\omega\varepsilon_0 k_\rho^2}\left[\frac{k_y k_x u_2}{D_{TM}} - \frac{k_0^2 k_y k_x}{D_{TE}}\right]\tilde{J}_x \tag{5.2}$$

Similarly, for a y directed dipole, the final expressions for $\tilde{E}_x$ and $\tilde{E}_y$ are given by

$$\tilde{E}_y = \frac{j}{\omega\varepsilon_0 k_\rho^2}\left[\frac{k_y^2 u_2}{D_{TM}} - \frac{k_0^2 k_x^2}{D_{TE}}\right]\tilde{J}_y \tag{5.3}$$

$$\tilde{E}_x = \frac{j}{\omega\varepsilon_0 k_\rho^2}\left[\frac{k_y k_x u_2}{D_{TM}} + \frac{k_0^2 k_y k_x}{D_{TE}}\right]\tilde{J}_y \tag{5.4}$$

The above expressions can be re written in matrix format as,

$$\begin{bmatrix}\tilde{E}_x \\ \tilde{E}_y\end{bmatrix} = \begin{bmatrix}\tilde{Z}_{xx} & \tilde{Z}_{xy} \\ \tilde{Z}_{yx} & \tilde{Z}_{yy}\end{bmatrix}\begin{bmatrix}\tilde{J}_x \\ \tilde{J}_y\end{bmatrix} \tag{5.5}$$

The elements of 2×2 matrix can be explicitly expressed as

$$\tilde{Z}_{xx} = \frac{j}{\omega \varepsilon_0 k_\rho^2} \left[\frac{k_x^2 u_2}{D_{TM}} - \frac{k_0^2 k_y^2}{D_{TE}} \right] \tag{5.6a}$$

$$\tilde{Z}_{yy} = \frac{j}{\omega \varepsilon_0 k_\rho^2} \left[\frac{k_y^2 u_2}{D_{TM}} - \frac{k_0^2 k_x^2}{D_{TE}} \right] \tag{5.6b}$$

$$\tilde{Z}_{xy} = \tilde{Z}_{yx} = \frac{j}{\omega \varepsilon_0 k_\rho^2} \left[\frac{k_y k_x u_2}{D_{TM}} + \frac{k_0^2 k_y k_x}{D_{TE}} \right] \tag{5.6c}$$

The far field radiation pattern of an x directed HED on an ungrounded dielectric layer in region 2 $(z > h)$ can be written as [53],

$$E_\theta = \frac{j k_0 e^{-j k_0 r}}{2\pi r} \left[\cos(\phi) \tilde{E}_x + \sin(\phi) \tilde{E}_y \right] \tag{5.7}$$

$$E_\phi = \frac{j k_0 e^{-j k_0 r}}{2\pi r} \left[-\sin(\phi) \cos(\theta) \tilde{E}_x + \cos(\phi) \cos(\theta) \tilde{E}_y \right] \tag{5.8}$$

Now, substituting equations (5.1), (5.2) in equation (5.7) and(5.8), $k_0 sin(\theta) cos(\phi)$, $k_0 sin(\theta) sin(\phi)$, $k_0 cos(\theta)$ in place of k_x, k_y and k_z we get the final far field expressions as,

$$E_\theta = \alpha_1 \frac{n(\theta) \cos(\theta) \{\varepsilon_r \cos(\theta) + j n(\theta) \tan(\beta_1 h)\}}{2\varepsilon_r n(\theta) \cos(\theta) + j \tan(\beta_1 h) \{n^2(\theta) + \varepsilon_r^2 \cos^2(\theta)\}} \tag{5.9}$$

$$E_\phi = \alpha_2 \frac{\{n(\theta) \sec(\theta) + j \tan(\beta_1 h)\}}{2n(\theta) \sec(\theta) + j \tan(\beta_1 h) \{n^2(\theta) \sec^2(\theta) + 1\}} \tag{5.10}$$

where $\alpha_1 = -\cos(\phi) \left(\frac{j\omega\mu_0}{4\pi r} \right) e^{-j k_0 r}$, $\alpha_2 = \sin(\phi) \left(\frac{j\omega\mu_0}{4\pi r} \right) e^{-j k_0 r}$, $\beta_1 = k_0 n(\theta)$ and $n(\theta) = \sqrt{\varepsilon_r - \sin^2(\theta)}$.

The theoretical gain (G) of a HED on an ungrounded dielectric layer in a given direction (θ, ϕ) can be expressed as [20],

$$G = \frac{4 \left(\sin^2\phi |E_\theta|^2 + \cos^2\phi |E_\phi|^2 \right)}{\int_0^{\frac{\pi}{2}} (\sin\theta) \left[|E_\theta|^2 + |E_\phi|^2 \right] d\theta} \tag{5.11}$$

It may be noted that the above Green's function for far field depend on both substrate thickness and dielectric constant (ε_r). Thus, the variation of thickness and dielectric material and their effects on the field as well as in the gain can be theoretically observed.

5.2.1 Derivation of Expressions for Radiated Fields of PMA

The above expressions in equations (5.9) and (5.10) give far fields of a HED on a dielectric substrate. The current supported by the feed in printed monopole antenna shown in Fig. 5.1 can be expressed in terms of incident traveling wave ($e^{-jk_0(x+f_g)}$) and reflected wave ($\Gamma e^{jk_0(x+f_g)}$) due to impedance discontinuity at the junction of feed and the patch. Note that, $x+f_g$ is the total length of the feed including feedgap (f_g) and Γ is the current reflection coefficient. Thus the net current given to PMA through the feed line can be given by [98],

$$J(x,y) = \hat{a}_x I_0 (e^{-jk_0(x+f_g)} + \Gamma e^{jk_0(x+f_g)}) \tag{5.12}$$

Hence,

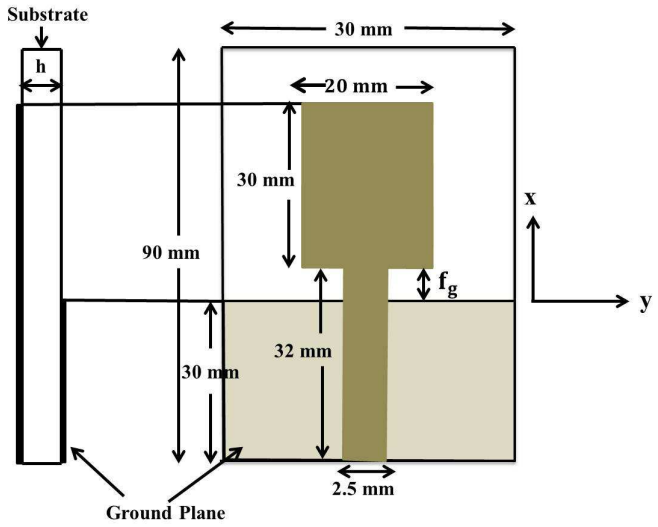

Figure 5.1: Geometry of rectangular printed monopole antenna on dielectric substrate ($\varepsilon_r = 4.3$, $tan\delta = 0.02$) of thickness $h = 1.52mm$

$$\tilde{J}(k_x,k_y) = \int_{-L/2}^{L/2} \int_{-W/2}^{W/2} J(x,y)\, e^{-j(k_x x + k_y y)} dxdy \tag{5.13}$$

So after replacing k_x and k_y by $k_0 sin(\theta) cos(\phi)$ and $k_0 sin(\theta) sin(\phi)$ and for $\Gamma = -1$, equation (5.13) can be written as,

$$\tilde{J}(\theta,\phi) = \frac{4W \sin c\,(05k_0 W \sin(\theta)\sin(\phi))\,[\sigma_1 - \sigma_2]}{\left((k_0 \sin(\theta)\cos(\phi))^2 - 1\right)} \tag{5.14}$$

where

$$\sigma_1 = 2\sin(0.5k_0 L \sin(\theta)\cos(\phi))\cos(0.5k_0 L)\left\{k_0 \cos(f_g k_0) + jk_0 \sin(\theta)\cos(\phi)\sin(f_g k_0)\right\}$$

$$\sigma_2 = 2\cos(0.5k_0 L \sin(\theta)\cos(\phi))\sin(0.5k_0 L)\left\{k_0 \sin(\theta)\cos(\phi)\cos(f_g k_0) + jk_0 \sin(f_g k_0)\right\}$$

It may be noted that current distribution in equation (5.14) includes a quadrature term. In

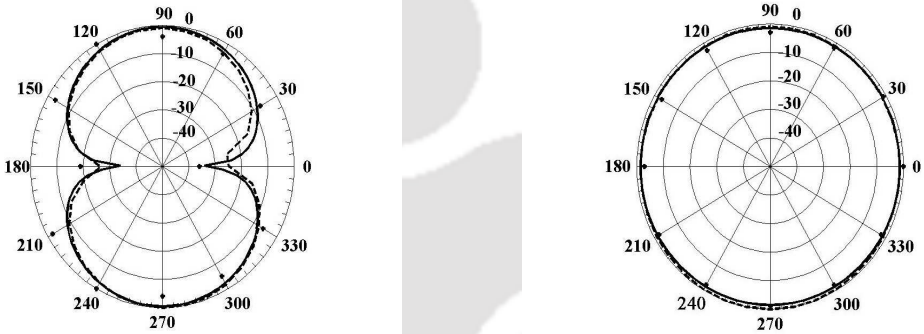

(a) $\phi = 0$ (b) $\theta = 90$

Figure 5.2: Radiation patterns of the rectangular printed monopole antenna shown in at 2.45 GHz (Theory (—), simulation using HFSS (– –) and measured (•)) .

case of printed monopole antennas, the ground plane also contributes to the radiation field. The ground plane acts as an asymmetric image of the monopole to form an asymmetrically driven dipole antenna. The current distribution in the ground plane can be given as,

$$\tilde{J_g}(\theta,\phi) = \frac{4W_g \sin c\,(05k_0 W_g \sin(\theta)\sin(\phi))\,[\sigma_{11} - \sigma_{12}]}{\left((k_0 \sin(\theta)\cos(\phi))^2 - 1\right)} \tag{5.15}$$

where

$$\sigma_{11} = 2k_0 \sin(0.5k_0 L_g \sin(\theta)\cos(\phi))\cos(0.5k_0 L_g)$$

$$\sigma_{12} = 2k_0 \cos(0.5k_0 L_g \sin(\theta)\cos(\phi))\sin(0.5k_0 L_g)\sin(\theta)\cos(\phi)$$

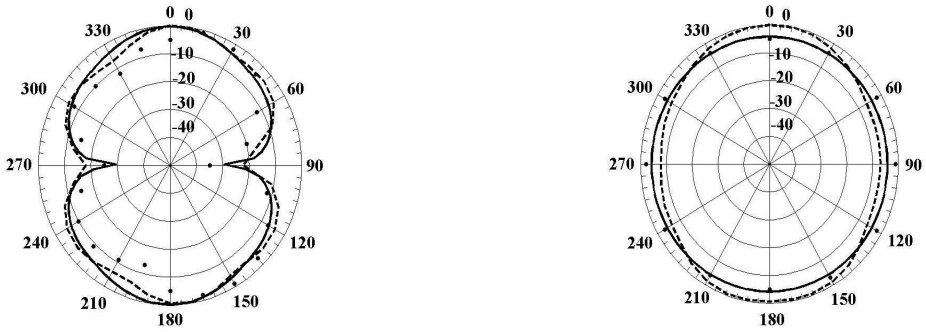

(a) $\phi = 0$ (b) $\theta = 90$

Figure 5.3: Radiation patterns of the rectangular printed monopole antenna shown in at 5.2 GHz (Theory (—), simulation using HFSS (– –) and measured (•)) .

L_g, W_g represents the length and width of the ground plane of PMA. Thus the overall radiation pattern for the rectangular printed monopole antenna, including the effect of the partial ground plane as shown in Fig. 5.1 can be written as,

$$E_{\theta pr} = \left(\frac{j\omega\mu_0}{4\pi r}\right) e^{-jk_0 r}(\widetilde{J}(\theta,\phi) + \widetilde{J_g}(\theta,\phi))E_\theta \tag{5.16}$$

$$E_{\phi pr} = \left(\frac{j\omega\mu_0}{4\pi r}\right) e^{-jk_0 r}(\widetilde{J}(\theta,\phi) + \widetilde{J_g}(\theta,\phi))E_\phi \tag{5.17}$$

The gain for the case of a rectangular printed monopole antenna can be calculated using equation (5.11). The closed form expressions for the far field radiation patterns of circular printed monopole antenna shown in Fig. 5.5, can be written as

$$E_{\theta pc} = \left(\frac{e^{-jk_0 r}}{r}\right) (\tilde{J}(\theta,\phi) + \tilde{J_g}(\theta,\phi))E_\theta \tag{5.18}$$

$$E_{\phi pc} = \left(\frac{e^{-jk_0 r}}{r}\right) (\tilde{J}(\theta,\phi) + \tilde{J_g}(\theta,\phi))E_\phi \tag{5.19}$$

For circular PMA, $\tilde{J}(\theta,\phi)$ can be written as,

$$\tilde{J}(\theta,\phi) = \int_0^{2\pi}\int_0^{a} J(a\cos(\theta), a\sin(\theta))\, e^{-j\left(k_x a\cos(\theta) + k_y a\sin(\theta)\right)} a\,da\,d\theta \tag{5.20}$$

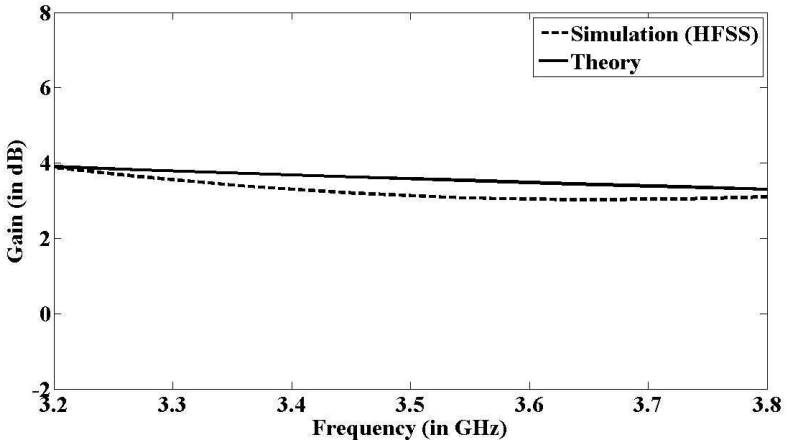

Figure 5.4: Gain of the rectangular printed monopole antenna on dielectric substrate ($\varepsilon_r = 4.3$, $tan\delta = 0.02$) of thickness $h = 1.52mm$.

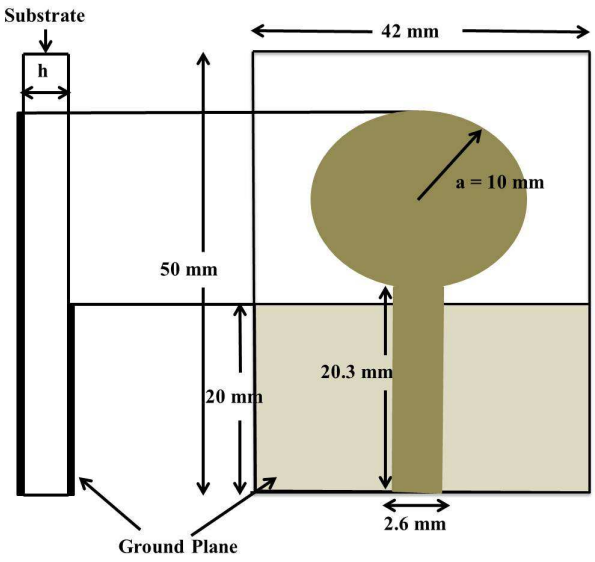

Figure 5.5: Geometry of circular printed monopole antenna on dielectric substrate ($\varepsilon_r = 4.7$, $tan\delta = 0.02$) of thickness $h = 1.5mm$

, where $k_x = k_0 sin(\theta)cos(\phi)$, $k_y = k_0 sin(\theta)sin(\phi)$ and a is the radius of the circle. Similar to rectangular PMA, the gain of circular printed monopole antenna can be found using equation (5.11).

5.3 Results

This section presents the results computed using the analytical expressions derived for the rectangular PMA and circular PMA and compares the same with the measured results available in literature [95] (for rectangular), [79] (for circular) as well with the results obtained through HFSS simulations. The radiation patterns of rectangular printed monopole antenna are shown in Fig. 5.2 and Fig. 5.3, whereas the gain plot is shown in Fig. 5.4.

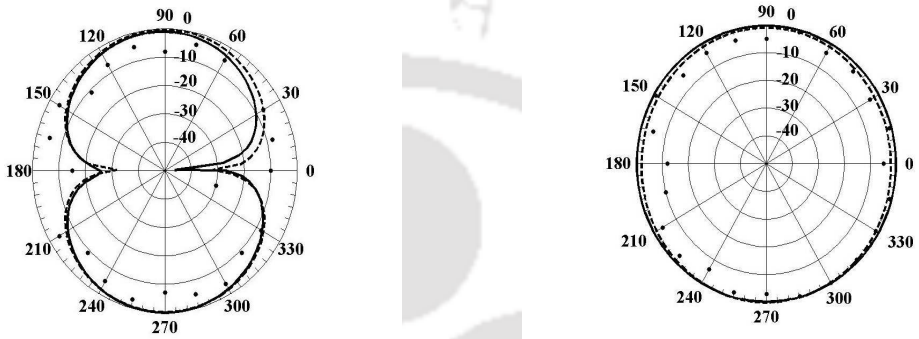

(a) E plane (b) H plane

Figure 5.6: Radiation patterns of the circular printed monopole antenna shown in Fig. 5.5 at 3 GHz (Theory (—), simulation using HFSS (– –) and measured (•)).

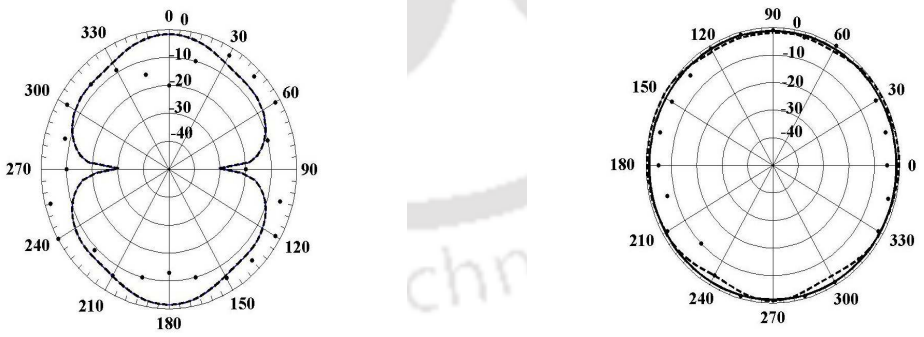

(a) E plane (b) H plane

Figure 5.7: Radiation patterns of the circular printed monopole antenna shown in Fig. 5.5 at 6.5 GHz (Theory (—), simulation using HFSS (– –) and measured (•)).

The radiation patterns of circular printed monopole antenna are shown in Fig. 5.6 and Fig. 5.7, whereas the gain plot is shown in Fig. 5.8.

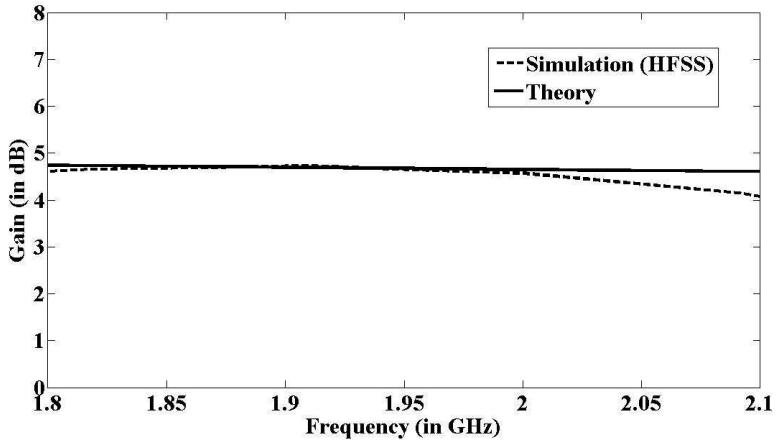

Figure 5.8: Gain of the circular printed monopole antenna on dielectric substrate ($\varepsilon_r = 4.7$, $tan\delta = 0.02$) of thickness $h = 1.5mm$.

5.4 Summary

This chapter presents the details of analytical evaluation of radiation patterns for rectangular and circular printed monopole antenna. Since the ground plane also affects the radiation characteristics of PMAs, taking the ground plane as an asymmetric image of the monopole the overall far field components of PMA are derived. Using the analytical expressions for the far field, the theoretical gain for the PMAs is computed. The theoretical results for the radiation pattern are in good agreement with HFSS simulated results and experimental results. Further, the theoretical gains of both PMAs are also verified using HFSS simulations.

CHAPTER 6

PERFORMANCE OF PRINTED MONOPOLE ANTENNA WITH MAGNETO-DIELECTRIC COVER

6.1 Introduction

As already mentioned, printed monopole antennas are suitable choices for ultrawideband (UWB) operation and for obtaining omnidirectional radiation characteristic. In general, UWB refers to an absolute bandwidth in excess of 500 MHz or percentage bandwidth more than 20 [99]. PMAs are generally fabricated on a dielectric substrate supported on a ground plane which extend upto feedline only [79], [95]. PMA design covering the UWB band (3.1 GHz-10.7 GHz) is reported in literature [79]. In order to achieve UWB operation in the 8 GHz to 18 GHz band, simple rectangular printed monopole antenna (RPMA) with a cover layer of magneto-dielectric material is proposed here. In [25], closed form expressions for far field radiation parameter has been evaluated for simple microstrip antenna by modeling the antenna as an horizontal electric dipole (HED) lying on an grounded dielectric layer. For the proposed antenna configuration, the metallic patch of PMA can be modeled as a horizontal electric dipole (HED) lying on a ungrounded dielectric layer covered by another magneto-dielectric layer, and both dielectric as well as magneto-dielectric layer can be modeled as a transmission line with characteristic impedance and propagation constant which depend on angle θ [20]. Since the characteristic impedance depends both on the substrate and the superstrate material, thus the change in radi-

ation properties of PMA with respect to variation in dielectric substrate and magneto-dielectric superstrate can be considered theoretically. Finally, theoretical results derived here for the radiation pattern of a rectangular PMA with magneto-dielectric cover fed by 50 Ω microstrip line on a dielectric substrate is compared with Ansoft High Frequency Structure Simulator (HFSS) results. In addition, return loss performance of the proposed antenna is compared with that of PMA with and without dielectric cover to demonstrate bandwidth enhancement for the proposed antenna.

6.2 Theory

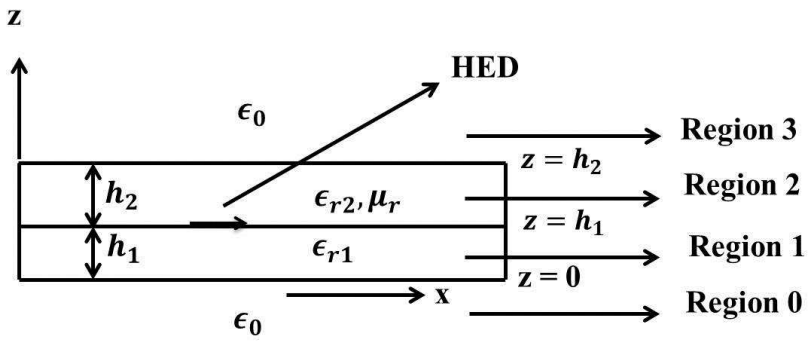

Figure 6.1: Geometry of HED along x- axis on the interface of ungrounded dielectric and magneto-dielectric cover.

Horizontal electric dipole (HED) lying at the interface of dielectric substrate and magneto-dielectric superstrate, and the substrate is backed by free space rather than metallic ground plane as shown in Fig. 6.1. Jackson et.al. [20] proposed that electric field along x direction at the interface ($z = h$) due to a far distant source either in θ or ϕ direction, by reciprocity theorem, will be equivalent to far field E_θ or E_ϕ due to HED at the interface. Thus, the substrate and the superstrate layer can be modelled as transmission line having length equal to thickness of the substrate and the superstrate respectively. In addition to this, characteristic impedance and propagation constant are θ dependent. Thus, the far field expression for a PMA covered by

a magneto-dielectric superstrate can be derived [20] as

$$E_\theta = -\cos(\phi)\left(\frac{j\omega\mu_0}{4\pi r}\right)e^{-jk_0 r}\tilde{J}(\theta,\phi)\frac{2\cos(\theta)(A+jB)}{(C+jD)} \tag{6.1}$$

$$E_\phi = \sin(\phi)\left(\frac{j\omega\mu_0}{4\pi r}\right)e^{-jk_0 r}\tilde{J}(\theta,\phi)\frac{2\cos(\theta)(A_1+jB_1)}{(C_1+jD_1)} \tag{6.2}$$

where $\widetilde{J}(\theta,\phi)$ can be written as given in [54]

$$\tilde{J}(\theta,\phi) = \frac{V_0}{Z_0}\frac{(2\pi/L)\cos(0.5k_0 L\sin(\theta)\cos(\phi))}{(\pi/L)^2-\left(k_0^2\sin^2(\theta)\cos^2(\phi)\right)} \times \sin c(0.5k_0 W\sin(\theta)\sin(\phi))$$

and

$$A = \cos(\theta)\left(1-\frac{\varepsilon_{r1}n_2(\theta)}{\varepsilon_{r2}n_1(\theta)}\tan(\beta_1 h_1)\tan(\beta_2 h_2)\right)$$

$$B = \frac{n_1(\theta)\tan(\beta_1 h_1)}{\varepsilon_{r1}}+\frac{n_2(\theta)\tan(\beta_2 h_2)}{\varepsilon_{r2}}$$

$$C = 1+\cos(\theta)-\tan(\beta_1 h_1)\tan(\beta_2 h_2)\left(\frac{\varepsilon_{r1}n_2(\theta)}{\varepsilon_{r2}n_1(\theta)}+\frac{\varepsilon_{r2}n_1(\theta)}{\varepsilon_{r1}n_2(\theta)}\cos(\theta)\right)$$

$$D = \left(\frac{n_1(\theta)\tan(\beta_1 h_1)}{\varepsilon_{r1}}+\frac{n_2(\theta)\tan(\beta_2 h_2)}{\varepsilon_{r2}}\right)+\cos^2(\theta)\left(\frac{\varepsilon_{r2}\tan(\beta_2 h_2)}{n_2(\theta)}+\frac{\varepsilon_{r1}\tan(\beta_1 h_1)}{n_1(\theta)}\right)$$

$$A_1 = \cos(\theta)\left(1-\frac{\mu_{r2}n_1(\theta)}{\mu_{r1}n_2(\theta)}\tan(\beta_1 h_1)\tan(\beta_2 h_2)\right)$$

$$B_1 = \frac{\mu_{r1}\tan(\beta_1 h_1)}{n_1(\theta)}+\frac{\mu_{r2}\tan(\beta_2 h_2)}{n_2(\theta)}$$

$$C_1 = 1+\cos(\theta)-\tan(\beta_1 h_1)\tan(\beta_2 h_2)\times\left(\frac{\mu_{r1}n_2(\theta)}{\mu_{r2}n_1(\theta)}+\frac{\mu_{r2}n_1(\theta)}{\mu_{r1}n_2(\theta)}\cos(\theta)\right)$$

$$D_1 = \left(\frac{n_1(\theta)\tan(\beta_1 h_1)}{\mu_{r1}}+\frac{n_2(\theta)\tan(\beta_2 h_2)}{\mu_{r2}}\right)+\cos^2(\theta)\left(\frac{\mu_{r1}\tan(\beta_1 h_1)}{n_1(\theta)}+\frac{\mu_{r2}\tan(\beta_2 h_2)}{n_2(\theta)}\right)$$

where $n_1(\theta)$, $n_2(\theta)$ are the effective refractive index which depend on angle θ equal to $\sqrt{\varepsilon_{r1}\mu_{r1}-\sin^2(\theta)}$ and $\sqrt{\varepsilon_{r2}\mu_{r2}-\sin^2(\theta)}$ respectively, propagation constant $\beta_1 = k_0 n_1(\theta)$ and $\beta_2 = k_0 n_2(\theta)$.

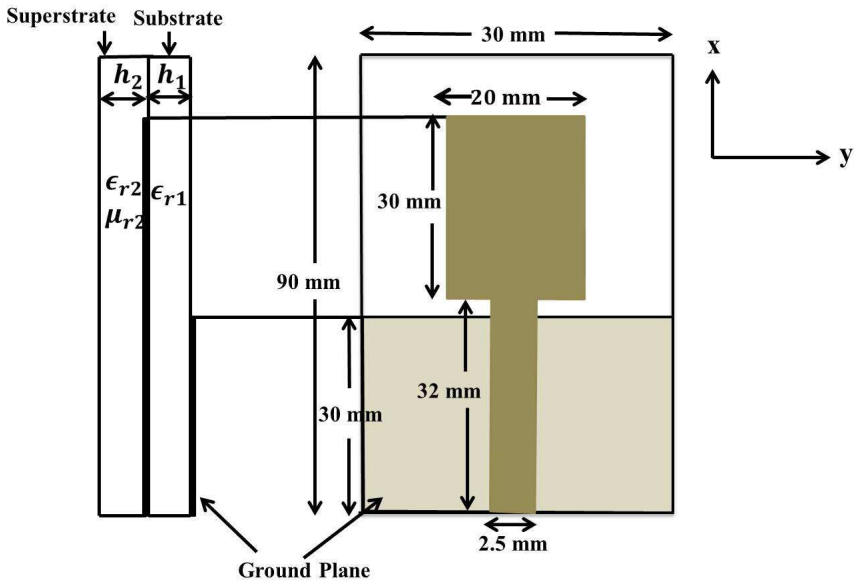

Figure 6.2: Geometry of rectangular printed monopole antenna on dielectric substrate ($\varepsilon_{r1} = 4.3$, $\mu_{r1} = 1$, $tan\delta_e = 0.02$) of thickness $h_1 = 1.52mm$ cover by magneto-dielectric superstrate ($\varepsilon_{r2} = 3$, $\mu_{r2} = 1.5$, $tan\delta_e = 0.02$, $tan\delta_m = 0.02$) of thickness $h_2 = 4mm$.

6.3 Results

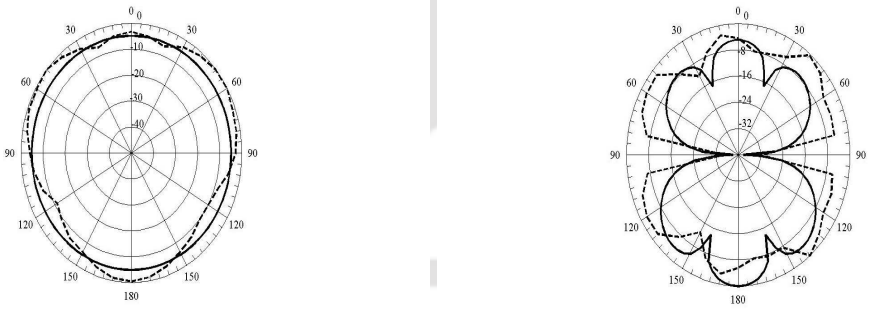

(a) X-Y plane (b) X-Z plane

Figure 6.3: Radiation patterns of rectangular printed monopole antenna with magneto-dielectric cover at 13 GHz (Theory (—), simulation using HFSS (– –)).

In order to show the validity of the proposed method, the theoretical results are compared with results simulated using HFSS. A simple rectangular printed monopole antenna fed by a 50 Ω transmission line covered with magneto-dielectric substrate is shown in Fig. 6.2. In Fig. 6.4,

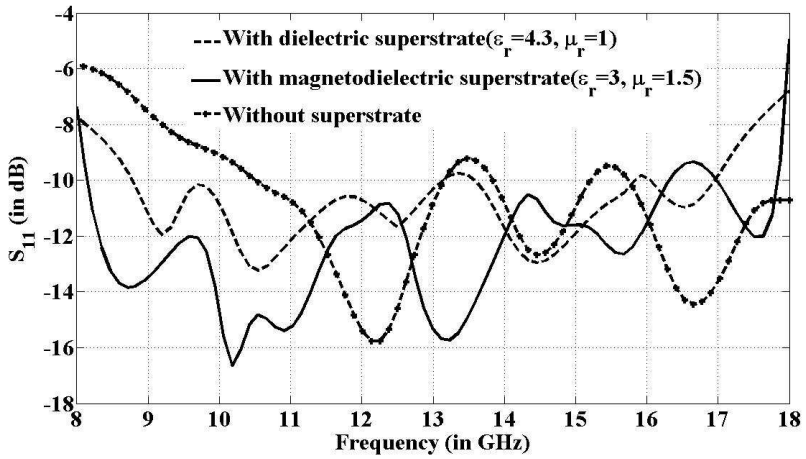

Figure 6.4: Simulation results (HFSS) for reflection coefficient of rectangular printed monopole antenna as shown in Fig. 6.2 for magneto-dielectric cover, dielectric cover and without cover

the comparison of reflection coefficient of printed rectangular monopole antenna with cover (magneto-dielectric and dielectric) and without cover is shown, whereas Fig. 6.3 shows the radiation plot of rectangular PMA with magneto-dielectric superstrate. Fig. 6.3(a) and Fig. 6.3(b) are the radiation plots in both the plane for rectangular PMA with magneto-dielectric cover whereas Fig. 6.4, shows the reflection coefficient of the same with dielectric, magneto-dielectric cover and without any cover, in which huge 8.1 GHz bandwidth is achieved with magnetodielectric cover in comparison to both dielectric cover and without cover.

6.4 Summary

The present chapter focusses on performance of a rectangular printed monopole antenna cover by a magneto-dielectric substrate. Using transmission line analogies, closed form expression for far field radiation pattern are theoretically derived and they are validated by HFSS. Some mismatch is observed between theory and simulation (HFSS) which can be attributed to fact that in theory the feed gap between the patch and the ground is not taken into consideration and the effect of ground plane is also neglected. PMA with magneto-dielectric cover is found to offer larger bandwidth as compared to PMA with dielectric cover or PMA without any cover.

CHAPTER 7

PERFORMANCE OF PRINTED MONOPOLE ANTENNA ON UNIAXIAL SUBSTRATE

7.1 Introduction

Spectral domain immittance approach is used to analyze multilayered microstrip structures. As mentioned earlier, Itoh et. al. [26], first proposed the immittance approach based analysis for dispersion characteristics of printed transmission lines. In general, patch portion of the microstrip structure is considered as an equivalent current source or a horizontal electric dipole (HED) to calculate Green's function. Similarly the metallic patch of printed monopole antenna (PMA) can be considered as HED with the difference that the ground plane below the patch is removed. However, in case of PMA, ground plane below the feed line is also a part of the radiator to form an asymmetric dipole antenna. Thus, immittance approach offers electric field formulation by avoiding the calculation of the coefficients of the field components from the boundary conditions at each interfaces. In earlier cases, studies of PMA is primarily done using dielectric substrate, but here the performance of the same is performed with uniaxial substrate and on the same note the PMA is also analyzed using immittance approach which was earlier used mainly for the analysis of microstrip antennas. In the following sections of the present chapter, theoretical analysis of rectangular PMA on uniaxial substrate using immittance approach is presented and validation of the analytical results using HFSS is performed in the results section. The simulation for the return loss of rectangular PMA on uniaxial substrate is also performed by High Frequency Structure Simulator (HFSS). It may be mentioned here that

the performance of microstrip antenna on uniaxial substrate has been reported in literature [33], but such studies for PMA is not available in literature.

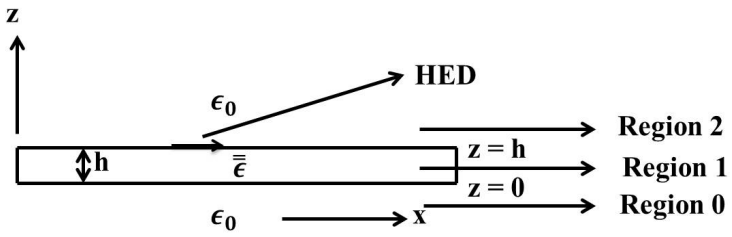

Figure 7.1: Geometry of HED along x- axis on the interface of dielectric and free space.

7.2 Theory

The uniaxial dielectric can be characterized using a permittivity tensor in the form

$$\bar{\bar{\varepsilon}} = \begin{bmatrix} \varepsilon_x & 0 & 0 \\ 0 & \varepsilon_x & 0 \\ 0 & 0 & \varepsilon_z \end{bmatrix} \tag{7.1}$$

In general, uniaxial dielectric can be subdivided into two groups in terms of Axial Ratio (AR) which is basically ratio of $\varepsilon_z/\varepsilon_x$. If, $\varepsilon_z/\varepsilon_x < 1$ then it is negative uniaxial and for $\varepsilon_z/\varepsilon_x > 1$ it is positive uniaxial [33].

To derive spectral domain Green's function, an HED lying on a ungrounded uniaxial dielectric layer is considered first since the ground plane under the patch is not present for PMAs as shown in Fig. 7.1. The spectral domain field components of a HED on lossless ungrounded uniaxial dielectric can be expressed in matrix form as,

$$\begin{bmatrix} \tilde{E}_x \\ \tilde{E}_y \end{bmatrix} = \begin{bmatrix} \tilde{Z}_{xx} & \tilde{Z}_{xy} \\ \tilde{Z}_{yx} & \tilde{Z}_{yy} \end{bmatrix} \begin{bmatrix} \tilde{J}_x \\ \tilde{J}_y \end{bmatrix} \tag{7.2}$$

Now the above matrix equation in (7.2), can be explicitly written using [26] as,

$$\tilde{E}_x = -\frac{1}{\alpha^2+\beta^2}\left(\alpha^2\tilde{Z}_e+\beta^2\tilde{Z}_h\right)\tilde{J}_x - \frac{\alpha\beta}{\alpha^2+\beta^2}\left(\tilde{Z}_e-\tilde{Z}_h\right)\tilde{J}_y \tag{7.3}$$

$$\tilde{E}_y = -\frac{1}{\alpha^2+\beta^2}\left(\beta^2\tilde{Z}_e+\alpha^2\tilde{Z}_h\right)\tilde{J}_x - \frac{\alpha\beta}{\alpha^2+\beta^2}\left(\tilde{Z}_e-\tilde{Z}_h\right)\tilde{J}_y \tag{7.4}$$

where $\alpha = jk_x$ and $\beta = jk_y$.

The terms $\tilde{Z}_e$, $\tilde{Z}_h$ in equation (7.3) and (7.4) are corresponding Green's function for TM and TE waves. $\tilde{Z}_e$, $\tilde{Z}_h$ are identified as inverse of wave admittances observed from HED located at the interface of free space and ungrounded dielectric. The expressions related to $\tilde{Z}_e$, $\tilde{Z}_h$ can be given by [100],

$$\tilde{Z}_e = \frac{1}{j\omega\left\{\frac{1}{u_2}+\frac{\varepsilon_x(u_a+\varepsilon_x u_0\tanh(u_a h))}{u_a(u_0\varepsilon_x+u_a\tanh(u_a h))}\right\}} \tag{7.5}$$

$$\tilde{Z}_h = \frac{j\omega}{\left\{u_0+\frac{u_b(u_0+u_b\tanh(u_b h))}{(u_b+u_0\tanh(u_b h))}\right\}} \tag{7.6}$$

where $u_0 = u_2 = \sqrt{\alpha^2+\beta^2-k_0^2}$, $u_a = \sqrt{\frac{\varepsilon_x}{\varepsilon_z}(\alpha^2+\beta^2)-\varepsilon_x k_0^2}$ and $u_b = \sqrt{\alpha^2+\beta^2-\varepsilon_x k_0^2}$.

The far field radiation pattern of a HED on an ungrounded uniaxial dielectric layer in air $(z > h)$ can be written as [53],

$$E_\theta = \frac{e^{-jk_0 r}}{2\pi r}\left[\cos(\phi)\tilde{E}_x+\sin(\phi)\tilde{E}_y\right] \tag{7.7}$$

$$E_\phi = \frac{e^{-jk_0 r}}{2\pi r}\left[-\sin(\phi)\cos(\theta)\tilde{E}_x+\cos(\phi)\cos(\theta)\tilde{E}_y\right] \tag{7.8}$$

The directivity of given antenna can be given as,

$$D = \frac{\frac{r^2}{2\eta_0}\left(|E_\theta|^2+\left|E_\phi\right|^2\right)|_{\theta=0}}{\frac{1}{2\eta_0}\int_0^{2\pi}\int_0^{\frac{\pi}{2}}\left(|E_\theta|^2+\left|E_\phi\right|^2\right)r^2\sin(\theta)\,d\theta\,d\phi} \tag{7.9}$$

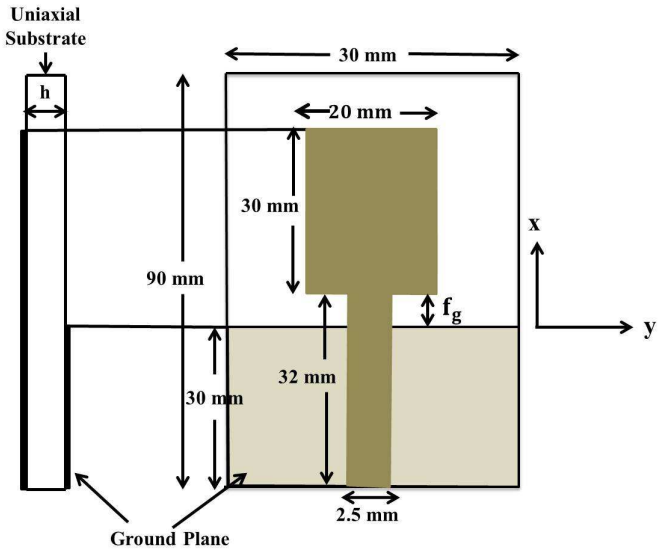

Figure 7.2: Geometry of printed rectangular monopole antenna on uniaxial substrate of thickness h = 1.5*mm*.

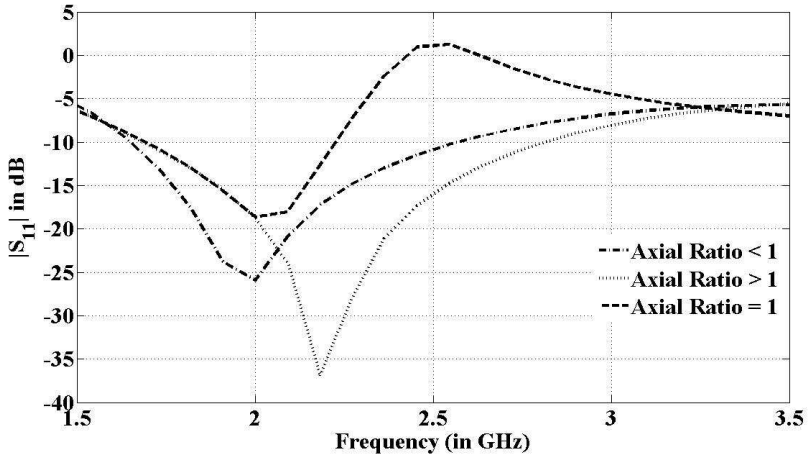

Figure 7.3: Comparison of reflection coefficient using positive uniaxial substrate ($\varepsilon_x = 1.2$, $\varepsilon_z = 2.1$), negative uniaxial substrate ($\varepsilon_x = 2.1$, $\varepsilon_z = 1.2$) and dielectric substrate ($\varepsilon_r = 2.2$) on a simple rectangular printed monopole antenna shown in Fig. 7.2.

7.3 Results

The geometry of simple rectangular PMA fed by 50 Ω microstrip line on an uniaxial substrate of thickness 1.5 mm is shown in Fig. 7.2. Here, we consider both positive as well as negative

uniaxial substrate cases, for negative uniaxial the values of the matrix in equation (7.1) are $\varepsilon_x = 2.1$, $\varepsilon_z = 1.2$ and for positive uniaxial $\varepsilon_x = 1.2$, $\varepsilon_z = 2.1$. The axial ratio (AR) becomes 1 for simple dielectric. It can be noted from Fig. 7.3 that uniaxial substrate offers greater

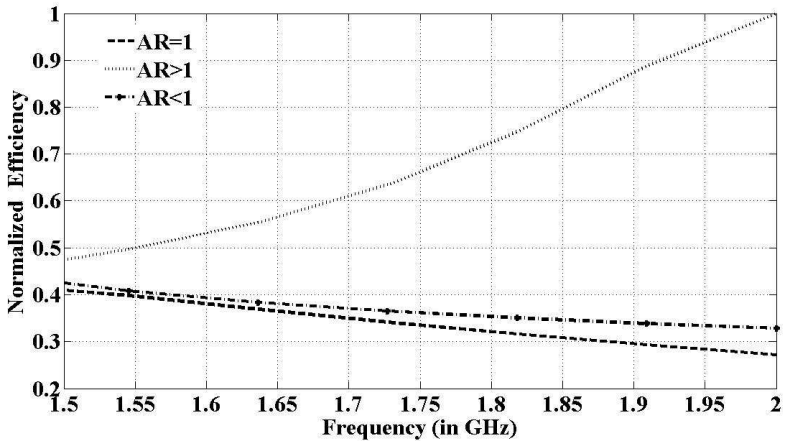

Figure 7.4: Comparison of efficiency using positive uniaxial substrate ($\varepsilon_x = 1.2$, $\varepsilon_z = 2.1$), negative uniaxial substrate ($\varepsilon_x = 2.1$, $\varepsilon_z = 1.2$) and dielectric substrate ($\varepsilon_r = 2.2$) on a simple rectangular printed monopole antenna shown in Fig. 7.2.

(a) $\phi = 0$ (b) $\theta = 90$

Figure 7.5: Theory (—) and simulation using HFSS (– –) for the radiation patterns of printed rectangular monopole antenna shown in Fig. 7.2 using positive uniaxial substrate at 1.7 GHz.

bandwidth compared to simple dielectric one. From Fig. 7.4 it can be be seen that the efficiency increases in the given band with increase in frequency for positive uniaxial substrate. But within the same range of frequency for negative uniaxial and dielectric substrate efficiency degrades. In dielectric case efficiency is much worse compared to negative uniaxial. The comparison

(a) $\phi = 0$ (b) $\theta = 90$

Figure 7.6: Theory (—) and simulation using HFSS (– –) for the radiation patterns of printed rectangular monopole antenna on shown in Fig. 7.2 using positive uniaxial substrate at 2.1 GHz.

of theoretical and simulation (HFSS) results for the radiation pattern of rectangular PMA on positive uniaxial substrate are shown in Fig. 7.5 and Fig. 7.6.

From Fig. 7.7 and Fig. 7.8, it can be concluded that PMA with positive uniaxial substrate offers greater directivity compared to negative uniaxial one. In other words, gain of PMA with positive uniaxial substrate is greater than negative uniaxial substrate since directivity is directly proportional to gain.

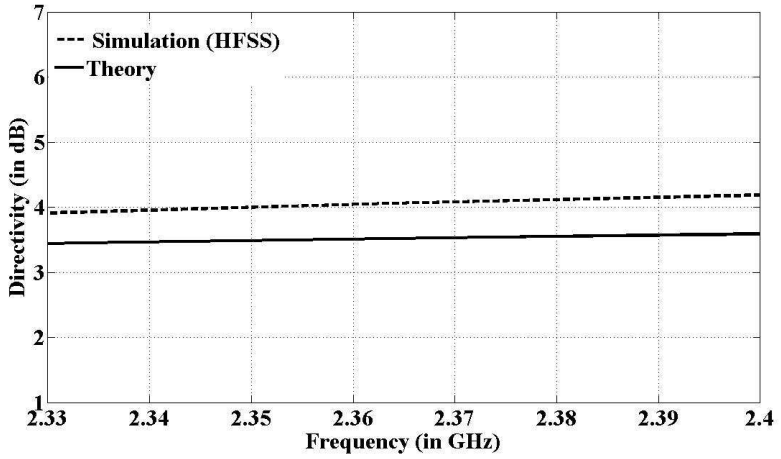

Figure 7.7: Plot of directivity of a simple rectangular printed monopole antenna on positive uniaxial substrate ($\varepsilon_x = 1.2$, $\varepsilon_z = 2.1$) shown in Fig. 7.2.

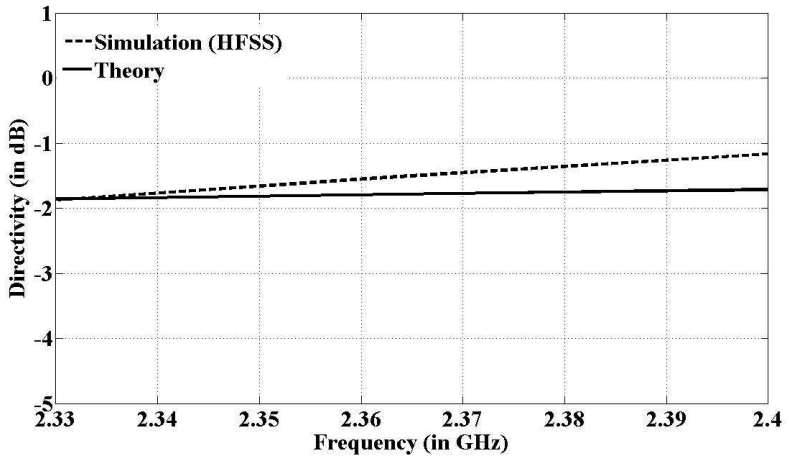

Figure 7.8: Plot of directivity of a simple rectangular printed monopole antenna on negative uniaxial substrate ($\varepsilon_x = 2.1$, $\varepsilon_z = 1.2$) shown in Fig. 7.2.

7.4 Summary

In this chapter spectral domain immittance approach is used to derive Green's function for horizontal electric dipole which lies on a uniaxial dielectric layer not backed by metallic ground plane. Expressions for far field Green functions for the same are derived here. The derived far field Green's function are utilized to calculate the radiation pattern for rectangular printed monopole antenna lying on a uniaxial substrate. From the results presented it can be seen that the uniaxial substrate performs better in comparison to dielectric substrate in terms of bandwidth, efficiency and directivity for PMAs. Among both type of uniaxial substrate, positive uniaxial substrate is better compared to negative one. Further, the theoretical results for the radiation pattern as well as directivity are in good agreement with simulated ones obtained using HFSS.

CHAPTER 8

CIRCUIT REPRESENTATION OF DIFFERENT PRINTED MONOPOLE ANTENNAS

8.1 Introduction

PMAs are preferred for UWB applications and some of the PMAs used as ultrawideband (UWB) antennas are available in [78, 79, 95]. Ammann et. al. in [101], give optimum size of the antenna as well as ground plane for proper radiation characteristics of PMA. Impedance should be matched properly between the feedline and the antenna in order to achieve proper radiation characteristics. Radiation pattern is almost independent of the frequency near the first resonance, but the same become strongly frequency dependent as the radiation pattern changes rapidly for next higher order resonances [102]. Circuit representation of a lossy one port device, for example antenna, can be represented in first canonical form of Foster [103], which consists of series inductance and capacitance with parallel R, L, C circuit. In case of printed antennas particularly for microstrip antenna the series capacitance is the static capacitance which arises due to patch and the ground plane, inductance represents contribution of different higher order modes which arises due to step impedance discontinuity at the junction of the feedline and the patch, the parallel R, L, C circuit represents particular radiating mode(s) only. In [102], ultra-wideband (UWB) antennas is represented in first canonical form of Foster. Printed monopole antenna with ground slot is presented in equivalent circuit form is given in [104]. But both of the two previous literatures didn't present the lumped element values of resistance, inductance and capacitances for the overall structures. Here, we presents the equivalent circuit of different

PMA cases with slight modification in existing form of equivalent circuits. Unlike microstrip antenna, PMA is devoid of ground plane below the patch so the static capacitance in series can be neglected. Thus a single inductance in series with parallel R, L, C circuit is enough to represent such antennas. In addition to this, each of the values of different elements such as resistance, inductance and capacitance for different PMA cases are presented in tabular form. The theoretical results for the different cases are then compared with simulation using High Frequency Structure Simulator(HFSS) and available experimental results.

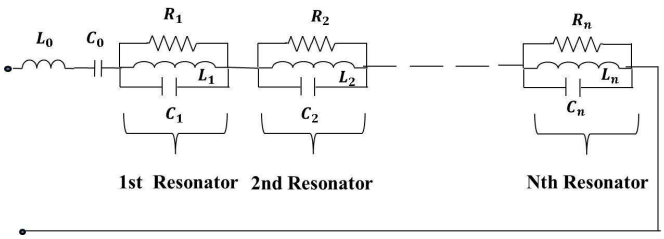

Figure 8.1: Equivalent circuit of multiple resonant antenna in first canonical form of Foster

8.2 Analysis of Antenna

Antennas operating in multiple resonating frequency are generally represented in first canonical form of Foster as shown in Fig. 8.1. The overall impedance of the above network can be given explicitly given as

$$Z_{in} = j\left(\omega L_0 - \frac{1}{\omega C_0}\right) + \sum_{n=1}^{N}\left(\frac{\omega^2 {L_n}^2 R_n}{\left(R_n - \omega^2 R_n L_n C_n\right)^2 + \omega^2 {L_n}^2} + j\frac{\omega {R_n}^2 L_n\left(1 - \omega^2 L_n C_n\right)}{\left(R_n - \omega^2 R_n L_n C_n\right)^2 + \omega^2 {L_n}^2}\right) \tag{8.1}$$

It may be noted from equation (8.1) that both real and the imaginary parts of the input impedance are varying with frequency.

For printed monopole antenna, the equivalent circuit as shown in Fig. 8.1 can be used with the modification that C_0 is not included in the equivalent circuit. In the following sections of the chapter different printed monopole antenna cases with their different circuit parameter values and their validation with simulation (in HFSS) and available experimental results are presented.

8.2.1 Case I: Printed Strip Monopole Antenna

A printed strip monopole antenna considered here is shown in Fig. 8.2. The circuit represen-

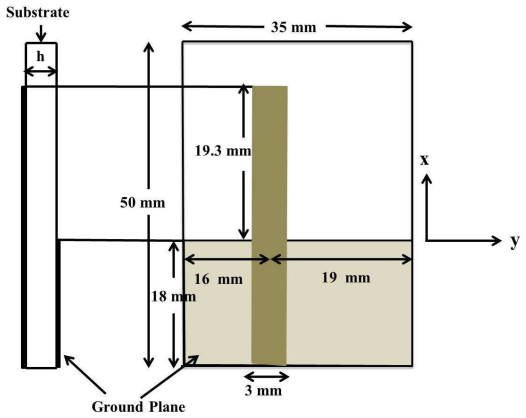

Figure 8.2: Geometry of printed strip monopole antenna on FR4 substrate having thickness 1.6 mm

tation of the printed strip monopole antenna is shown in Fig. 8.3. The different values of the

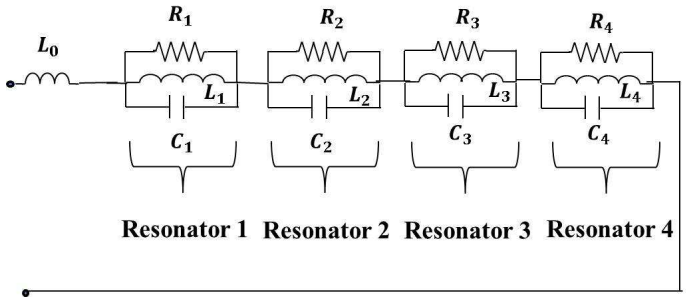

Figure 8.3: Circuit representation of strip printed monopole antenna

resistance, inductance and capacitance corresponding to strip printed monopole antenna are given below in Table. 8.1. The return loss for printed strip monopole antenna is shown in Fig. 8.4, whereas real and imaginary impedance are shown in Fig. 8.5 and Fig. 8.6 respectively. The number of resonator chosen for a given antenna is depend on the number of zero crossing in the imaginary impedance plot. In Fig. 8.6, it can be observed that the number of zero crossing is four. But on the same note, the radiation would be proper on the frequency band in which

Table. 8.1: Lumped element values of strip printed monopole antenna

Z_{in}	Z_0	Z_1	Z_2	Z_3	Z_4
R_n		79.49	195.94	49.63	28.77
L_n	0.178 nH	0.190 nH	1.3 nH	0.189 nH	0.226 nH
C_n		21.4 pF	1.1 pF	2 pF	0.528 pF

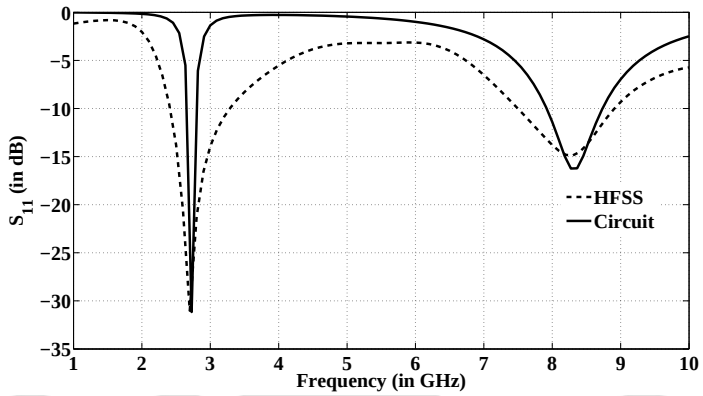

Figure 8.4: Return loss of printed strip monopole antenna

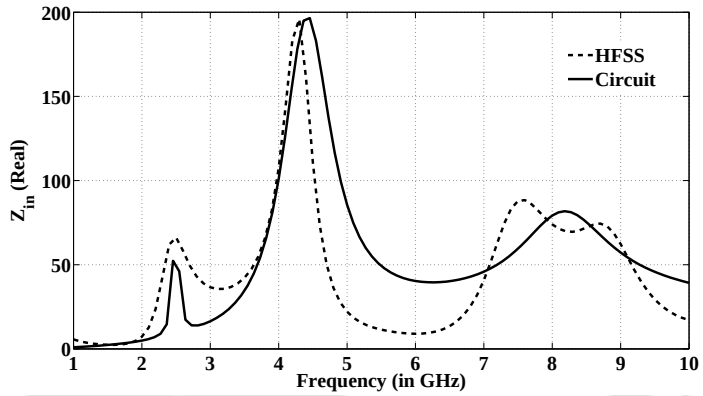

Figure 8.5: Real part of input impedance of printed strip monopole antenna

reactance is zero or very low and resistance part is 50 Ω or near by 50 Ω. Antenna depicts in Fig. 8.2 shows good impedance matching near about 2.8 GHz and 8.1 GHz. The value of real part of the impedance i.e. resistance, can be obtained directly from the real impedance plot. In order to obtain the value of imaginary part of the impedance one can use equation $X_L = \omega L$ or $X_C = 1/\omega C$ to get inductive or capacitive values.

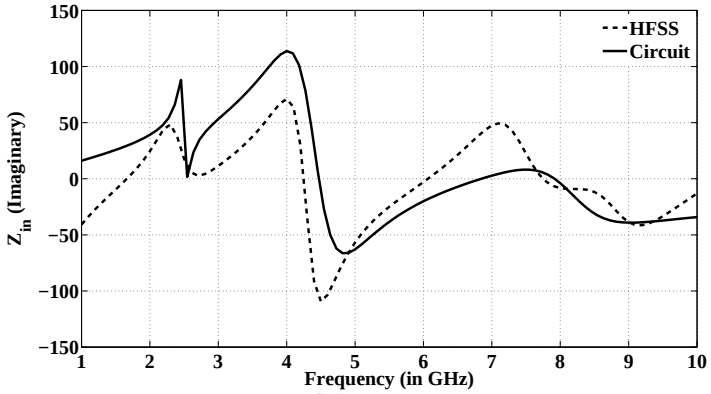

Figure 8.6: Imaginary part of input impedance of strip printed monopole antenna

8.2.2 Case II: Rectangular Printed Monopole Antenna

The geometry of rectangular PMA considered in [95], is shown in Fig. 8.7 and it is being tested through circuit approach and validated by simulation in HFSS. In Fig. 8.8, return loss for

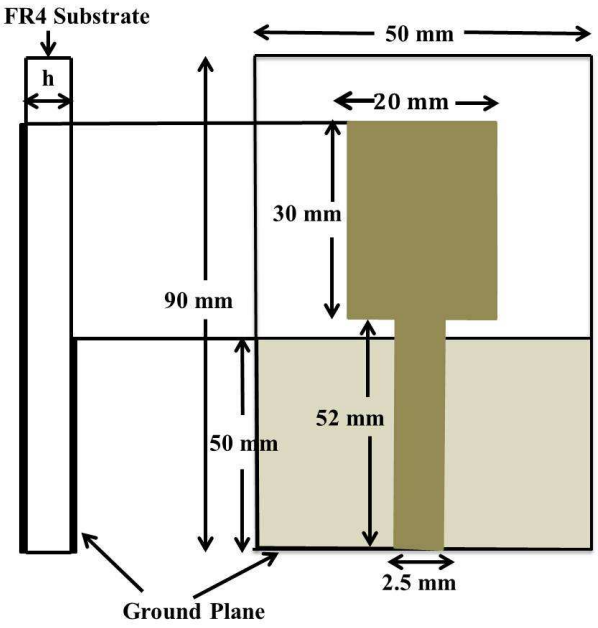

Figure 8.7: Geometry of rectangular printed monopole antenna on substrate having dielectric constant 4.3 and thickness h= 1.52 mm

rectangular PMA is shown and it is observed that the available measured result in [95] is close to theoretical one. The width of the strip increases the bandwidth increases drastically. The Fig. 8.9 and Fig. 8.10 are input impedance (real and imaginary) plot for the rectangular PMA.

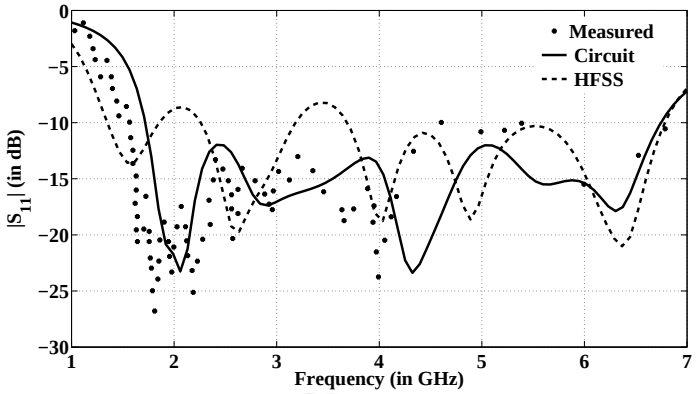

Figure 8.8: Return loss of rectangular printed monopole antenna

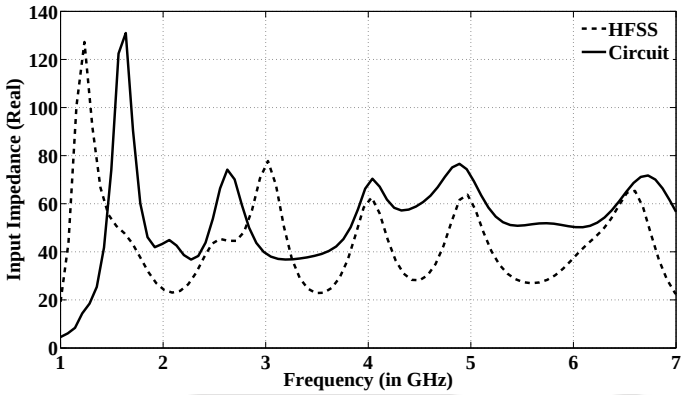

Figure 8.9: Real part of input impedance of rectangular printed monopole antenna

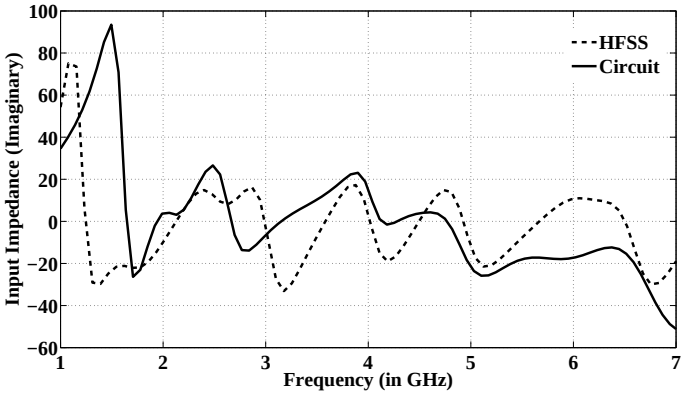

Figure 8.10: Imaginary part of input impedance of rectangular printed monopole antenna

The different values of the resistance, inductance (in nH) and capacitance (in pF) corresponding to rectangular printed monopole antenna are shown in Table. 8.2. From Fig. 8.10, it has been observed that the number of zero crossing is nine in reactive impedance plot. For this type of antennas the resonance takes place at the frequencies which are very nearer to each other to get

Table. 8.2: Lumped element values of rectangular printed monopole antenna

Z_{in}	Z_0	Z_1	Z_2	Z_3	Z_4	Z_5	Z_6	Z_7	Z_8	Z_9
R_n		122	130.3	23.24	54.67	24.01	32.58	20.31	41.7	27.22
L_n	0.178	0.43	2	0.328	0.5	0.59	0.12	0.15	0.17	0.16
C_n		126	4.9	18	7.3	3.6	13	8.4	6.2	4.8

huge bandwidth.

8.2.3 Case III: Bend Strip Printed Monopole Antenna

In this section bend strip monopole antenna is analyzed. The geometry of the antenna is shown in Fig. 8.11. The different values of the resistance, inductance and capacitance corresponding to

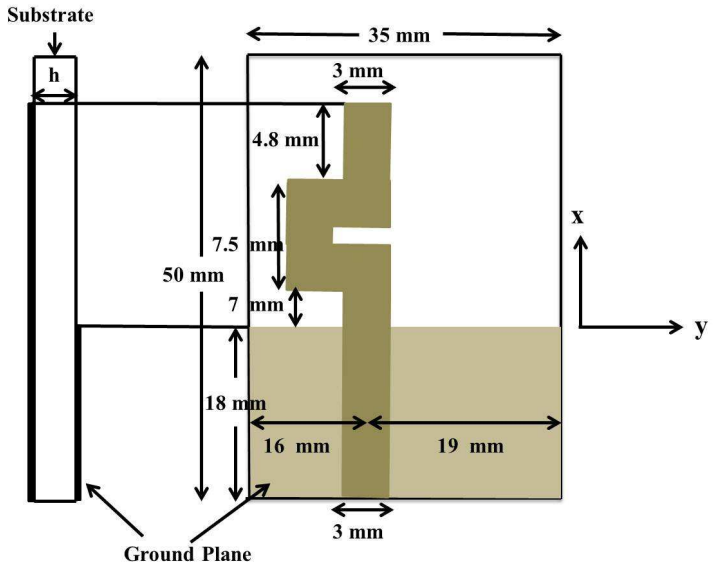

Figure 8.11: Geometry of bend strip printed monopole antenna on FR4 substrate having thickness 1.6 mm

bend strip printed monopole antenna are given below in Table. 8.3. In case of bend strip printed

Table. 8.3: Lumped element values of bend strip printed monopole antenna

Z_{in}	Z_0	Z_1	Z_2	Z_3	Z_4
R_n		47.09	264.77	24.30	89.67
L_n	0.178 nH	0.7 nH	0.127 nH	0.35 nH	0.38 nH
C_n		6.2 pF	11.3 pF	2.5 pF	0.94 pF

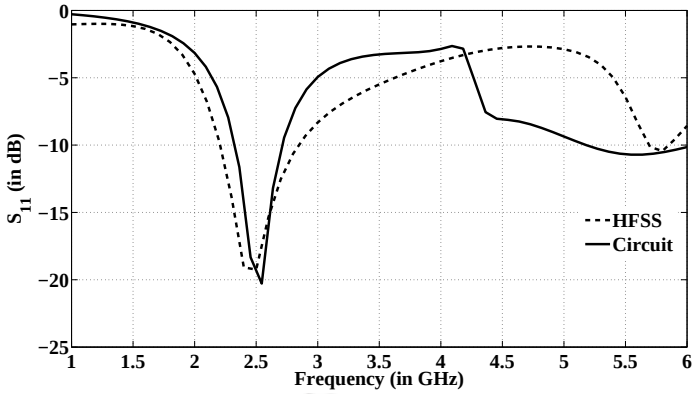

Figure 8.12: Return loss of bend strip printed monopole antenna

monopole antenna overall current path length is increased compared to simple strip monopole antenna, so the first resonant frequency get lowered near 2.5 GHz as shown in Fig. 8.12. The

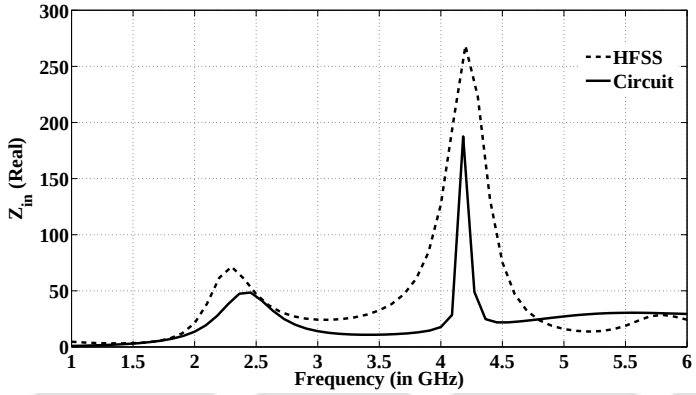

Figure 8.13: Real part of input impedance of bend strip printed monopole antenna

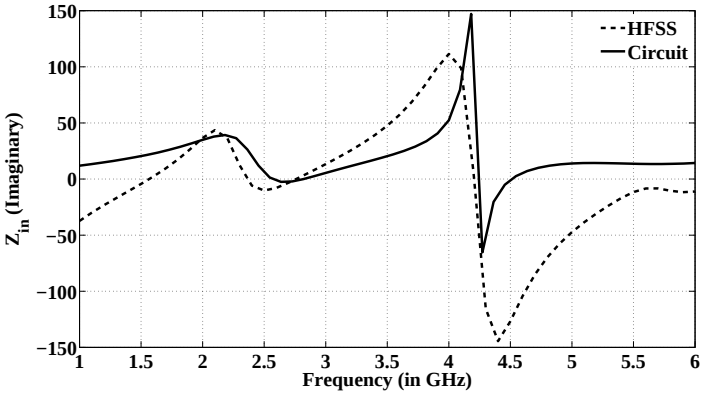

Figure 8.14: Imaginary part of input impedance of bend strip printed monopole antenna

input impedance plot of bend strip printed monopole antenna shown in Fig. 8.13 and Fig. 8.14.

The number of resonator considered here is four since zero crossing point observed in Fig. 8.14 is four.

8.2.4 Case IV: Bend Strip Printed Monopole Antenna with Protruding Stub in the Ground Plane

In [105], simulated and measured results are produced for bend strip printed monopole antenna with protruding stub in the ground plane. Here, the circuit representation with corresponding values of lumped elements of printed monopole antenna with protruding stub in the ground are presented. The results are both verified by simulation and available measured result in [105] for the return loss. The layout for the said configuration is shown in Fig. 8.15. The values of

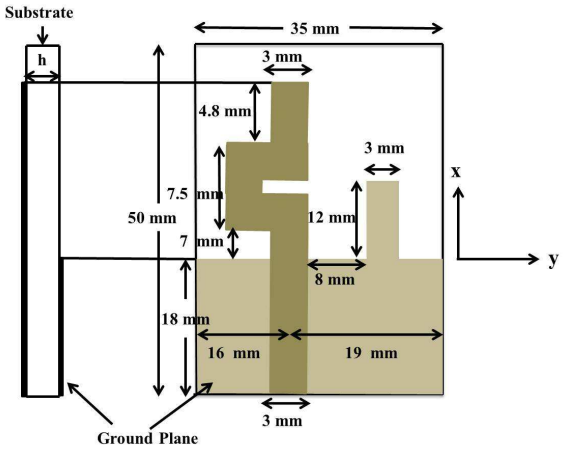

Figure 8.15: Geometry of bend strip printed monopole antenna with protruding stub in the ground plane on FR4 substrate having thickness 1.6 mm.

the resistance, inductance and capacitance related to bend strip printed monopole antenna with protruding stub in the ground plane are given below in Table. 8.4. In Fig. 8.16, it has been

Table. 8.4: Lumped element values of bend strip printed monopole antenna with protruding stub in the ground plane

Z_{in}	Z_0	Z_1	Z_2	Z_3	Z_4
R_n		79.25	250.72	92.39	20.31
L_n	0.178 nH	0.83 nH	1.0 nH	0.20 nH	0.9 nH
C_n		6.5 pF	1.2 pF	3.4 pF	1 pF

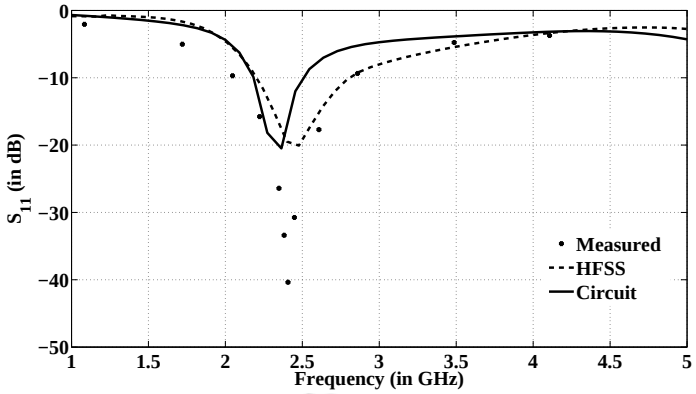

Figure 8.16: Return loss of bend strip printed monopole antenna with protruding stub in the ground plane

observed that second resonance become more specific in 5.8 GHz due to addition of the stub in the ground plane which provides an another path for the current to radiate. But in Fig. 8.12 due to absence of the stub in the ground the small amount of radiation is occurring at 5.8 GHz due to presence of ground plane only. The theoretical result in Fig. 8.16 is verified with measurement result available in [105]. The input impedance both real and imaginary for the present case is shown in Fig. 8.17 and Fig. 8.18. The number of resonator considered here is four since zero

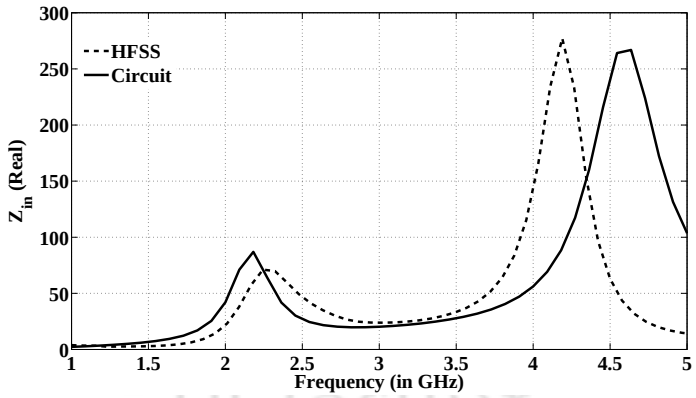

Figure 8.17: Real part of input impedance of bend strip printed monopole antenna with protruding stub in the ground plane

crossing point observed in Fig. 8.18 is four.

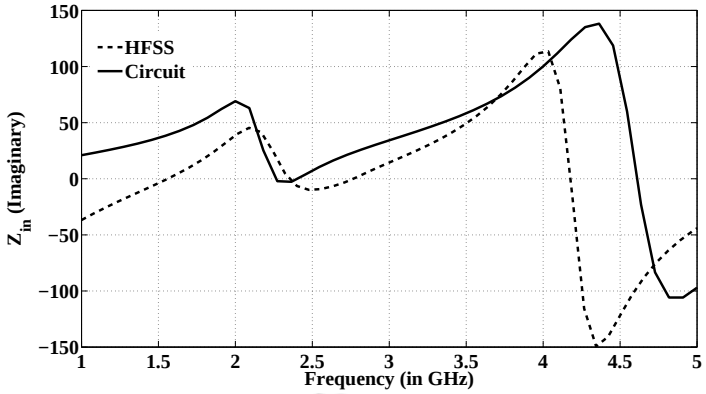

Figure 8.18: Imaginary part of input impedance of bend strip printed monopole antenna with protruding stub in the ground plane

8.3 Summary

This chapter presents a circuit representation approach for the analysis of printed monopole antenna for different cases. Modified circuit representation is presented for PMA cases. The work not only focussed on presenting circuit representation of the different cases of PMA but also provides the values of different lumped elements which constitute the circuit. Further, the performance of such equivalent circuit are compared with simulation using HFSS via input impedance and return loss calculation. In addition, the return loss plot for rectangular PMA, circular PMA and printed monopole antenna with protruding stub in the ground plane are verified with available experimental results.

CHAPTER 9

CONCLUSIONS AND FUTURE WORK

9.1 Conclusions

Many research work on printed monopole antenna based on simulation and measurements have been reported in literatures. However, detailed theoretical investigation on PMA have not been reported. In this thesis, theoretical analysis for PMA is presented in detail and theoretical results are verified with simulation (HFSS) and available experimental data from published works. Briefly, the approach used for the analysis of PMA are summarized as follows:

A. Full wave analysis of PMA

Spatial domain potential Green's functions of a horizontal electric dipole (HED) lying on an ungrounded dielectric slab is derived. The full wave technique (MoM) based on Mixed Potential Integral Equation (MPIE), involving the derived potential Green's functions, is used to calculate the input impedance as well as the refection coefficient of printed monopole antennas (PMAs). The performance of rectangular and F shaped PMAs are evaluated using MPIE-MoM. The computed results for the input impedance and reflection coefficient of rectangular PMA are verified with HFSS results. Further, refection coefficient of F-shaped PMA is computed using MPIE-MoM which is verified by HFSS simulation and available experimental result.

B. Approximate analysis of PMA using transmission line analogy

Derivation of a closed form expression for input admittance of horizontal electric dipole over an ungrounded substrate using transmission line analogy is presented. The derived expres-

sion is then used to calculate reflection coefficient of rectangular and circular printed monopole antenna (PMA) fed by a microstrip line. Analytical result for the reflection coefficient of both rectangular and circular PMA is verified using HFSS. For circular PMA, analytical and simulated results are also compared with the measured results available in literature. Effect of the dimension and dielectric material parameters on the antenna bandwidth is also studied and verified by HFSS.

C. Circuit Representation of Different Printed Monopole Antennas

Circuit representation of printed monopole antennas for different antenna cases is presented here. In general, a simple parallel R, L, C circuit is enough to represent a particular band of an antenna. Similarly for multi-band antenna, each resonance can be replace by their equivalent parallel R, L, C circuit. Thus overall circuit of a lossy one port device such as antenna can be modeled by series inductance and capacitance with parallel R, L, C circuit(s). But the effect of capacitance in series is not relevant for printed monopole antennas since ground plane below the patch is absent for such cases. Circuit representation is presented for different printed monopole antennas cases with their individual lumped element values for each design of the antenna which are further verified by HFSS and available experimental results.

9.2 Suggestions for Future Research

Following the proposed methods described in this thesis, a number of possible directions for extensions to this work are discussed below:

- In this work basically microstrip line fed PMA have been analyzed. Coplanar waveguide fed PMA is not considered here so further study of such structure would be interesting.
- In the present work, polarization aspect of PMA is not considered theoretically. Such investigation may be carried out for further analysis of PMA.
- Theoretical investigation for any arbitrary shape patch and ground plane would be interesting.

- It will be interesting to carry out the theoretical analysis of PMA with notches.

LIST OF PUBLICATIONS

Journal Publications

1. Bhattacharjee S., Kshetrimayum R. S. and Bhattacharjee R., "On the equivalent circuit, input impedance, reflection coefficient and bandwidth of printed monopole antenna", *Microwave and Optical Technology Letter, Wiley*, vol. 57(7), 1535-1538, 2015.

2. Bhattacharjee S., Kshetrimayum R. S. and Bhattacharjee R., "Derivation of potential Green functions for ungrounded dielectric slab and its application in full wave analysis of PMAs", *Journal of Electromagnetic Waves and Applications, Taylor & Francis*, vol. 29(16), 2242-2256, 2015.

3. Bhattacharjee, S., Kshetrimayum, R. S. and Bhattacharjee, R., "Printed monopole antennas on uniaxial substrate: Theory and Simulation", *Electronics Letters, IET*, vol. 52(10), 796-798, 2016.

Journal Under Publication Process

1. Bhattacharjee, S., Kshetrimayum, R. S. and Bhattacharjee, R., "Theoretical analysis of radiation characteristics of printed monopole antennas", *Applied Computational Electromagnetics Society Journal* To be accepted after major revision.

Conference Publications

1. Bhattacharjee, S., Kshetrimayum R. S. and Bhattacharjee, R.,"Bandwidth enhancement of printed monopole antennas using magneto-dielectric cover", *in Proc. IEEE AEMC 2015, Guwahati*.

Manuscript under preparation

1. Bhattacharjee, S., Kshetrimayum, R. S. and Bhattacharjee, R., “Circuit representation of different printed monopole antennas”, *to be submitted* .

REFERENCES

[1] G. A. Deschamps, "Microstrip microwave antennas," in *3rd USAF Symposium on Antennas*, 1953.

[2] J. R. James and P. S. Hall-(Eds.), *Handbook of Microstrip Antennas*. IEE Electromagnetic Wave Series, 1989.

[3] J. Huang and A. C. Densmore, "Microstrip Yagi array antenna for mobile satellite vehicle applications," *IEEE Trans. on Antennas and Propagation.*, vol. 39(7), pp. 1024–1030, 1991.

[4] J. Huang and R. J. Pogorzelski, "A Ka-band microstrip reflectarray with elements having variable rotation angles," *IEEE Trans. on Antennas and Propagation.*, vol. 46(5), pp. 650–656, 1998.

[5] S. Nishimura, K. Nakano, and T. Makimoto, "Franklin type microstrip line antenna," in *IEEE Antennas and Propagation Society International Symposium*, 1979, pp. 134–137.

[6] I. J. Bahl, S. S. Stuchly, and M. A. Stuchly, "A new microstrip radiator for medical applications," *IEEE Trans. on Microwave Theory and Techniques*, vol. 28(12), pp. 1464–1469, 1980.

[7] C. A. Balanis, *Antenna Theory, Analysis and Design*, 2nd ed. John Wiley and Sons, 1996.

[8] H. Lebbar, M. Himdi, and J. P. Daniel, "Analysis and size reduction of various printed monopoles with different shapes," *Electronics Letters*, vol. 30(21), pp. 1725–1726, 1994.

[9] ——, "Transmission line analysis of printed monopole," *Electronics Letters*, vol. 28(14), pp. 1326–1327, 1992.

[10] Y. L. Kuo and K. L. Wong, "Printed double T monopole antenna for 2.4/5.2 Ghz dual-band WLAN operations," *IEEE Trans. on Antennas and Propagation*, vol. 51(9), pp. 2187–2192, 2003.

[11] W. C. Liu, C. M. Wu, and N. C. Chu, "A compact CPW fed slotted patch antenna for dual-band operation," *IEEE Antennas and Wireless Propagation Letters*, vol. 9, pp. 110–113, 2010.

[12] J. Liang, C. C. Chiau, X. Chen, and C. G. Parini, "Printed circular disc monopole antenna for ultra-wideband applications," *Electronics Letters*, vol. 40(20), pp. 1246–1247, 2004.

[13] S. T. Choi, K. Hamaguchi, and R. Kohno, "Small printed CPW fed triangular monopole antenna for ultra-wideband applications," *Microwave and Optical Technology Letters*, vol. 51(5), pp. 1180–1182, 2009.

[14] D. M. Pozar, *Microwave Engineering*, 2nd ed. John Wiley and Sons, 1998.

[15] R. Munson, "Conformal microstrip antennas and microstrip phased arrays," *IEEE Trans. on Antennas and Propagation*, vol. 22(1), pp. 74–78, 1974.

[16] H. Pues and A. Van de Capelle, "Accurate transmission-line model for the rectangular microstrip antenna," *IEE Proc. Microwaves, Optics and Antennas*, vol. 131(6), pp. 334–340, 1984.

[17] A. Bhattacharyya and R. Garg, "Generalised transmission line model for microstrip patches," *IEE Proc. Microwaves, Antennas and Propagation*, vol. 132(2), pp. 93–98, 1985.

[18] ——, "Analysis of annular sector and circular sector microstrip patch antenna," *Electromagnetics*, vol. 6(3), pp. 229–242, 1986.

[19] A. Bhattacharyya and L. Shafai, "Theoretical and experimental investigation of the elliptical annular ring antenna," *IEEE Trans. on Antennas and Propagation*, vol. 36(11), pp. 1526–1530, 1988.

[20] D. R. Jackson and N. G. Alexopoulos, "Gain enhancement methods for printed circuit antennas," *IEEE Trans. on Antennas and Propagation*, vol. 33(9), pp. 976–987, 1985.

[21] T. Itoh-(Ed.), *Numerical Techniques for Microwave and Millimeter-Wave Passive Structures*. John Wiley, 1989.

[22] J. R. Mosig and F. E. Gardiol, *Advances in Electronics and Electron Physics*, 1982, vol. 59.

[23] A. Reineix and B. Jecko, "Analysis of microstrip patch antennas using finite difference time domain method," *IEEE Trans. on Antennas and Propagation*, vol. 37(11), pp. 1361–1369, 1989.

[24] C. Wu, K.-L. Wu, Z. Q. Bi, and J. Litva, "Accurate characterization of planar printed antennas using finite-difference time-domain method," *IEEE Trans. on Antennas and Propagation*, vol. 40(5), pp. 526–534, 1992.

[25] D. R. Jackson and N. G. Alexopoulos, "Simple approximate formulas for input resistance, bandwidth, and efficiency of a resonant rectangular patch," *IEEE Trans. on Antennas and Propagation*, vol. 39(3), pp. 407–410, 1991.

[26] T. Itoh, "Spectral domain immitance approach for dispersion characteristics of generalized printed transmission lines," *IEEE Trans. on Microwave Theory and Techniques*, vol. 28(7), pp. 733–736, 1980.

[27] A. G. Derneryd, "Linearly polarized microstrip antennas," *IEEE Trans. on Antennas and Propagation*, vol. 24(6), pp. 846–851, 1976.

[28] G. Dubost, "Transmission-line model analysis of a lossy rectangular microstrip patch," *Electronics Letters*, vol. 18(7), pp. 281–282, 1982.

[29] M. Himdi, J. P. Daniel, and C. Terret, "Transmission line analysis of aperture coupled microstrip antenna," *Electronics Letters*, vol. 25(18), pp. 1229–1230, 1989.

[30] G. Dubost and G. Beauquet, "Linear transmission-line model analysis of a circular patch antenna," *Electronics Letters*, vol. 22(22), pp. 1174–1176, 1986.

[31] G. Dubost, "Linear transmission-line model analysis of arbitrary-shape patch antennas," *Electronics Letters*, vol. 22(15), pp. 798–799, 1986.

[32] M. D. Deshpande and M. C. Bailey, "Input impedance of microstrip antennas," *IEEE Trans. on Antennas and Propagation*, vol. 30(4), pp. 645–650, 1982.

[33] D. M. Pozar, "Radiation and scattering from a microstrip patch on a uniaxial substrate," *IEEE Trans. on Antennas and Propagation*, vol. 35(6), pp. 613–621, 1987.

[34] J. R. Mosig and F. E. Gardiol, "Analytical and numerical techniques in the green's function treatment of microstrip antennas and scatterers," *IEE Proc. Microwaves, Optics and Antennas*, vol. 130(2), pp. 175–182, 1983.

[35] C. H. Stoyer, "Electromagnetic fields of dipoles in stratified media," *IEEE Trans. on Antennas and Propagation*, vol. 25(4), pp. 547–552, 1977.

[36] N. K. Das and D. M. Pozar, "A generalized spectral-domain Green's function for multilayer dielectric substrates with application to multilayer transmission lines," *IEEE Trans. on Microwave Theory and Techniques*, vol. 35(3), pp. 326–335, 1987.

[37] G. Dural and M. I. Aksun, "Closed-form Green's functions for general sources and stratified media," *IEEE Trans. on Microwave Theory and Techniques*, vol. 43(7), pp. 1545–1552, 1995.

[38] R. W. P. King, "The electromagnetic field of a horizontal electric dipole in the presence of a three-layered region," *Journal of Applied Physics*, vol. 69(12), pp. 7987–7995, 1991.

[39] Y. L. Lu, Y. L. Wang, Y. H. Xu, and K. Li, "Electromagnetic fields of a horizontal electric dipole buried in a four-layered region," *Progress In Electromagnetics Research B*, vol. 16, pp. 247–275, 2009.

[40] Y. H. Xu, K. Li, and Y. L. Lu, "Electromagnetic fields of a horizontal electric dipole in the presence of a four layered region," *Progress In Electromagnetics Research*, vol. 81, pp. 371–391, 2008.

[41] N. K. Uzunoglu, N. G. Alexopoulos, and J. G. Fikioris, "Radiation properties of microstrip dipoles," *IEEE Trans. on Antennas and Propagation*, vol. 27(6), pp. 853–858, 1979.

[42] J. R. Mosig and T. K. Sarkar, "Comparison of quasi-static and exact electromagnetic fields from a horizontal electric dipole above a lossy dielectric backed by an imperfect ground plane," *IEEE Trans. on Microwave Theory and Techniques*, vol. 34(4), pp. 379–387, 1986.

[43] D. M. Pozar, "Input impedance and mutual coupling of rectangular microstrip antennas," *IEEE Trans. on Antennas and Propagation*, vol. 30(6), pp. 1191–1196, 1982.

[44] W. C. Chew and J. A. Kong, "Analysis of a circular microstrip disk antenna with a thick dielectric substrate," *IEEE Trans. on Antennas and Propagation*, vol. 29(1), pp. 68–76, 1981.

[45] M. C. Bailey and M. D. Deshpande, "Analysis of elliptical and circular microstrip antennas using moment method," *IEEE Trans. on Antennas and Propagation*, vol. 33(9), pp. 954–959, 1985.

[46] S. M. Ali, W. Chew, and J. Kong, "Vector hankel transform analysis of annular-ring microstrip antenna," *IEEE Trans. on Antennas and Propagation*, vol. 30(4), pp. 637–644, 1982.

[47] D. G. Shively, "Scattering from microstrip patch antennas using subdomain basis function," *Electromagnetics*, vol. 14, pp. 1–18, 1994.

[48] D. M. Pozar and S. Voda, "A rigorous analysis of a microstripline fed patch antenna," *IEEE Trans. on Antennas and Propagation*, vol. 35(12), pp. 1343–1350, 1987.

[49] X. H. Yang and L. Shafai, "Characteristics of aperture coupled microstrip antennas with various radiating patches and coupling apertures," *IEEE Trans. on Antennas and Propagation*, vol. 43(1), pp. 72–78, 1995.

[50] D. M. Pozar, "A reciprocity method of analysis for printed slot and slot-coupled microstrip antennas," *IEEE Trans. on Antennas and Propagation*, vol. 34(12), pp. 1439–1446, 1986.

[51] P. Sullivan and D. H. Schaubert, "Analysis of an aperture coupled microstrip antenna," *IEEE Trans. on Antennas and Propagation*, vol. 34(8), pp. 977–984, 1986.

[52] N. I. Herscovici and D. M. Pozar, "Analysis and design of multilayer printed antennas: a modular approach," *IEEE Trans. on Antennas and Propagation*, vol. 41(10), pp. 1371–1378, 1993.

[53] D. G. Fang, *Antenna Theory and Microstrip Antennas*. CRC Press, 2010.

[54] P. Perlmutter, S. Shtrikman, and D. Treves, "Electric surface current model for the analysis of microstrip antennas with application to rectangular elements," *IEEE Trans. on Antennas and Propagation*, vol. 33(3), pp. 301–311, 1985.

[55] T. Itoh and W. Menzel, "A full-wave analysis method for open microstrip structures," *IEEE Trans. on Antennas and Propagation*, vol. 29(1), pp. 63–68, 1981.

[56] F. J. Demuynck, G. A. E. Vandenbosch, and A. R. Van de Capelle, "The expansion wave concept: partI. efficient calculation of spatial green's functions in a stratified dielectric medium," *IEEE Trans. on Antennas and Propagation*, vol. 46(3), pp. 397–406, 1998.

[57] R. C. Hall and J. R. Mosig, "Analysis of coaxially fed microstrip antenna with electrically thick substrates," *Electromagnetics*, vol. 9, pp. 367–384, 1989.

[58] K. A. Michalski and C. I. G. Hsu, "RCS computation of coax-loaded microstrip patch antennas of arbitrary shape," *Electromagnetics*, vol. 14, pp. 33–42, 1994.

[59] S. Uckun, T. K. Sarkar, S. M. Rao, and M. Salazar-Palma, "A novel technique for analysis of electromagnetic scattering from microstrip antennas of arbitrary shape," *IEEE Trans. on Microwave Theory and Techniques*, vol. 45(4), pp. 485–491, 1997.

[60] R. C. Hall and J. R. Mosig, "The analysis of arbitrarily shaped aperture-coupled patch antennas via a mixed-potential integral equation," *IEEE Trans. on Antennas and Propagation*, vol. 44(5), pp. 608–614, 1996.

[61] G. A. E. Vandenbosch and F. J. Demuynck, "The expansion wave concept:Part II. a new way to model mutual coupling in microstrip arrays," *IEEE Trans. on Antennas and Propagation*, vol. 46(3), pp. 407–413, 1998.

[62] Y. Hua and T. K. Sarkar, "Generalized pencil-of-function method for extracting poles of an em system from its transient response," *IEEE Trans. on Antennas and Propagation*, vol. 37(2), pp. 229–234, 1989.

[63] R. A. Kipp and C. H. Chan, "Complex image method for sources in bounded regions of multilayer structures," *IEEE Trans. on Microwave Theory and Techniques*, vol. 42(5), pp. 860–865, 1994.

[64] D. G. Fang, J. J. Yang, and G. Y. Delisle, "Discrete image theory for horizontal electric dipoles in a multilayered medium," *IEE Proc. Microwaves, Antennas and Propagation*, vol. 135(5), pp. 297–303, 1988.

[65] J. R. Mosig, "Arbitrarily shaped microstrip structures and their analysis with a mixed potential integral equation," *IEEE Trans. on Microwave Theory and Techniques*, vol. 36(2), pp. 314–323, 1988.

[66] R. F. Harrington, *Field computation by moment method*. IEEE Series, 1968.

[67] J. P. Damiano, J. Bennegueouche, and A. Papiernik, "Study of multilayer microstrip antennas with radiating elements of various geometry," *IEE Proc. Microwaves, Antennas and Propagation*, vol. 137(3), pp. 163–170, 1990.

[68] J. R. Mosig and F. E. Gardiol, "General integral equation formulation for microstrip antennas and scatterers," *IEE Proc. Microwaves, Antennas and Propagation*, vol. 132(7), pp. 424–432, 1985.

[69] R. C. Hansen and M. Burke, "Antennas with magneto-dielectrics," *Microwave and Optical Technology Letters*, vol. 26(2), pp. 75–78, 2000.

[70] H. Mosallaei and K. Sarabandi, "Magneto-dielectrics in electromagnetics: concept and applications," *IEEE Trans. on Antennas and Propagation*, vol. 52(6), pp. 1558–1567, 2004.

[71] K. Han, M. Swaminathan, R. Pulugurtha, H. Sharma, R. Tummala, S. Yang, and V. Nair, "Magneto-dielectric nanocomposite for antenna miniaturization and sar reduction," *IEEE Antennas and Wireless Propagation Letters*, vol. pp(99), pp. 1–1, 2015.

[72] P. M. T. Ikonen, K. N. Rozanov, A. V. Osipov, P. Alitalo, and S. A. Tretyakov, "Magnetodielectric substrates in antenna miniaturization: Potential and limitations," *IEEE Trans. on Antennas and Propagation*, vol. 54(11), pp. 3391–3399, 2006.

[73] C. Niamien, S. Collardey, A. Sharaiha, and K. Mahdjoubi, "Compact expressions for efficiency and bandwidth of patch antennas over lossy magneto-dielectric materials," *IEEE Antennas and Wireless Propagation Letters*, vol. 10, pp. 63–66, 2011.

[74] F. Farzami, K. Forooraghi, and M. Norooziarab, "Miniaturization of a microstrip antenna using a compact and thin magneto-dielectric substrate," *IEEE Antennas and Wireless Propagation Letters*, vol. 10, pp. 1540–1542, 2011.

[75] J. Plet, M. Drissi, and J. Citerne, "Mixed-potential integral equation technique for the characterization of microstrip antennas printed on uniaxial substrates," *Antennas and Propagation Society International Symposium, AP-S. Digest*, vol. 2, pp. 1266–1269, 1995.

[76] R. M. Nelson, D. A. Rogers, and A. G. d'Assuncao, "Resonant frequency of a rectangular microstrip patch on several uniaxial substrates," *IEEE Trans. on Antennas and Propagation*, vol. 38(7), pp. 973–981, 1990.

[77] H. Lee and V. K. Tripathi, "Spectral domain analysis of frequency dependent propagation characteristics of planar structures on uniaxial medium," *IEEE Trans. on Microwave Theory and Techniques*, vol. 30(8), pp. 1188–1193, 1982.

[78] M. N. Srifi, S. K. Podilchak, M. Essaaidi, and Y. M. M. Antar, "Compact disc monopole antennas for current and future ultrawideband UWB applications," *IEEE Transactions on Antennas and Propagation*, vol. 59, no. 12, pp. 4470–4480, Dec 2011.

[79] J. xin Liang, C. Chiau, X. Chen, and C. Parini, "Study of a printed circular disc monopole antenna for UWB system," *IEEE Transactions on Antennas and Propagation*, vol. 53, no. 11, pp. 3500–3504, Nov 2005.

[80] J. R. Panda and R. S. Kshetrimayum, "An F-shaped printed monopole antenna for dual-band RFID and WLAN applications," *Microwave and Optical Technology Letters*, vol. 53, pp. 1478–1481, 2011.

[81] J. Kim, T. Yoon, J. Kim, and J. Choi, "Design of an ultra wide-band printed monopole antenna using FDTD and genetic algorithm," *IEEE Microwave and Wireless Components Letters*, vol. 15, no. 6, pp. 395–397, June 2005.

[82] W. Wu and Y. P. Zhang, "Analysis of ultra-wideband printed planar quasi-monopole antennas using the theory of characteristic modes," *IEEE Antennas and Propagation Magazine*, vol. 52, no. 6, pp. 67–77, Dec 2010.

[83] C. Laohapensaeng, C. Free, and I. D. Robertson, "Simplified analysis of printed strip monopole antenna fed by a cpw," vol. 5, Dec 2005.

[84] R. Garg, I. Bahl, P. Bhartia, and A. Ittipiboon, *Microstrip Antenna Design Handbook*. Artech House, 2010.

[85] A. K. Bhattacharjee, S. R. B. Chaudhuri, D. R. Poddar, and S. K. Chowdhury, "Equivalence of radiation properties of square and circular microstrip patch antennas," *IEEE Transactions on Antennas and Propagation*, vol. 38, no. 10, pp. 1710–1711, Oct 1990.

[86] N. V. Shuley, R. R. Boix, F. Medina, and M. Horno, "On the fast approximation of green's functions in MPIE formulations for planar layered media," *IEEE Transactions on Microwave Theory and Techniques*, vol. 50, no. 9, pp. 2185–2192, Sep 2002.

[87] M. I. Aksun, "A robust approach for the derivation of closed-form green's functions," *IEEE Transactions on Microwave Theory and Techniques*, vol. 44, no. 5, pp. 651–658, May 1996.

[88] Y. P. Chen, W. C. Chew, and L. Jiang, "A new green's function formulation for modeling homogeneous objects in layered medium," *IEEE Transactions on Antennas and Propagation*, vol. 60, no. 10, pp. 4766–4776, Oct 2012.

[89] J. R. Mosig and A. A. Melcon, "Green's functions in lossy layered media: integration along the imaginary axis and asymptotic behavior," *IEEE Transactions on Antennas and Propagation*, vol. 51, no. 12, pp. 3200–3208, Dec 2003.

[90] Y. L. Chow, J. J. Yang, D. G. Fang, and G. E. Howard, "A closed-form spatial green's function for the thick microstrip substrate," *IEEE Transactions on Microwave Theory and Techniques*, vol. 39, no. 3, pp. 588–592, Mar 1991.

[91] N. Alexopoulos, D. Jackson, and P. Katehi, "Criteria for nearly omnidirectional radiation patterns for printed antennas," *IEEE Transactions on Antennas and Propagation*, vol. 33, no. 2, pp. 195–205, Feb 1985.

[92] V. Volski and G. A. E. Vandenbosch, "Quasi 3-d mixed potential integral equation formulation for periodic structures," *IEEE Transactions on Antennas and Propagation*, vol. 61, no. 4, pp. 2068–2076, April 2013.

[93] G. A. E. Vandenbosch and A. R. V. de Capelle, "Mixed-potential integral expression formulation of the electric field in a stratified dielectric medium-application to the case

of a probe current source," *IEEE Transactions on Antennas and Propagation*, vol. 40, no. 7, pp. 806–817, Jul 1992.

[94] L. Barlately, J. R. Mosig, and T. Sphicopoulos, "Analysis of stacked microstrip patches with a mixed potential integral equation," *IEEE Transactions on Antennas and Propagation*, vol. 38, no. 5, pp. 608–615, May 1990.

[95] M. John, J. Evans, M. J. Ammann, J. Modro, and Z. Chen, "Reduction of ground-plane-dependent effects on microstrip-fed printed rectangular monopoles," *IET Microw. Antennas Propag*, vol. 2, pp. 42–47, 2008.

[96] A. Panahi, X. L. Bao, G. Ruvio, and M. J. Ammann, "A printed triangular monopole with wideband circular polarization," *IEEE Transactions on Antennas and Propagation*, vol. 63, no. 1, pp. 415–418, Jan 2015.

[97] H. J. Visser, *Approximate Antenna Analysis for CAD*. John Wiley and Sons, 2009.

[98] A. K. Bhattacharyya, "Long rectangular patch antenna with a single feed," *IEEE Transactions on Antennas and Propagation*, vol. 38, no. 7, pp. 987–993, Jul 1990.

[99] D. Porcino and W. Hirt, "Ultra-wideband radio technology: Potential and challenges ahead," *IEEE Communication Magazine*, vol. 41, pp. 66–74, July 2003.

[100] M. L. Tounsi, R. Touhami, and M. C. E. Yagoub, "Generic spectral immittance approach for fast design of multilayered bilateral structuresincluding anisotropic media," *Microwave and Wireless Components Letters, IEEE*, vol. 17, pp. 409–411, 2007.

[101] M. J. Ammann and M. John, "Optimum design of the printed strip monopole," *IEEE Antennas Propag. Mag.*, vol. 47, Dec 2005.

[102] S. B. T. Wang, A. M. Niknejad, and R. W. Brodersen, "Circuit modeling methodology for UWB omnidirectional small antennas," *Selected Areas in Communications, IEEE Journal on*, vol. 24, no. 4, pp. 871–877, April 2006.

[103] S. Ramo, J. R. Whinnery, and T. V. Duzer, *Fields and Waves in Communication Electronics*, 3rd ed. John Wiley and Sons, 1994.

[104] Y. Lu, Y. Huang, H. T. Chattha, and P. Cao, "Reducing ground-plane effects on UWB monopole antennas," *Antennas and Wireless Propagation Letters, IEEE*, vol. 10, pp. 147–150, March 2011.

[105] J. R. Panda and R. S. Kshetrimayum, "A printed 2.4 GHz/5.8 GHz dual band monopole antenna with a protruding stub in the ground plane for WLAN and RFID applications," *Progress In Electromagnetics Research*, vol. 117, pp. 425–434, 2011.